

LEVEL II

THE JOURNAL OF THE DOD FUZE ENGINEERING WORKING GROUP (FESWG)

(JOINT ARMY - NAVY - AIR FORCE)

(1)

FEASIBILITY OF STANDARDIZED RAIN TESTING FOR FUZES

APPROVED FOR PUBLICATION

BY THE DOD FESWG

JUNE 1981

SERIAL NO. 1.0

PREPARED BY

JOHN K. DOMEN

**DTIC
ELECTE
FEB 5 1982
H**

US ARMY ARMAMENT RESEARCH AND DEVELOPMENT COMMAND

PRODUCT ASSURANCE DIRECTORATE

DOVER, NJ 07801

Requests for additional copies of this document shall be addressed to the
Defense Technical Information Center.

82 02 04 077

DISTRIBUTION STATEMENT A
Approved for public release
Distribution Unlimited

DTIC FILE COPY AD A110513

The citation in this report of the names of commercial firms or commercially available products or services does not constitute official endorsement or approval of such commercial firms, products, or services by the U.S. Government.

The views, opinions, and/or findings contained in this report are those of the author and should not be construed as an official Department of the Army position, policy, or decision, unless so designated by other documentation.

①
THE JOURNAL OF THE DOD FUZE ENGINEERING WORKING GROUP (FESWG)

(JOINT ARMY - NAVY - AIR FORCE)

FEASIBILITY OF STANDARDIZED RAIN TESTING
FOR FUZES

Approved for Publication

by the DOD FESWG

June 1981

DTIC
SELECTED
FEB 5 1982
H

Serial No. 1.0

Prepared by

John K. Domen

US ARMY ARMAMENT RESEARCH AND DEVELOPMENT COMMAND

PRODUCT ASSURANCE DIRECTORATE

Dover, NJ 07801

Requests for additional copies of this document shall be
addressed to the Defense Technical Information Center.

REPORT DOCUMENTATION PAGE		READ INSTRUCTIONS BEFORE COMPLETING FORM
1. REPORT NUMBER	2. GOVT ACCESSION NO. AD-A110 513	3. RECIPIENT'S CATALOG NUMBER
4. TITLE (and Subtitle) FEASIBILITY OF STANDARDIZED RAIN TESTING FOR FUZES <i>Serial Number 100</i>		5. TYPE OF REPORT & PERIOD COVERED Final, July 79-June 81
7. AUTHOR(s) John K. Domen		6. PERFORMING ORG. REPORT NUMBER
9. PERFORMING ORGANIZATION NAME AND ADDRESS ARRADCOM DRDAR-QAS-T Dover, NJ 07801 <i>141</i>		8. CONTRACT OR GRANT NUMBER(s)
11. CONTROLLING OFFICE NAME AND ADDRESS ARRADCOM DRDAR-TSS Dover, NJ 07801		10. PROGRAM ELEMENT, PROJECT, TASK AREA & WORK UNIT NUMBERS AMCMS Code No. 6910.00.63400
14. MONITORING AGENCY NAME & ADDRESS (if different from Controlling Office) Co-sponsored by the Joint Service Fuze Managers and the DOD Fuze Engineering Standardization Working Group		12. REPORT DATE June 1981
		13. NUMBER OF PAGES 145
		15. SECURITY CLASS. (of this report) Unclassified
		15a. DECLASSIFICATION/DOWNGRADING SCHEDULE
16. DISTRIBUTION STATEMENT (of this Report) Approved for public release, distribution unlimited.		
17. DISTRIBUTION STATEMENT (of the abstract entered in Block 20, if different from Report)		
18. SUPPLEMENTARY NOTES		
19. KEY WORDS (Continue on reverse side if necessary and identify by block number) Rain, Fuzes, Simulation.		
20. ABSTRACT (Continue on reverse side if necessary and identify by block number) Rain can cause a fuze to function prior to arriving at a designated target. This report addresses those aspects of a rainfield that relate to the potential problem of preinitiating fuzes designed to function on impact with a target as the primary mode.		

Data on worldwide natural and spray rainfields is reviewed from the aspect of spacial and drop size variations and their relevance to standardizing a rain test.

Inherent in spray and natural rainfields is the statistical uncertainty of what specific encounters occurred during the high velocity portion of the flight. The physics of rain encounter with impact fuzes indicates large drop sizes toward 6 mm diameter are important. A heavy rainfall of at least 20 in/hr biased with larger drops appears feasible for testing. (h.)

However, to reduce statistical uncertainties on impacting with raindrops, an overhead channel orifice system is described, but the practical assurance of uniform drop spacial distribution militates against such a system.

A more feasible system analytically investigated is a "rain web" consisting of a single or sequence of planar matrices holding 5 or 6 mm diameter drops. This approach allows a firmer determination of the distribution of intercepted drops in any firing, and is easily implemented.

A confirmatory test at a facility similar to that of Holloman AFB is recommended to investigate the possibility of an undesired response of a fuze when subjected to a field with many drops with sizes in the range 4 mm diameter and smaller, integrated over the flight through the rainfield.

F E S W G Journal Articles

<u>Serial No.</u>	<u>Title</u>	<u>Date Approved</u>
1.0	Feasibility of Standardized Rain Testing for Fuzes	June 1981



Accession For		
DTIC GRA&I	<input checked="" type="checkbox"/>	
DTIC TDS	<input type="checkbox"/>	
Unprocessed	<input type="checkbox"/>	
Classification		
Distribution/		
Availability Codes		
Serial and/or		
Dist	Special	
A		

Table of Contents

Conclusions	5
Introduction	8
Concepts Relating to Rainfall	
Measurement of Raindrop Size and Number	10
Number and Size in Log-Linear Distribution	12
Water Content Comparison	13
Exponential Approximation Distribution	14
Liquid Content of Rain	15
Median Drop Diameter	16
Rainfall Rate	16
Acceleration and Terminal Velocity of Drops	16
Wind Effect on Spatial Distribution	20
Equivalent Rain Rate	22
Published Natural and Spray Rainfields	
Introduction	23
List of 25 Fields, Distributions and Parameters	24
Plots of 22 Fields, and Comparisons	27
Rain Distributions in Radar Handbook	32
Rainfields Reported in MIL STD 210B	33
Cumulative Water Content of 22 Rainfields	39
Holloman Air Force Base Facilities	
Rocket Test Track	42
Artillery (Ballistic) Test Facility	47
Fuze Encounter through Rain	
Mechanical and Electronic Fuzing	49
Specific Case with Tropical Rainfield	50
Rain Web for Fuze Rain Testing	
Introduction	54
Fabrication of the Drops	54
Frequency Distribution of the Encounter	56
Fractional Drops Intercepted and Water Content	64
Mechanical Impact for Rain Impulse Simulation	70
Experimental-Photographic Study of O-C-O System	
Concept	73
Experiment and Tabulation of Results	75
References	79
Appendix A Photos from Study of O-C-O System	80
Appendix B Rain Impact on PD Fuzes	86
Distribution List	141

Figures

1	Histogram of drop sizes in a rainfield	11
2	Spherical drops accelerating under gravity	19
3.	Spherical drops with initial velocity	19
4	Drop trajectory in 3 knot cross wind	21
5	Drop trajectory in 8 knot cross wind	21
6	Canal Zone distributions	28
7	Standard and tropical rain	28
8	Marshall Islands and North Carolina distributions	29
9	Miami distributions	29
10	Holloman rocket and ballistic rain	30
11	Tropical and Holloman comparison	30
12	Standard, Tropical, Holloman comparison	31
13	Canal Zone E and Holloman comparison	31
14	MIL STD 210B distribution comparison	38
15	Water content for Canal Zone distributions	39
16	Water content for Standard and Tropical rain	39
17	Water content for Marshall Islands and NC rain	40
18	Water content for Miami rain	40
19	Water content for Holloman distributions	41
20	Lateral view of Holloman rocket track	42
21	Axial view of Holloman rocket track	42
22	Holloman rocket track rain at 5 psi	45
23	Holloman rocket track average rain at 5 psi	46
24	Holloman ballistic rain test facility	47
25	Holloman ballistic facility cross section	48

Figures

26	Tropical rain increased 4 and 8 times	52
27	Basic 13 drop pattern for Rain Web simulation	56
28	Web-Fuze configuration for $L = 11$ mm	61
29	Calculated drop interception distribution for $L = 11$ mm	61
30	Web-Fuze configuration for $L = 15$ mm	62
31	Calculated drop interception distribution for $L = 15$ mm	62
32	Web-Fuze configuration for $L = 19$ mm	63
33	Calculated drop interception distribution for $L = 19$ mm	63
34	Calculated drop interception distribution for $L = 23$ mm	64
35	Water content for fractions of 5 mm intercepted drops	65
36	Cumulative water content for fractions of 5 mm intercepted drops	66
37	Drops from 1.6 mm orifice	81
38	Drops from 1.6 mm orifice	82
39	Drops from 2.38 mm orifice	83
40	Drops from 3.10 mm orifice	84
41	Drops from 4.76 mm orifice	85

Tables

1	Raindrop terminal velocities	17
2	Natural and spray rainfields considered	23
3	Rainfield number-size drop distributions	25
4	Calculated rainfield parameters	26
5	Radar handbook and Canal Zone E rain comparison	32
6	MIL STD 210B drop size distributions	33
7	Liquid content for MIL STD 210B rain	35
8	Distributions after reduction to 1mm intervals	36
9	Calculated parameters for 1 mm interval rainfields	37
10	Rain parameters for Holloman rocket track at 5 psi	44
11	Average encounter values in Tropical rain	51
12	Drop sizes and number in orifice flow experiment	76

CONCLUSIONS

1. The nature of natural and spray rainfields is such that only a statistical estimate can be made of what drops were encountered in any test. The variability of the size distribution of drops along a trajectory can be appreciable.

2. Drop sizes around 0.5 mm diameter have negligible water content and can be ignored for momentum transfer.

3. For impact responding fuzes, the larger drops from 4 to 6 mm are most effective, and the test facility should characterize the number of such drops intercepted by the fuze on the average, and their standard deviation.

4. The question of how high a rain rate can be used depends on the time needed by essential fuze components to react and then relax sufficiently to an impulse encounter. Though collision time with a raindrop is less than 10 microseconds for weapon firings, the response of the fuze depends on its configuration, that is, the stiffness and mass values of all significant discrete elements in the fuze. However, there is some reservation in trying to determine these times analytically, as the analyst may omit a key consideration, or some design features may be intractable analytically. Each fuze needs individual consideration.

5. If an intense spray rainfield is chosen, an intensity of at least 20 in/hr and biased with larger drops should be suitable. There should be sufficient time between impacts to avoid the question of multiple impacts in having a subsequent

drop strike before the fuze has effectively relaxed from a previous impact.

6. The deluge nozzle (80200) used at Holloman appears reasonable. It is biased toward the larger size drops.

7. The O-C-O (overhead channel orifice) system is possible for better determination of the drop size distribution. However, horizontal spacing of the drops is needed by some initial motion in the channel itself, since otherwise the drops would be spaced too closely. The practicality of this system is questionable.

8. Statistical uncertainty is practically eliminated if a specific drop pattern with larger drops (principally 5 mm) can be positioned on a planar "web" matrix, normal to the shell trajectory. The matrix is envisioned as a thin plastic sheet with discrete, gelatinized blobs positioned such that at least one of them will intercept the frontal fuze area with high probability. (See the section on Rain Web for details). The drops should be sealed with a protective coating. Such sheets can be positioned so at least 20 milliseconds of travel time exist between them. This deterministic field, while preserving the essentials of the physics of the encounter, will provide the designer with an idea of the loads to be imparted on the fuze.

9. Proximity type fuzes (radio frequency, optical, capacitance) require further consideration of the effect of the test site on the fuze electronic response.

10. Aerodynamic heating would soften plastic fuze frontal structures. Ordinarily this cannot be fully simulated and preheating of the fuze may not be possible because of internal explosive loads.

INTRODUCTION

This study investigates known properties of rain fields and describes technical uncertainties that are associated with rain. The feasibility of establishing a military standard must address such technical uncertainties both on the part of the rainfield itself and the response of the fuze. The literature on rain phenomena is extensive and information that pertains to such a standard is collected in this study.

Topics associated with rain encounter with fuzes are: rainfield distributions, for both natural and artificially produced (spray) rain; reaction time of fuzes; accelerated testing with a high rainfall rate; the practical length of a test facility; and the method of obtaining precise rain-drop distributions.

This study addresses principally impact initiated fuzes, as proximity fuzes (e.g. RF, optical, capacitance) are also affected by the proximity to the ground and the test site structures.

To state the problem succinctly: What test arrangement is most feasible from an economic and practical aspect that is sufficiently representative of the physics of the encounter of an impact fuze or a fuze with an impact sensor with rain? Can the test facility convey a predetermined loading pattern on the fuze so the designer can anticipate

loading levels on the fuze? Can a sprinkler type system satisfy these goals? What are the least number of fuzes that can be fired in the shortest possible rain distance without appreciable statistical uncertainty about which and how many drops intercepted the fuze on each firing? What maximum rain rate should be allowed for accelerated testing?

A further discussion of these topics is delayed until page 67 after a treatment of the essential elements of the rain web approach.

A previous summary study on rain encounter with point detonating fuzes appeared as a paper in the Proceedings of the Fuze/Munitions Environment Characterization Symposium (Picatinny Arsenal, Dover, NJ, November 1972) and is contained as appendix B in this report since it serves as a basis for this report. (Reference 1)

CONCEPTS RELATING TO RAINFALL

Measurement of Raindrop Size and Number

Various drop sizes and their number that are instantaneously present in some small volume are measured. After many measurements of such volumes, the average number of drops according to some drop size intervals is reported. This drop size-number distribution is normalized to a representative volume which is usually one cubic meter. (References 2,3)

Questions:

1. What different size drops are in the sample volume?
2. How many of each size are present (some size-diameter interval must be specified)?
3. What is the spacial distribution of such drops?
4. What is the effect of wind in shifting the distribution?

The answer to question 3 might be a Poisson distribution, but for a spray rainfield it is highly dependent on the hardware installation. Question 4 may be treated analytically by wind drag factors.

In answer to questions 1 and 2: Sizes of drops vary from a fraction of a millimeter to about 6 mm diameter (the very large drops especially may not be very spherical). Sizes have been measured in various ways, from sizes of pellets of flour formed, by photography, and to expected laser beam measurement of shadows produced by the drops.

Many of these small volume measurements are needed to obtain a representative average drop distribution, e.g.

if the sample volume were as large as 100 cubic inches, about 600 such inspection volumes are needed to obtain one cubic meter of representative volume.

Publications that report raindrop distributions differ in the drop diameter interval (ΔD) used for grouping the range of drop diameters. Some reports use 0.1 mm, 0.2 mm, 0.5 mm or 1 mm. If measured in 0.5 mm intervals, the number of drops of mean 2.5 mm diameter actually comes from drops in a range from 2.25 to 2.75 mm in size.

Reported distributions are then a histogram plot of the number of drops of a particular diameter D_1 (within a diameter range ΔD) as shown in figure 1.

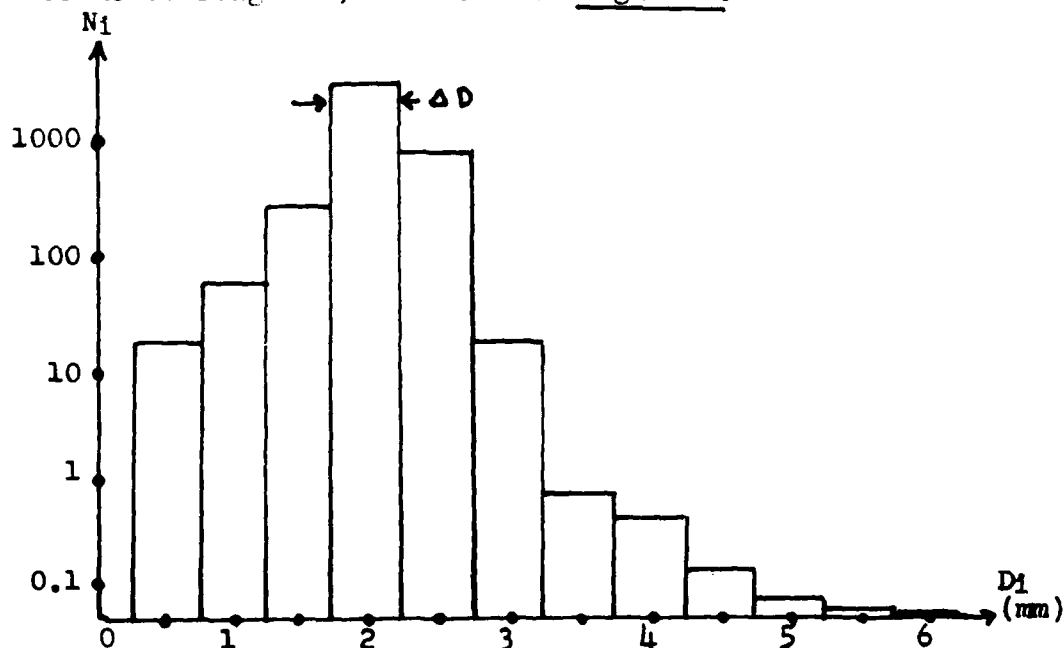


Figure 1. Histogram of average number N_1 of drops of diameter D_1 for a diameter range ΔD (here 0.5 mm) for a representative volume in the rainfield.

The ordinate is plotted on a log scale since the number of various sizes changes from a possible several thousand small ones to a fraction of a drop of a 5 mm diameter in a cubic meter.

The total number of drops, N , in this cubic meter, is not too meaningful. It is the sum of the drops at any mean drop size, D_1 , over all the drop diameter increments, ΔD . If the drop diameter interval is large, say 0.5 mm, then there are fewer intervals, but a larger number in an interval.

S represents the number of discrete average drop diameters D_1 :

$$N = \sum_{i=1}^S N_1 \quad (1)$$

Number and Size in Log-Linear Distribution

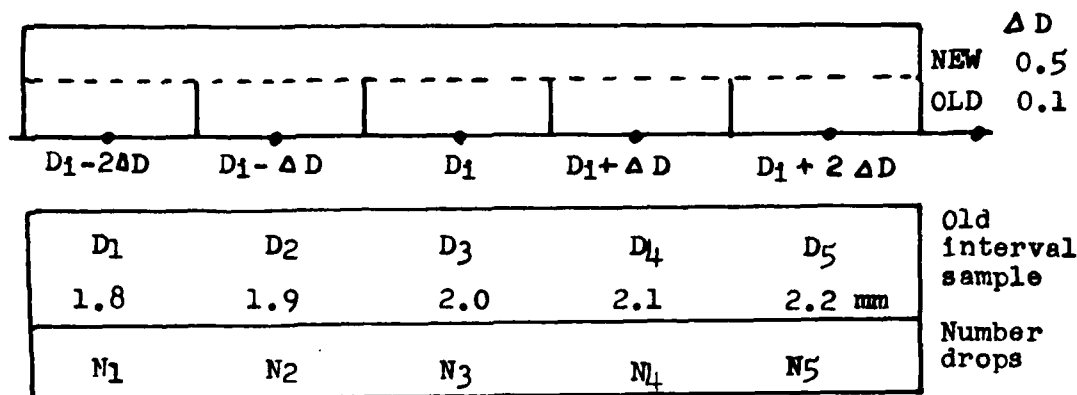
In this report, in order that the reported natural and spray rainfields may be compared in a convenient manner, all the raindrop distributions were resolved to the same ΔD drop diameter interval, 0.5 mm. This was the interval used in the Holloman report of 1975 on the rocket test facility.

Some of the earlier reported distributions used 0.1 mm intervals. The following procedure is sufficiently accurate in converting, for example, 0.1 to 0.5 mm intervals by testing the water content of the transformed distribution.

This approach was used to reduce all rain distributions to a common graphical representation. The Synopsis of Background Material for MIL STD 210B (references 5 and 6) reports distributions on a 1.0 mm interval, and only

a crude method could be used to go in reverse, to a smaller 0.5 mm interval.

Water Content Comparison



The mean of 2.0 mm diameter will be used. Change the range from 0.1 to 0.5 mm, and see the effect on the liquid content, which goes as $N_1 D_1^3$. The liquid content in the OLD system, correct to terms in $(\Delta D)^2$ is:

$$L_{OLD} = \sum_{i=1}^5 D_i^3 N_i = D_1^3 N_1 + D_2^3 N_2 + D_3^3 N_3 + D_4^3 N_4 + D_5^3 N_5 \quad (2)$$

$$L_{OLD} = (D_3 - 2\Delta D)^3 N_1 + (D_3 - \Delta D)^3 N_2 + D_3^3 N_3 + (D_3 + \Delta D)^3 N_4 + (D_3 + 2\Delta D)^3 N_5$$

$$L_{OLD} = [D_3^3 - 3D_3^2(2\Delta D) + 3D_3(2\Delta D)^2] N_1 + [D_3^3 - 3D_3^2(\Delta D) + 3D_3(\Delta D)^2] N_2 + D_3^3 N_3 + [D_3^3 + 3D_3^2(\Delta D) + 3D_3(\Delta D)^2] N_4 + [D_3^3 + 3D_3^2(2\Delta D) + 3D_3(2\Delta D)^2] N_5 \quad (3)$$

The liquid content of the old interval system is expressed in terms of the liquid content of the new with correction terms:

$$L_{0.10} = D_3^3 [N_1 + N_2 + N_3 + N_4 + N_5] \leftarrow \begin{array}{l} \text{Approximation for the} \\ \text{liquid content for the} \\ \text{new transformed system,} \\ \text{LNEW.} \end{array}$$

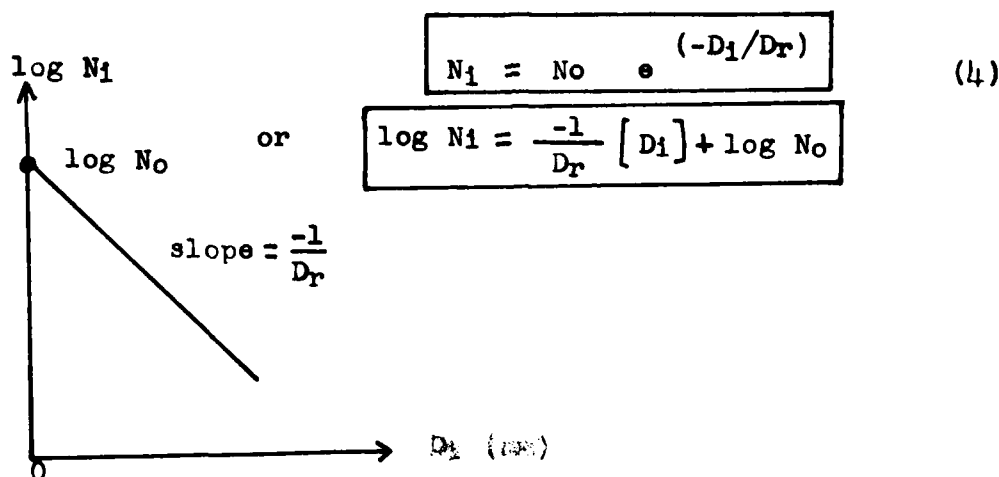
$$\left. \begin{array}{l} + 3 D_3^4 \Delta D [-2N_1 - N_2 + N_4 + 2N_5] \\ + 3 D_3 (\Delta D)^2 [4N_1 + N_2 + N_4 + 4N_5] \end{array} \right\} \begin{array}{l} \text{Correction terms} \\ \text{neglected in this 0.1} \\ \text{to 0.5 mm interval} \\ \text{transformation.} \end{array}$$

This liquid content correction is small and depends on what drop size is being considered (D_3 in this case), and the specific rain distribution. For example, for Marshall Islands A, the correction for the 1 mm drop is plus 8% of the term, LNEW. For the 2 mm drop, it is -2% of LNEW.

Since the number of drops changes dramatically from several hundred or thousand small drops, to a fraction of a drop of the very large size in a cubic meter, several orders of magnitude are suitably plotted on a log scale. Natural rainfields so plotted are NOT a straight line, but have a maximum around 2 mm diameter. For natural rain, such a plot is close to a straight line from about 2.5 to 5 mm drops.

Exponential Approximation Distribution

Artificial spray fields do produce a large number of small drops. For simplicity of presentation, many measured distributions, as for the Holloman data, are reduced by a least squares fit to a straight line. The mathematical form of the equation of the line that shows this distribution is:



N_1 - number of drops in a cubic meter of size D_1 (mm) around a range diameter ΔD (mm).

N_0 - hypothetical number of zero diameter drops = $8000 \Delta D$, which can be a very large number.

D_r - the calculated inverse slope of the line. It is sometimes called a reference diameter.

There is reference to work by Marshall and Palmer who related this diameter to the rain rate:

$$D_r(\text{mm}) = 0.244 R^{0.21} (\text{mm/hr}) \quad (5)$$

The drop size distribution becomes:

$$N_1 = 8000 \Delta D \exp(-4.1 D_1 / R^{0.21}) \quad (6)$$

Liquid Content of Rain

Liquid content (grams per cubic meter) is the average liquid volume of water that would be obtained in a specified volume (usually cubic meter) cut out of a specific rainfield. Liquid content is surprisingly small, even for heavy rains. For a 40 inches/hour fall, the water content is only about 0.004% of the volume of the rainfield.

Definition of liquid content based on the measured distribution:

$$L (\text{g/m}^3) = \frac{\pi \rho}{6} \sum_{i=1}^S N_i D_i^3 = \frac{\pi}{6000} \sum_{i=1}^S N_i D_i^3 \quad (7)$$

with the dimensions: D_1 (mm)
 N_1 (drops/cubic meter)
 ρ = one gram/cc
 S = number of discrete drop diameters

Median Drop Diameter

In summing the liquid content of all the drops, that diameter of a drop at which 50% of the liquid content lies below this diameter is called the median drop diameter. The size is about 2 mm.

Rainfall Rate

A convenient unit to use here is inches/hour, because by a numerical coincidence, the rainfall rate and liquid content (g/m³) are about identical numerically if each is expressed in the units given.

Definition of rain rate:

$$R \text{ (in/hr)} = \frac{\pi}{6} \sum_{i=1}^S v_i N_i D_i^3 = \frac{7.2 \pi}{10^6} \sum_{i=1}^S v_i N_i D_i^3 \quad (8)$$

where the units are: v_i (ft/sec) terminal velocity of drop of diameter D_i
 D_i (mm)
 N_i (/m³)

The important term is the velocity of raindrops. The higher the velocity, the higher the rain rate for the same drop size-number distribution.

Acceleration and Terminal Velocity of Drops

One reported expression for the measured terminal velocity of raindrops is a quartic polynomial, where the velocity V_i is in (m/sec), and the diameter D_i in (mm): (Reference 12)

$$V_1 = C_0 + C_1 D_1 + C_2 D_1^2 + C_3 D_1^3 + C_4 D_1^4 \quad (9)$$

The coefficients are:

$$C_0 = -0.27128$$

$$C_1 = 5.22306$$

$$C_2 = -1.10757$$

$$C_3 = 0.11115$$

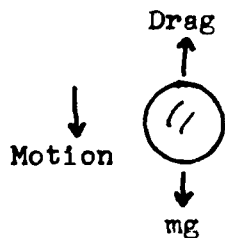
$$C_4 = -0.0046884$$

Table 1 expresses formula 9 with velocity in ft/sec:

Table 1. Raindrop terminal velocity

D(mm)	V(fps)
0.5	6.8
1.0	13.0
1.5	17.8
2.0	21.5
2.5	24.3
3.0	26.4
3.5	28.0
4.0	29.0
4.5	29.5
5.0	30.0
5.5	30.0

It is profitable at this point to go one step further and calculate the velocity of drops as they accelerate from rest. There are two reasons: (1) to find this dynamic fall under gravity from a liquid stream; (2) to find the horizontal induced velocity from a wind gust to estimate the disturbed spacial distribution. The velocity of spherical liquid drops starting from rest under gravity is calculated:



Use the drag force expression:

$$\text{Drag force} = C_D \frac{\rho_{\text{air}} v^2}{2} \frac{\pi D^2}{4} \quad (10)$$

C_D = experimental drag coefficient (which is a function of Reynolds number)

ρ_{air} = air density

$v = \dot{x}$ = instantaneous drop velocity

D = drop diameter

m = mass of drop = $\rho_{\text{water}} \pi D^3 / 6$

Equation of motion of drop for vertical motion:

$$m \ddot{x} = m g - \frac{C_D \rho_{AIR} v^2 \pi D^2}{8}$$

$$\ddot{x} = g - C_D \left[\frac{\rho_{AIR}}{\rho_{WATER}} \right] \frac{3}{4} \frac{v^2}{D} \quad (11)$$

Air-water density ratio for ordinary conditions:

$$0.00238/1.94 = 0.0012268$$

The acceleration equation:

$$\ddot{x} = g - \frac{0.00092 C_D \dot{x}^2}{D} \quad (12)$$

The drag coefficient C_D is a function of Reynolds number Re :

$$Re \equiv \frac{\dot{x} D \rho_{AIR}}{\mu_{OYN}} = \frac{\dot{x} D}{\nu_{KIN}} = \frac{\dot{x} D [ft^2/sec]}{0.00016 [ft^2/sec]} \quad (13)$$

where the Reynolds number itself is a function of:

\dot{x} - instantaneous velocity of the drop
 D - drop diameter
 ρ_{AIR} - air density
 μ_{OYN} - dynamic viscosity of air

The kinematic viscosity of air ($\nu_{KIN} \equiv \mu_{OYN} / \rho_{AIR}$) at ordinary temperature is about 0.00016 ft²/sec. Experimental data for spheres in air is from Fluid Mechanics by Binder, p. 180. The drag coefficient is determined from the current Reynolds

number:	Re	C_D	Re	C_D	} Range of interest
	1	30	200	0.8	
	2	18	500	0.58	
	5	7	1000	0.49	
	10	4.5	2000	0.42	
	20	3.0	4000	0.40	
	50	1.7			
	100	1.1			

These equations were solved for drops from 1 to 6 mm diameter to find their time-fall-velocity relation. Figure 2 plots the velocity as a function of fall distance. Circles represent 0.5 second increments of flight time. Also plotted

is a dotted line for the free fall of any object with no air drag. The calculated terminal velocity of the 5 and 6 mm drops exceed the experimental value of 30 fps. This may be due to treating these drops as spherical, when in nature they are not.

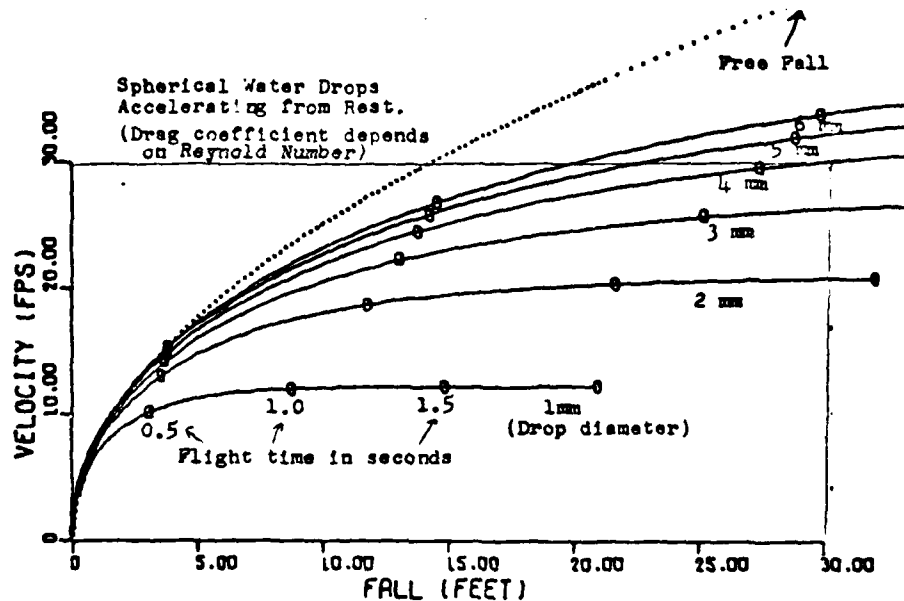


Figure 2. Spherical drops accelerating from rest.

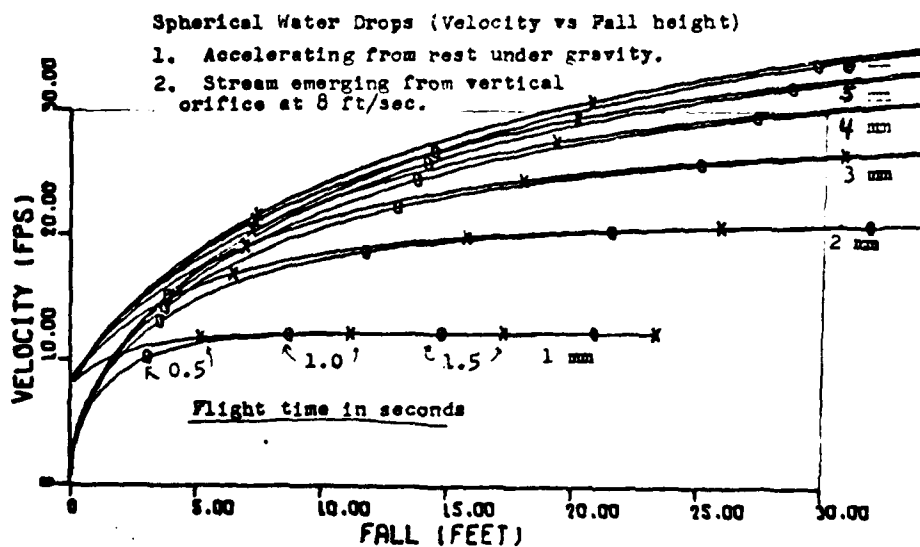


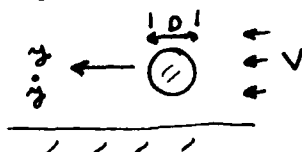
Figure 3. Spherical drops at 0 and 8 fps initial velocity.

Figure 3 shows superimposed on the results of figure 2 the specific case when drops have been formed from a stream which has already reached an initial velocity of 8 fps. After only 5 feet of fall, drops with no initial velocity are approaching the velocities of these drops.

These plots were made in consideration of an overhead-channel-orifice (OCO) system where the channel has about 6 inches of water, with an exit velocity of $\sqrt{2gh} = 5.7$ fps. In experimentally quiet conditions, about one foot of fall of the stream is needed before full drop formation emerges. The initial velocity is set at about 8 ft/sec, and this system is discussed in a later section.

Wind Effect on Spacial Distribution

To obtain an analytical estimate of the motion of various drops for a horizontal wind, an expression similar to equation 12 can be used. Consider drops with no initial horizontal velocity. A constant wind velocity, V , is applied. The absolute speed of the drops relative to the ground is \dot{y} . The velocity that appears in the acceleration and drag expressions is the relative velocity $(V - \dot{y})$:



$$\ddot{y} = 0.00092 C_D (V - \dot{y})^2 / D \quad (14)$$

$$Re = (V - \dot{y})D / \nu$$

The consequent horizontal velocity versus horizontal displacement is obtained for two cross winds of 1.55 and 4.11 meters/sec, for drops from 1 to 6 mm.

Figures 4 and 5 show these trajectories. The total length of the trajectories is equivalent to the time these drops should fall about 4 feet vertically in air under gravity, as expressed in equation 12. Though the use of drag coefficients for spherical objects is not valid, some qualitative idea is obtained of the sweeping away of the drops.

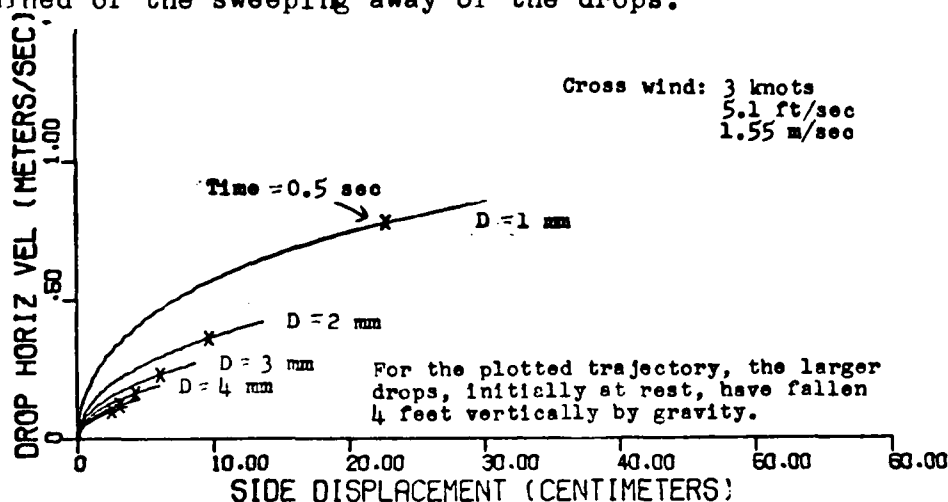


Figure 4. Trajectory of stationary drops (1 to 6 mm diameter) suddenly exposed to cross wind of 3 knots.

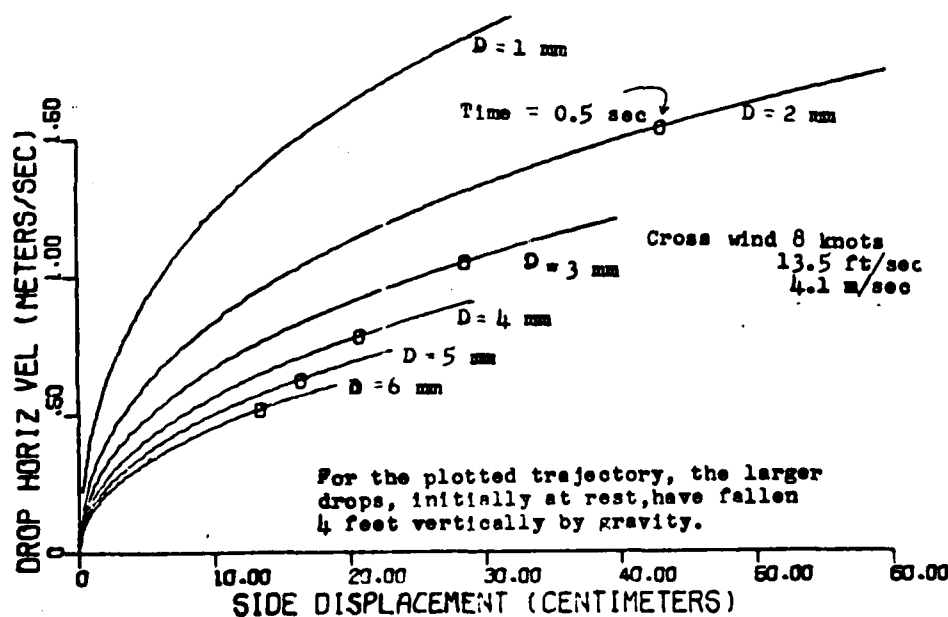
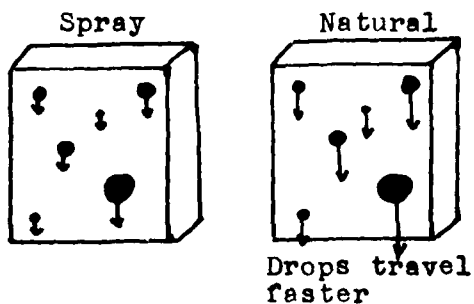


Figure 5. Trajectory of stationary drops (1 to 6 mm diameter) suddenly exposed to cross wind of 8 knots.

Equivalent Rain Rate

By table 1, it takes an appreciable fall for larger drops to attain terminal velocity. A worse condition occurs in a spray rainfield if the nozzles are pointed upward. Their vertical component of velocity becomes zero at the top of the trajectory. The Holloman ROCKET track nozzles spray downward, whereas the ARTILLERY range nozzles spray upward.

If a specific volume is cut out of a natural rainfield, and the drops allowed to accumulate at the bottom of this volume, we obtain a rain gage type measurement of liquid content. If by chance we cut out the same volume from a spray rainfield and find that the liquid content is the same (assume drop size distribution about the same), the rain rate will NOT be the same.



In natural rain, the drops are travelling at a higher velocity than in a spray rainfield. The rain rate for the spray rainfield is not that obtained with a rain gage. To find its equivalent in

nature, the drop size distribution of the spray rainfield is needed, and the terminal velocity applied to the various drops. This was done in finding the rain rate of such rainfields with experimental terminal velocities in equation 9.

PUBLISHED NATURAL AND SPRAY RAINFIELDS

Introduction

Table 2 lists the 25 rainfields investigated. Most of them are from reference 1. Due to the difficulty in comparing one field with another because of different drop diameter range (ΔD) used, all the distributions were reduced to the same 0.5 mm interval.

Table 2. Natural and Spray Rainfields

1	CANAL ZONE A
2	CANAL ZONE B
3	CANAL ZONE C
4	CANAL ZONE D
5	CANAL ZONE E
6	STANDARD RAINFALL U.S.
7	TROPICAL RAIN
8	MARSHALL ISLANDS A
9	MARSHALL ISLANDS B
10	MARSHALL ISLANDS C
11	NORTH CAROLINA A
12	NORTH CAROLINA B
13	NORTH CAROLINA C
14	MIAMI CONTINUOUS RAIN
15	MIAMI THUNDERSHOWER A
16	MIAMI THUNDERSHOWER B
17	HOLLOMAN ROCK 10-26-3
18	HOLLOMAN ROCK 10-26-5
19	HOLLOMAN ROCK 10-26-5SD
20	HOLLOMAN ROCK 10-26-6
21	HOLLOMAN ROCK R070
22	HOLLOMAN ARTL 80200
23	MILSTD-2108, MAX. ALT=0KM
24	MILSTD-2108, 0.1% MAX
25	MILSTD-2108, 0.5% MAX

Distributions 1-5 are the heavier rates from a published series for the Canal Zone.

Distribution 6 is a formulated (theoretical) rainfall for the U.S.

Distributions 15-16 are extremely high rates recorded in Miami.

Distributions 17, 18 and 20 are Holloman spray rainfields in the rocket test facility, measured along the repeating horizontal locations from 10 to 26, and at the water pressures of 3.5, 5, and 6.5 psi. The designation HOLLOMAN ROCK 10-26-6 refers to the average distribution from locations 10 to 26 at a water pressure 6.5 psi.

Distribution 19 (HOLLOMAN ROCK 10-26-5SD) represents, not a real distribution, but the standard deviation of measurements made at the discrete physical locations from 10 to 26. It shows the appreciable SPACIAL variability along the repeating 8 foot sections of the rocket track.

Distribution 21 (HOLLOMAN ROCK 8070) are measurements around 1970 at the rocket facility, but with a different nozzle (8070) which produced a higher rain rate of about 6 in/hr. (Reference 2)

Distribution 22 (HOLLOMAN ARTL 80200) are measurements at the Holloman artillery (ballistic) site around 1969 with the deluge nozzle 80200 with rates from 40 to 60 in/hr, depending where along the rainfield measurements were made.

Distributions 23-25 are from MIL STD 210B, and will be discussed in another section. It was difficult to fit these in as they are reported in gross 1.0 mm intervals. To achieve 0.5 mm increments, the number of drops at the center diameters, 1,2,3... was considered one half the number reported. The number of drops at the half intervals, 1.5, 2.5... are calculated by taking one fourth of the drops on each side of the associated integer. The calculation of rain rate and liquid content in Table 4 is done with these 0.5 mm increment transformed distributions, and with equations 7 and 8.

List of 25 Fields, Distributions, and Parameters

Table 3 lists the average number of drops per cubic meter of the 25 rainfields considered, at each diameter from 0.5 to 6 mm, within a range of 0.5 mm.

For example, the number 65 on line 7 (Tropical Rain) under 3.0 mm diameter, means that on the average, 65 drops should be expected in a cubic meter for this rainfield, for drop sizes from 2.75 to 3.25 mm diameter.

Note the spaces for Holloman listings 17-20. The data

Table 3. Drop size distributions for natural and spray rainfields

DROP DIAMETER MM		.5	1.0	1.5	2.0	2.5	3.0	3.5	4.0	4.5	5.0	5.5	6.0
AVERAGE NUMBR OF DROPS/ CUBIC METER AT EACH DIAMETER D WITHIN A RANGE ΔD=0.5MM													
1	CANAL ZONE A	5.	58.	115.	70.	20.	5.60	1.25	.43	.06	0.00	0.00	.01
2	CANAL ZONE R	8.	82.	140.	96.	35.	11.70	3.20	1.03	.20	.06	.02	0.00
3	CANAL ZONE C	18.	138.	165.	130.	55.	21.00	8.10	2.80	.68	.29	.08	.03
4	CANAL ZONE D	44.	275.	230.	181.	98.	38.00	13.00	3.60	1.00	.42	.20	.02
5	CANAL ZONE E	88.	535.	374.	250.	134.	55.00	20.00	6.10	1.44	.32	.21	.07
6	STANDARD RAINFALL U.S.	1480.	372.	183.	93.	49.	19.70	8.20	3.00	1.08	.40	.19	.06
7	TROPICAL RAIN	110.	450.	360.	250.	135.	65.00	25.00	10.00	3.00	1.25	.50	.25
8	MARSHALL ISLANDS A	146.	466.	395.	190.	38.	7.70	1.52	.21	.12	.03	0.00	0.00
9	MARSHALL ISLANDS B	510.	785.	475.	318.	120.	29.00	4.80	.73	.21	.21	.21	0.00
10	MARSHALL ISLANDS C	200.	688.	635.	422.	218.	75.00	19.00	7.20	1.46	.82	.30	0.00
11	NORTH CAROLINA A	15.	350.	350.	150.	50.	15.00	4.50	1.10	.35	.15	0.00	0.00
12	NORTH CAROLINA B	200.	1200.	600.	300.	100.	35.00	13.00	5.00	2.00	.60	.20	0.00
13	NORTH CAROLINA C	250.	2250.	1200.	500.	170.	50.00	17.00	7.00	2.50	.90	.35	.02
14	MIAMI CONTINUOUS RAIN	20.	1110.	3300.	2000.	780.	320.00	65.00	16.00	3.00	0.00	0.00	0.00
15	MIAMI THUNDERSHOWER A	1340.	7950.	9990.	7500.	2880.	680.00	210.00	60.00	30.00	11.00	4.00	0.00
16	MIAMI THUNDERSHOWER B	1050.	6600.	8350.	6270.	2670.	1140.00	440.00	270.00	75.00	36.00	13.00	0.00
17	HOLLOMAN ROCK 10-26-3	2200.	900.	260.	100.	46.	20.00	10.00	3.60				
18	HOLLOMAN ROCK 10-26-5	2850.	1024.	320.	120.	48.	18.00	7.00	2.40				
19	HOLLOMAN ROCK 10-26-5SD	980.	400.	145.	60.	24.	10.00	5.00	2.00				
20	HOLLOMAN ROCK 10-26-6	3500.	1050.	370.	140.	45.	14.00	4.80	1.50				
21	HOLLOMAN ROCK 8070.	3000.	1750.	1250.	520.	140.	40.00	7.00	1.75	.50			
22	HOLLOMAN ARTL 80200	9999.	4250.	1750.	1000.	700.	450.00	260.00	150.00	85.00	40.00	15.00	7.00
23	MILSTD-2108, MAX, ALT=0KM	39500.	79000.	43000.	7500.	5160.	2820.00	1676.00	532.00	316.00	100.00	60.00	19.00
24	MILSTD-2108, 0.1% MAX	2900.	5880.	3326.	852.	488.	123.00	71.00	18.00	10.30	2.50	1.55	0.00
25	MILSTD-2108, 0.5% MAX	656.	1313.	750.	171.	96.	22.50	12.80	3.00	1.75	.50	.30	.10

was taken from a 1975 report. The instrumentation could not read drop diameters above about 4 mm. Such larger drops are expected, and Holloman intended to update the instrumentation.

Table 4 lists typical rainfield parameters calculated from the drop distribution in a computer program. The total number of drops, N, in the last column is not too meaningful because of the large number of very small drops, which have little water content and little net momentum transfer.

Table 4. Calculated Rainfield Parameters

NATURAL AND SPRAY RAINFIELDS		RATE (MM/HR)	RATE (IN/HR)	L10 (G/M3)	MEDIAN (MM)	N DROPS (/M3)
1	CANAL ZONE A	19.	.8	.8	1.8	275.
2	CANAL ZONE B	31.	1.2	1.3	1.9	377.
3	CANAL ZONE C	51.	2.0	2.0	2.1	539.
4	CANAL ZONE D	81.	3.2	3.2	2.2	884.
5	CANAL ZONE E	117.	4.6	4.6	2.1	1464.
6	STANDARD RAINFALL U.S.	50.	2.0	2.1	2.0	2210.
7	TROPICAL RAIN	134.	5.3	5.1	2.3	1410.
8	MARSHALL ISLANDS A	49.	1.9	2.2	1.6	1245.
9	MARSHALL ISLANDS B	97.	3.8	4.2	1.8	2243.
10	MARSHALL ISLANDS C	174.	6.9	7.0	2.0	2467.
11	NORTH CAROLINA A	52.	2.0	2.2	1.7	936.
12	NORTH CAROLINA B	115.	4.5	4.9	1.8	2456.
13	NORTH CAROLINA C	191.	7.5	8.3	1.7	4448.
14	MIAMI CONTINUOUS RAIN	688.	27.1	27.8	1.9	7614.
15	MIAMI THUNDERSHOWER A	2344.	92.3	95.7	1.9	30664.
16	MIAMI THUNDERSHOWER B	2829.	111.4	108.5	2.2	26914.
17	HOLLOMAN ROCK 10-26-3	56.	2.2	2.5	1.7	3540.
18	HOLLOMAN ROCK 10-26-5	57.	2.3	2.7	1.5	4389.
19	HOLLOMAN ROCK 10-26-5SD	29.	1.2	1.3	1.7	1626.
20	HOLLOMAN ROCK 10-26-6	57.	2.2	2.7	1.5	5125.
21	HOLLOMAN ROCK 8070	163.	6.4	7.5	1.6	6709.
22	HOLLOMAN ARTL 80200	1158.	45.6	41.9	2.9	18706.
23	MILSTD-2108, MAX, ALT=0KM	7780.	306.3	317.9	2.1	179683.
24	MILSTD-2108, 0.1% MAX	495.	19.5	21.4	1.7	13672.
25	MILSTD-2108, 0.5% MAX	100.	3.9	4.4	1.6	3027.

Plots of 22 Fields, and Comparisons

Figures 6 to 10 plot the distributions listed in table 2 on the usual log-linear scale. A brief summary of features:

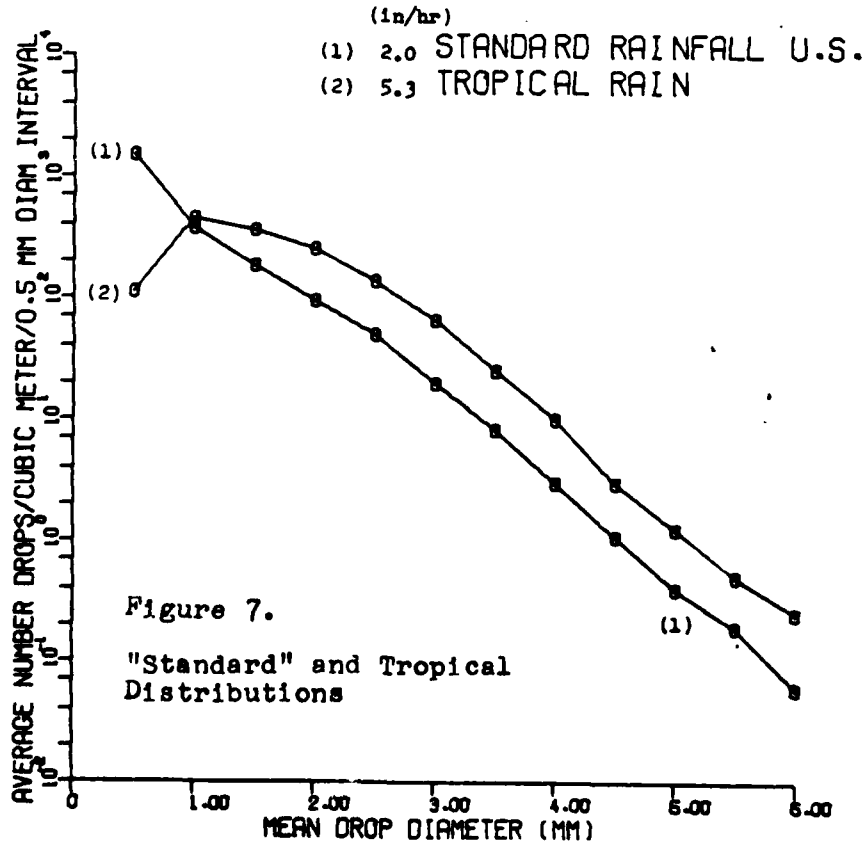
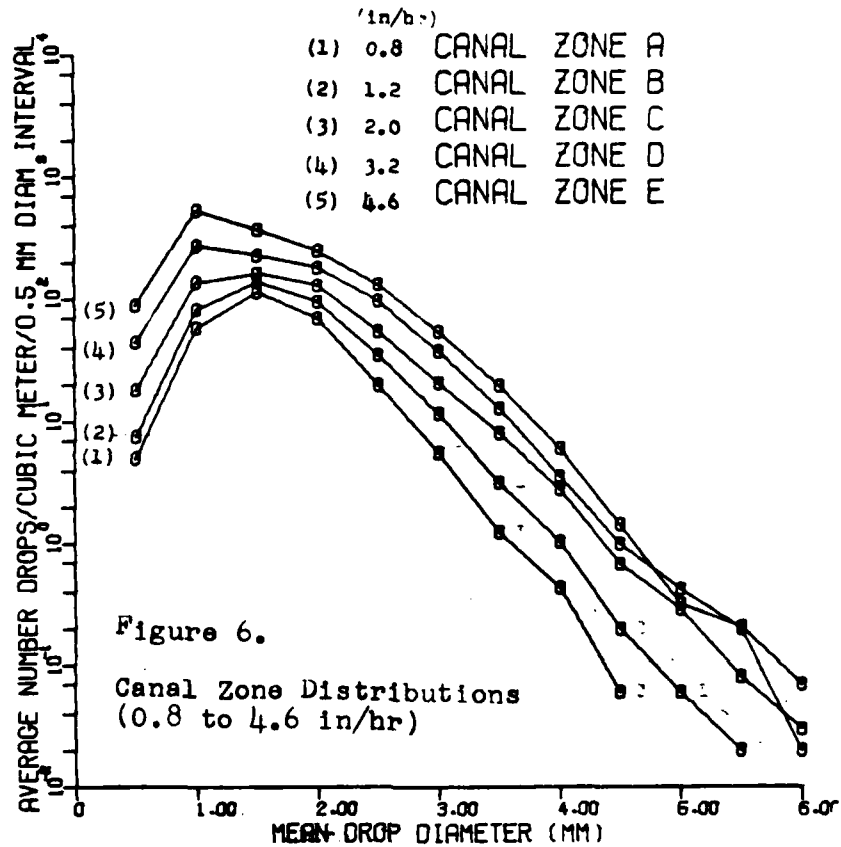
- Figure 6. General trend for natural fields: As rain rate goes up, the curve shifts up rather uniformly.
- Figure 7. The "standard" rainfield looks like a spray rainfield with the large number of 0.5mm drops. The tropical rain here is a heavy fall.
- Figure 8. These plots of Marshall Islands and North Carolina distributions show typical upward displacement of the curve as the rain rate goes up.
- Figure 9. The two Miami thundershowers are extreme rainfalls. Note the appreciable difference for the larger drop sizes.
- Figure 10. Holloman spray fields:

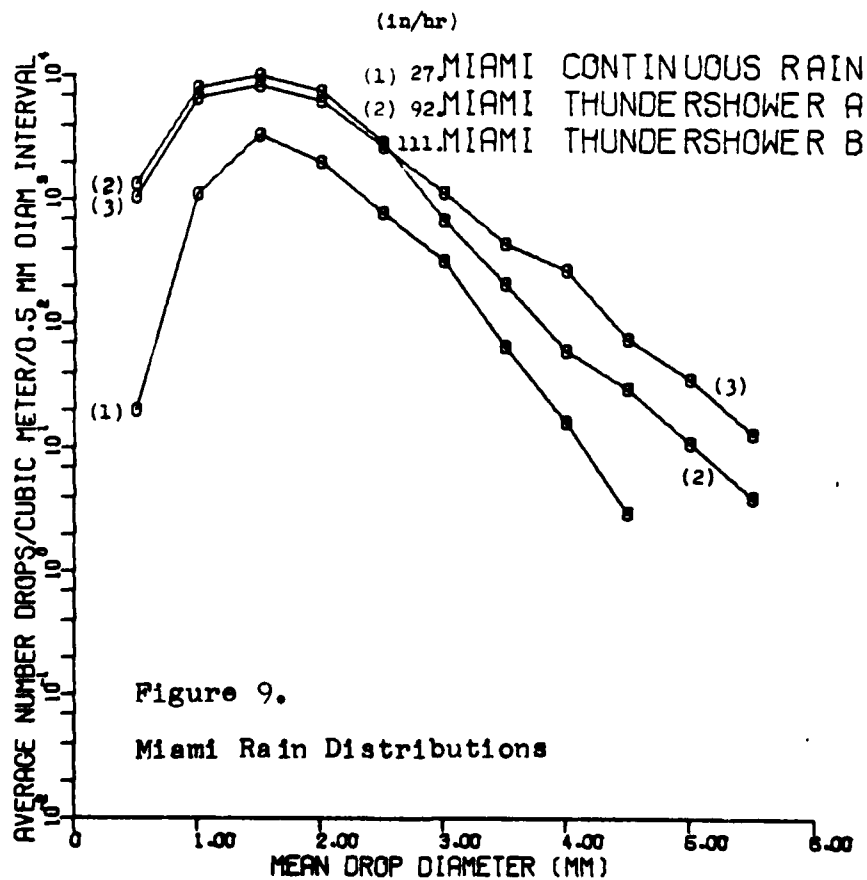
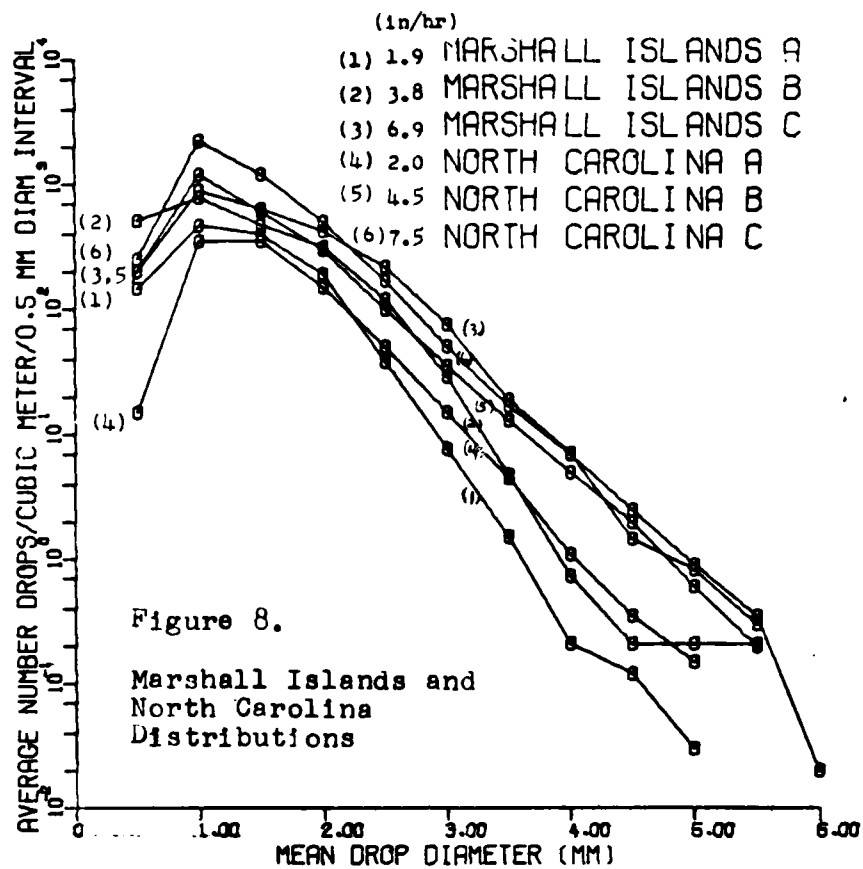
The three distributions for the 10-26 distance designation are about the same in rain rate. As the water pressure increased, the number of SMALLER drops increased, as the number of LARGER drops decreased.

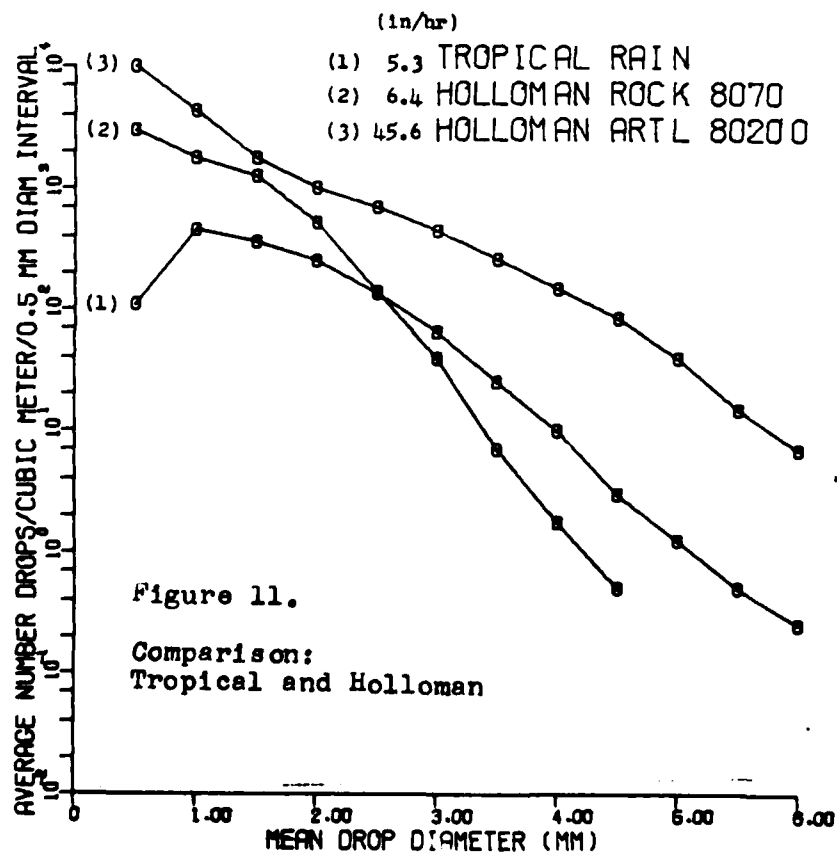
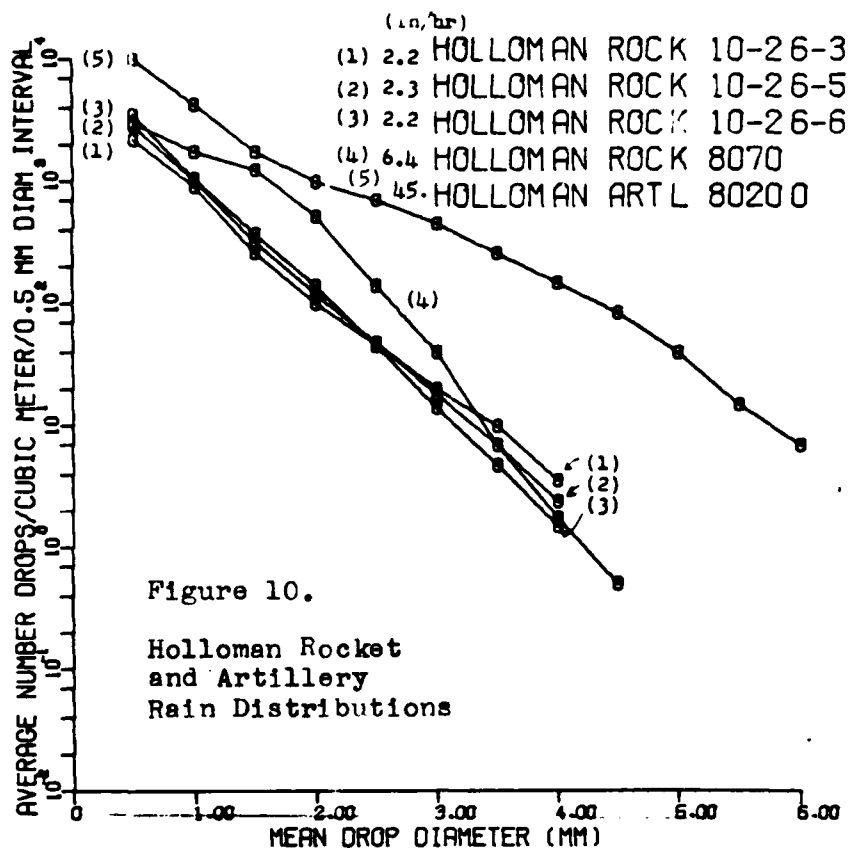
The rocket range 8070 nozzle, and artillery deluge 80200 nozzle results are plotted.

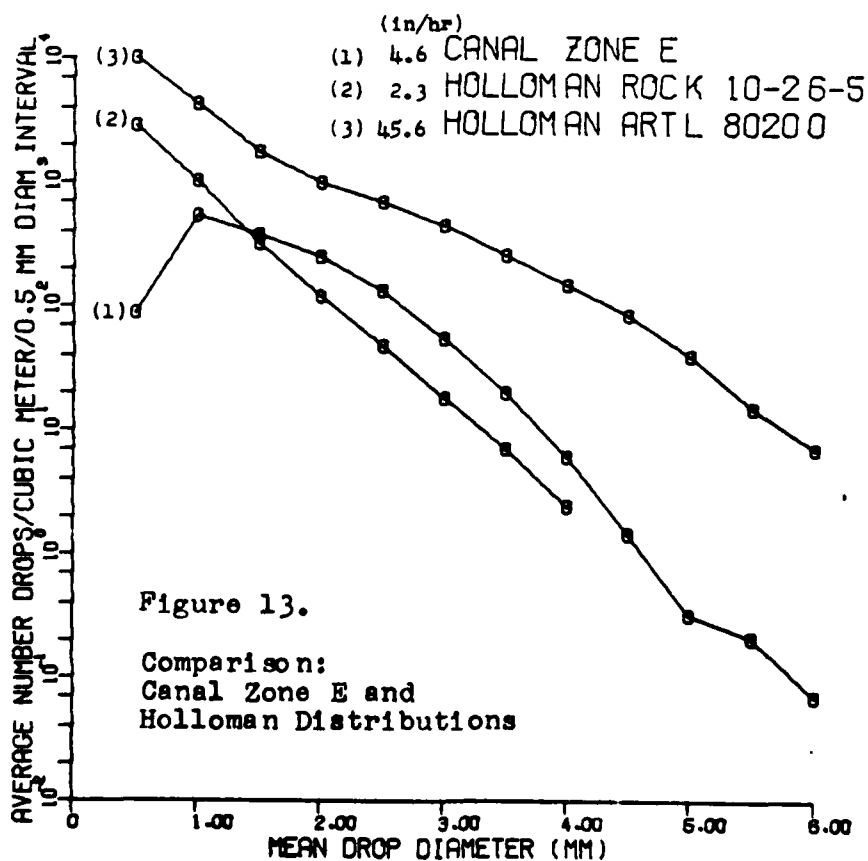
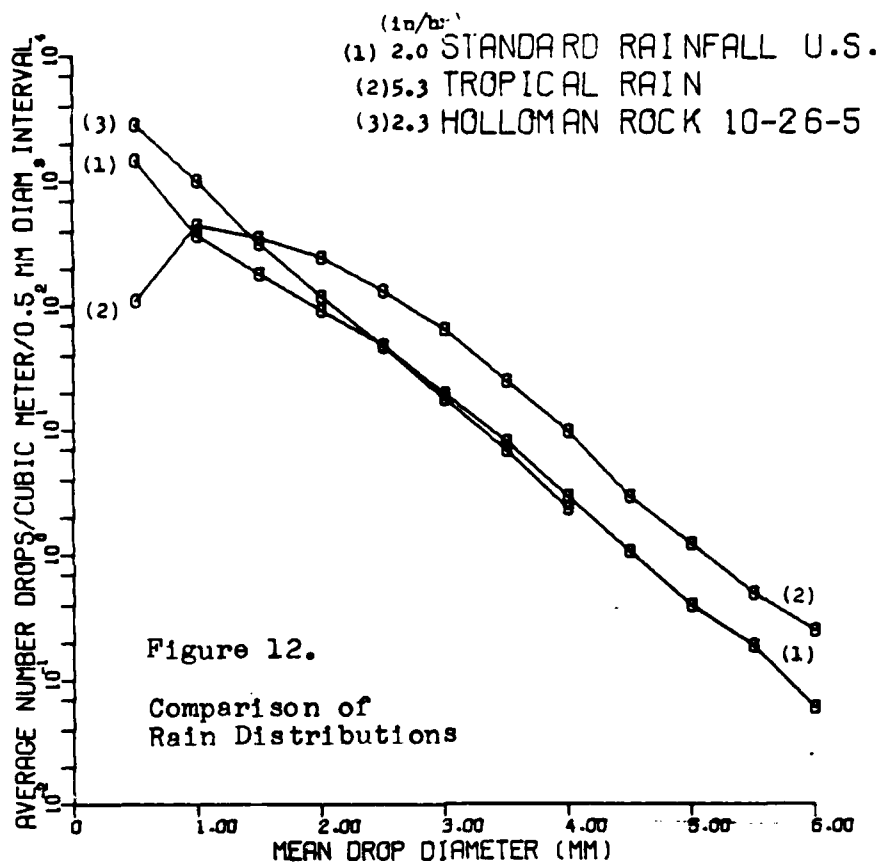
Comparison plots:

- Figure 11. Heavy natural rain (TROPICAL) is quite different from the 1970 reported Holloman rocket and ballistic ranges (8070 and 80200 nozzles).
- Figure 12. TROPICAL distribution is again plotted. The "standard" field, and optimum configuration of Holloman 10-26-5 track rather well with the TROPICAL. (Again, no data on large size drops from Holloman).
- Figure 13. The Holloman deluge 80200 nozzle is optimum for creating large size drops.









Rain Distributions in Radar Handbook

In the Radar Handbook by Skolnik (reference 4), eight drop distributions for precipitation rates from 0.25 to 150 mm/hr are given in 0.5 mm diameter increments as a function of percent of water volume from each of these drop increments. The book cites the work of Laws and Parsons reported in 1943.

To see how the distributions differ, compare the 100 mm/hr (3.94 in/hr) rate in the radar handbook with Canal Zone E field of 4.6 in/hr. The number of drops per cubic meter in the handbook is obtained by using the rain rate equations:

$$R = 3.94 \text{ in/hr} = 7.2 \pi \sum_i v_i N_i P_i D_i^3 / 10^6$$

$$N = 165$$

$$N_i = N P_i$$

The calculated liquid content L is close to the rain rate in inches per hour:

$$L = \pi \sum_i N_i D_i^3 / 6000 = 3.22 \text{ g/m}^3$$

Table 5 shows the comparison when the percentage of liquid content of Canal Zone E is calculated.

Table 5. Comparison of Radar Handbook with Canal Zone E Rain Distribution

Size (mm)	Radar Handbook (3.94 in/hr)		Canal Zone E (4.6 in/hr)	
	Percent volume P_i	Drops/m ³ N_i	Percent volume P_i	Drops/m ³ N_i
0.5	1.0	1.7	6.	88
1.0	4.6	7.6	36.	535
1.5	8.8	14.7	25.	574
2.0	14.	23	17.	250
2.5	17.1	28	9.	134
3.0	18.4	30.5	3.7	55
3.5	15.	25	1.4	20
4.0	9.	15	0.42	6.1
4.5	5.8	9.6	0.1	1.44
5.0	3.0	5.	0.02	0.32
5.5	1.7	2.8	0.01	0.21
6.0	1.0	1.7	-	0.07
6.5	0.7	1.1	-	-

Though the rain rates are similar, the distributions are quite different. The radar handbook distributions are shifted toward larger size drops.

Rainfields Reported in MIL STD 210B

MIL STD 210B (Climatic Extremes for Military Equipment, 15 December 1973) lists environments on a world wide basis (references 5,6). Rain distributions are listed in 1 mm diameter intervals from an analytical expression synthesized from the work of previous authors. Only three distributions are given in table 6 for sea level. These respective distributions are listed in the references as increasing by about 30% at an altitude of 4 kilometers, and returning to about the same sea level value at around 8 kilometers (4.6 miles). The distributions decay to about half the 8 kilometer value rain intensity around a 12 kilometer altitude.

Table 6. Sea level and 8 kilometer distributions for Maximum, 0.1% and 0.5% probability levels. (MIL STD 210B)

Rain type	Rate		Prec. mass (g/m ³)	N _i = Drops/meter ³ for drop diameter range given:					
	(mm/hr)	(in/hr)		0.5 1.4	1.5 2.4	2.5 3.4	3.5 4.4	4.5 5.4	5.5 6.4
MAX ^a	1860.	73.	77.	159,000	30,000	5,640	1064	201	38
0.1% ^b	188.	7.4	8.3	11,800	1,700	247	36	5	1
0.5% ^c	48.	1.9	2.2	2,626	342	45	6	1	1

^a Maximum rate ever recorded for one minute.

^b Rain rate should not exceed this 0.1% of time in wettest part of the world, in wettest month.

^c Rain rate should not exceed this 0.5% of time in wettest part of the world, in wettest month.

A correlation was found between the rain rate R and the liquid content L, and expressed as:

$$L \text{ (g/m}^3\text{)} = 0.052 R^{0.97} \text{ (mm/hr)} \quad (15)$$

For a given rain rate, the pred pitation mass (liquid content) is calculated from equation 15. This is the precipitation mass in table 6. To go one step further, and express the drop size distribution, first a median drop of diameter D_0 was calculated analytically, again from the rain rate:

$$D_0 \text{ (mm)} = 1.48 R^{0.05} \text{ (mm/hr)} \quad (16)$$

All the data was then fit to a log-exponential function to generate the original drop distribution, N_1 , for a drop diameter interval of 1 mm:

$$N_1 = 389 R^{1.02} \text{ (mm/hr)} e^{-3.67 D_1/D_0} \quad (17)$$

where $D_1 = 1, 2, 3, 4, 5, 6$ mm. N_1 are numbers reported in MIL STD 210B.

With this understanding, the numbers for drop distributions in MIL STD 210B are obtained roundabout, through analytical fit of original data. Care has to be used in using these numbers directly because of the coarseness of the drop diameter interval ΔD , and it is not expected that one analytical expression should fit the extreme maximum fall.

Table 7 shows the liquid content for the three fields calculated with equation 15, which is a valid empirical expression, and with the general liquid content expression, equation 5, directly from a distribution.

Table 7. Liquid content (g/m³) for MIL STD 210B
Distributions by three approaches

	$L = 0.052 R^{0.97}$	$L = \frac{\pi}{6000} \sum N_i D_i^3$ Use lower limit $D_i = 0.5, 1.5, \dots$	Use mid point $D_i = 1, 2, \dots$
MAX	77.	146.	340.
0.1%	8.3	7.0	18.5
0.5%	2.2	1.4	3.8

Even the use of the lower limit of the drop sizes results in a rain rate twice what it should be for the MAXIMUM fall. The actual liquid content for the 0.1 and 0.5% fields are bracketed by the two choices of D_i . A finer reporting of the distributions is needed to work with them directly.

There is little loss in accuracy in liquid content and rain rate in going to a coarser diameter interval ΔD . If the first 22 distributions in this report, already listed for $\Delta D = 0.5$ mm, are further reduced to $\Delta D = 1$ mm by taking the number of drops at the integer diameter, and adding to it one half the number at both sides of the integer, the resulting distributions are listed in table 8. The distributions are distorted at the smaller drop size, but this is not significant as drops around one millimeter have little water content.

If the same computer program is used to reduce these distributions to obtain rain rate and liquid content, the result is table 9. The overall effect is to artificially enhance the rate by about 9%. In the program, the median diameter $D_i = 1, 2, \dots$ is used as the diameter in the liquid content and rate expressions of equations 7 and 8.

Table 8. Distributions reduced to 1 mm diameter intervals for comparison with MIL STD 210B

		DROP DIAMETER MM 1.0	2.0	3.0	4.0	5.0	6.0
1	CANAL ZONE A	118.	138.	16.	1.1	.0	.01
2	CANAL ZONE B	156.	184.	31.	2.7	.2	.01
3	CANAL ZONE C	230.	240.	53.	7.2	.7	.07
4	CANAL ZONE D	412.	345.	94.	10.6	1.0	.12
5	CANAL ZONE E	766.	504.	132.	16.8	1.1	.18
6	STANDARD RAINFALL U.S.	1204.	209.	48.	7.6	1.0	.16
7	TROPICAL RAIN	685.	498.	145.	24.0	3.0	.50
8	MARSHALL ISLANDS A	737.	407.	27.	1.0	.1	0.00
9	MARSHALL ISLANDS B	1278.	616.	91.	3.2	.4	.11
10	MARSHALL ISLANDS C	1306.	849.	194.	17.4	1.7	.15
11	NORTH CAROLINA A	533.	350.	42.	3.5	.3	0.00
12	NORTH CAROLINA B	1600.	650.	92.	12.5	1.7	.10
13	NORTH CAROLINA C	2975.	1185.	144.	16.8	2.3	.20
14	MIAMI CONTINUOUS RAIN	2770.	4040.	743.	50.0	1.5	0.00
15	MIAMI THUNDERSHOWER A	13620.	13940.	2225.	180.0	28.0	2.00
16	MIAMI THUNDERSHOWER B	11300.	11780.	2695.	527.5	80.0	6.50
17	HOLLOMAN ROCK 10-26-3	2130.	253.	48.	8.6	0.0	0.00
18	HOLLOMAN ROCK 10-26-5	2609.	304.	46.	5.9	0.0	0.00
19	HOLLOMAN ROCK 10-26-5SD	963.	145.	25.	4.5	0.0	0.00
20	HOLLOMAN ROCK 10-26-6	2985.	348.	39.	3.9	0.0	0.00
21	HOLLOMAN ROCK 8070	3875.	1215.	114.	5.5	.3	0.00
22	HOLLOMAN ARTL 80200	10125.	2225.	930.	322.5	90.0	14.50

If the rate is calculated for MIL STD 210B distributions by also taking the integer diameter $D_1 = 1, 2, \dots$ the rain rate is highly enhanced:

	Rate (in/hr) ^a	Rate (in/hr) ^b
Maximum	320.	73.
0.1%	16.	7.4
0.5%	3.2	1.9

(^a Integer diameter in eq. 8. ^b Reported rate.)

The three MIL STD 210B distributions are plotted in figure 14 for comparison with 1) tropical rain, 2) Holloman ballistic, and 3) Holloman rocket mean field.

Table 9. Calculated rain quantities for distributions reduced to 1 mm diameter intervals.

NATURAL AND SPRAY RAINFIELDS		RATE (MM/HR)	RATE (IN/HR)	LIO (G/M3)	N DROPS (/M3)
1	CANAL ZONE A	22.	.9	.9	273.
2	CANAL ZONE B	35.	1.4	1.4	373.
3	CANAL ZONE C	56.	2.2	2.2	530.
4	CANAL ZONE D	89.	3.5	3.4	862.
5	CANAL ZONE E	131.	5.1	5.0	1420.
6	STANDARD RAINFALL U.S.	60.	2.4	2.5	1470.
7	TROPICAL RAIN	148.	5.8	5.5	1355.
8	MARSHALL ISLANDS A	58.	2.3	2.5	1172.
9	MARSHALL ISLANDS B	113.	4.4	4.7	1988.
10	MARSHALL ISLANDS C	196.	7.7	7.7	2367.
11	NORTH CAROLINA A	60.	2.4	2.5	929.
12	NORTH CAROLINA B	131.	5.2	5.4	2356.
13	NORTH CAROLINA C	222.	8.7	9.3	4323.
14	MIAMI CONTINUOUS RAIN	781.	30.7	30.6	7604.
15	MIAMI THUNDERSHOWER A	2651.	104.4	105.1	29994.
16	MIAMI THUNDERSHOWER B	3110.	122.5	117.0	26389.
17	HOLLOMAN ROCK 10-26-3	70.	2.7	3.1	2440.
18	HOLLOMAN ROCK 10-26-5	74.	2.9	3.5	2964.
19	HOLLOMAN ROCK 10-26-SSD	36.	1.4	1.6	1136.
20	HOLLOMAN ROCK 10-26-6	77.	3.0	3.7	3375.
21	HOLLOMAN ROCK 8070	202.	7.9	8.9	5209.
22	HOLLOMAN ARTL 80200	1267.	49.9	46.1	13707.

The object of this exercise is to show that although distributions are readily plotted for comparison, the calculation of rain rate and liquid content for good accuracy need a ΔD of 0.5 mm or smaller.

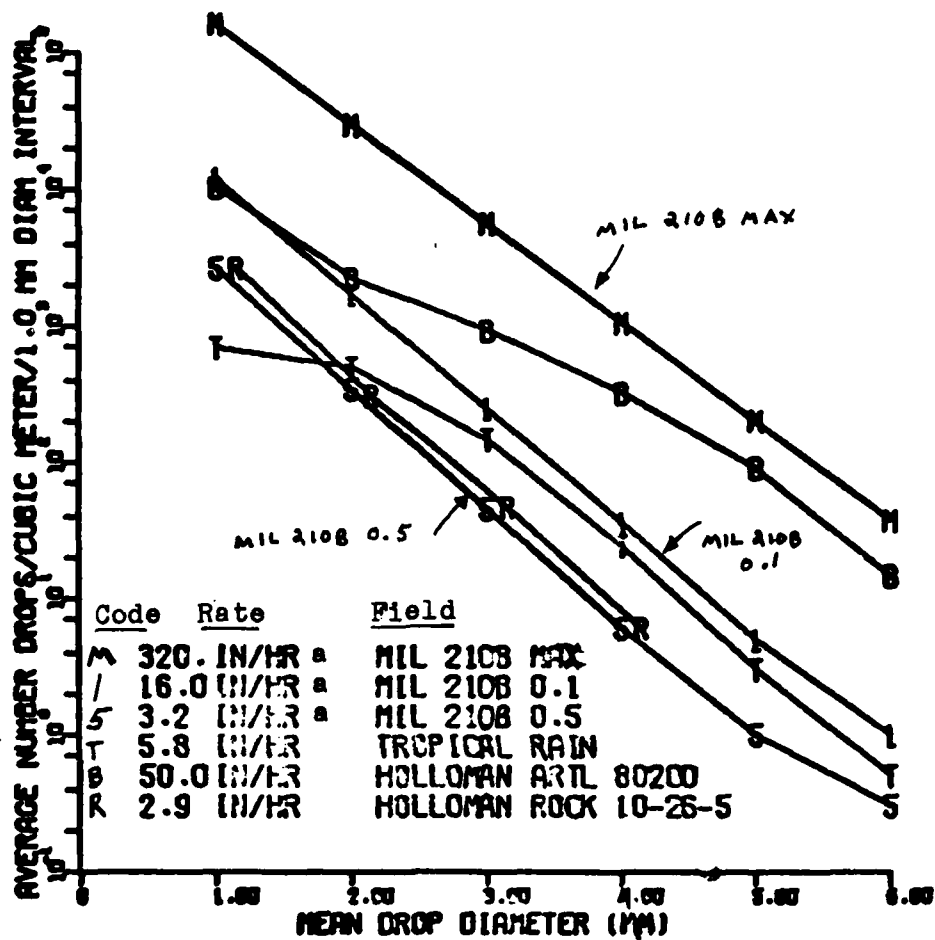


Figure 14. Comparison of MIL STD 210B distributions with three others.

^a MIL STD rain rates are artificially enhanced if the integer diameter is used in the rain rate equation 8. The three comparison distributions' rate is little affected by the same mathematics.

Cumulative Water Content of 22 Rainfields

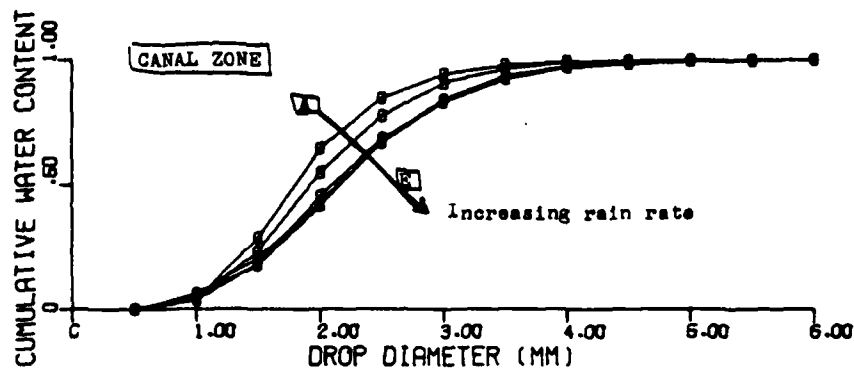


Figure 15. Cumulative water content for Canal Zone distributions.

For these natural rains, as the rain rate increases, the water content curve moves downward. Although the drop distribution curves move rather uniformly upward, the addition of larger drops, though small in number, contribute appreciably to delaying the curve rise.

Note the insignificant water content for smallest drop sizes.

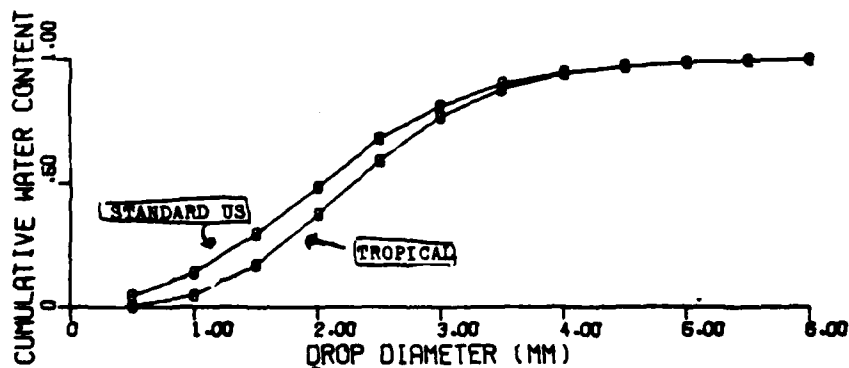


Figure 16. Cumulative water content for "Standard" and tropical distributions.

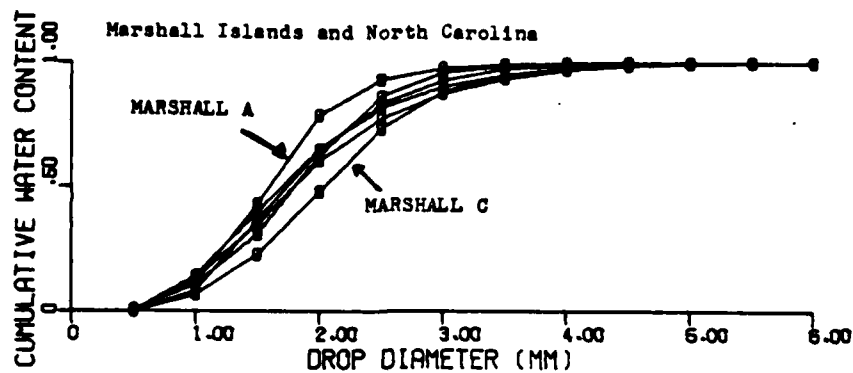


Figure 17. Marshall Islands and North Carolina again show the shift downward in water content as natural rain rate increases.

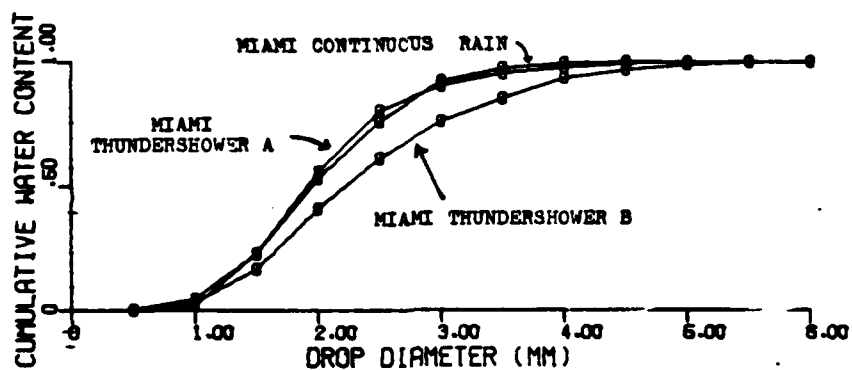


Figure 18. Cumulative water content for Miami thundershowers.

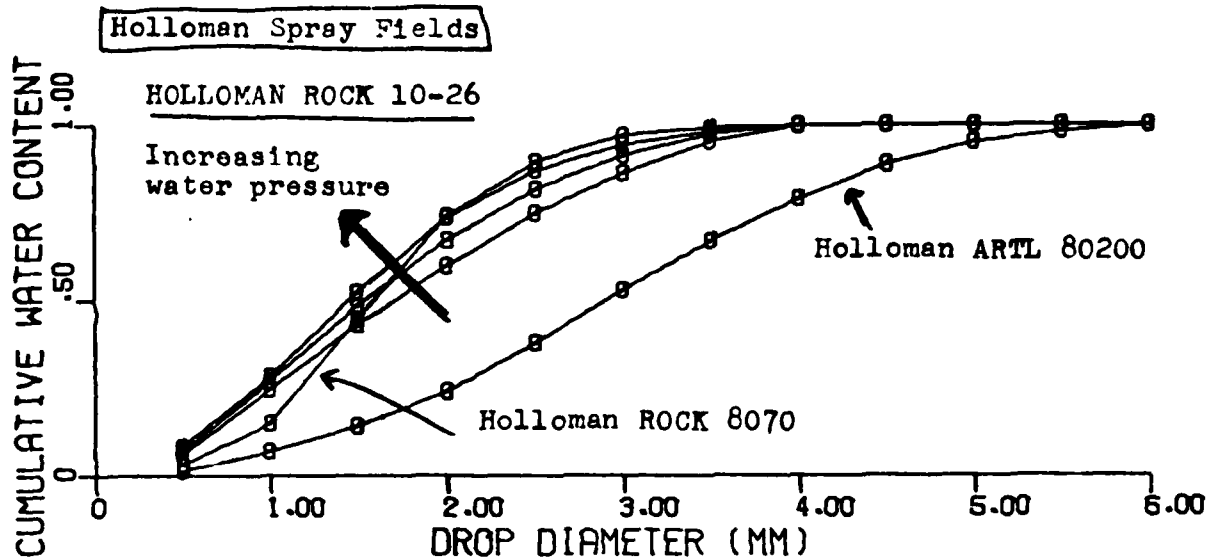


Figure 19. Cumulative water content for the Holloman rocket and artillery (ballistic) ranges.

The rates for the three curves for the 10-26 optimum locations are about the same, but as the water pressure increases, the small drops are increased at the expense of the larger ones. Higher pressure for these nozzles appears not to result in a greater efflux of water, but probably a more turbulent outflow to tear up larger drops.

The curve for the Holloman deluge 80200 is unique. This field is a good candidate for assuring encounters with larger drops in as short a field as possible.

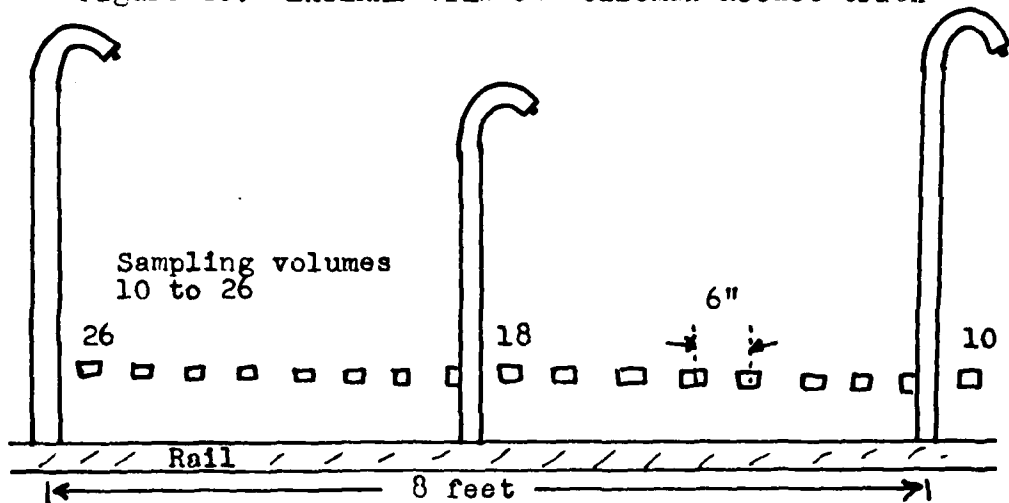
Noticeable for the Holloman ROCKET facility is that already at 1 mm mean diameter, the water content is over 25%, whereas it is only a few percent for heavy natural rains.

HOLLOMAN AIR FORCE BASE FACILITIES

Rocket Test Track

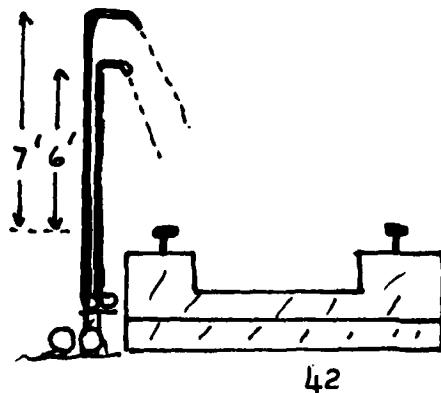
The rail track is 50,000 feet for rocket acceleration and deceleration. 18,000 feet of this length is available for a rain field (45 sections, each 400 feet long). Each 400 foot section has 50 nozzles. Two types of nozzles were used in the same field in the 1975 report. (References 7,8,9)

Figure 20. LATERAL VIEW of Holloman Rocket track



This pattern is repeated every 8 feet as shown in figure 20. Note the locations 10 to 26 where rain measurements were made. An optimum pattern was produced along this line. Nozzles are positioned about 6 and 7 feet from the track, and spray downward, about 60°, toward the track as shown in figure 21.

Figure 21. AXIAL VIEW of Holloman rocket track

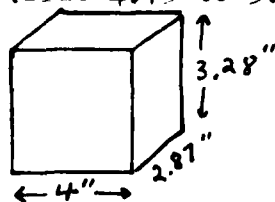


In 1969, a single type 8070 nozzle was used on this facility, with the following parameters:

Nozzle: VEE JET H14U 8070 (Standard)
 31,000 optical volumes measured, each 38 in³ (net volume 19.2 m³)
 Rain rate: 6.6 in/hr
 Liquid content: 6.87 g/m³
 Median diameter: 1.89 mm
 Nozzle water pressure: 9 psig.
 Average wind: Cross track - 0.9 knots, SD 1.5
 Along track - 1.3 knots, SD 1.7

Drop sizes were measured to about 4.5 mm diameter.

It is interesting to note how many sample volumes are needed before, on the AVERAGE, even one 5 mm drop might be seen (size 4.75 to 5.25 mm). The inspection volume is:



Volume = 38 in³ = 0.000623 m³ = 0.022 ft³

With the 8070 nozzle, about 0.6 drops

in this 5 mm range might be present in

one cubic meter. The sample volumes needed

before on the AVERAGE, one such size interval drop is met is:

$$\frac{1 \text{ inspection volume}}{0.00063 \text{ m}^3} \frac{\text{m}^3}{0.6 \text{ drop}} = 2700 \text{ sample volumes}$$

This represents a volume of 60 cubic feet in the rainfield. If a fuze with an effective frontal diameter of 1.5 cm passed through the entire 18,000 feet of rain, this is equivalent to only about half this volume. Thus, this front portion of the fuze, in two flights through the field, would on the AVERAGE meet only ONE drop in the interval, 4.75 to 5.25 mm. This is for the 6 in/hr rate, 8070 nozzle!

Lower (2.2 in/hr) rate nozzles used for 1975 report:

Table 10 lists the rain distribution for the optimum locations 10 to 26 at 5 psi pressure. Note the spacial variation within this 8 feet.

Table 10. Number drops/m³ at locations 10 to 26
at 5 psi at Holloman rocket track

LOC	10	12	14	16	18	20	22	24	26	ROW AVG
ER	43.1	67.4	38.7	88.5	101	50.2	21.2	87.3	61.6	62.1
LWC	1.92	4.43	1.98	3.99	4.57	2.47	1.21	4.01	2.70	3.03
MMD	1.62	1.45	1.09	1.56	1.56	1.21	0.82	1.43	1.66	1.38
N(0.5)	1,120.0	3,640.0	3,820.0	2,990.0	3,020.0	3,640.0	3,250.0	3,060.0	1,330.0	2,874.0
N(1.0)	498.0	1,530.0	783.0	1,300.0	1,420.0	994.0	575.0	1,400.0	714.0	1,020.0
N(1.5)	217.0	485.0	181.0	397.0	490.0	249.0	100.0	474.0	294.0	321.0
N(2.0)	104.0	151.0	58.7	160.0	222.0	73.8	28.5	158.0	139.0	122.0
N(2.5)	26.9	56.9	27.5	74.2	85.5	32.7	11.3	69.6	47.6	48.7
N(3.0)	13.3	25.9	7.79	28.3	26.0	13.5	1.38	23.7	24.7	18.3
N(3.5)	3.23	16.2	1.86	8.79	12.1	6.62	0.46	8.33	9.55	7.02
N(4.0)	0.94	6.57	1.88	4.23	1.88	0.48	0.94	3.29	1.41	2.40

ER - equivalent rain rate (mm/hr)

LWC - liquid water content (g/m³)

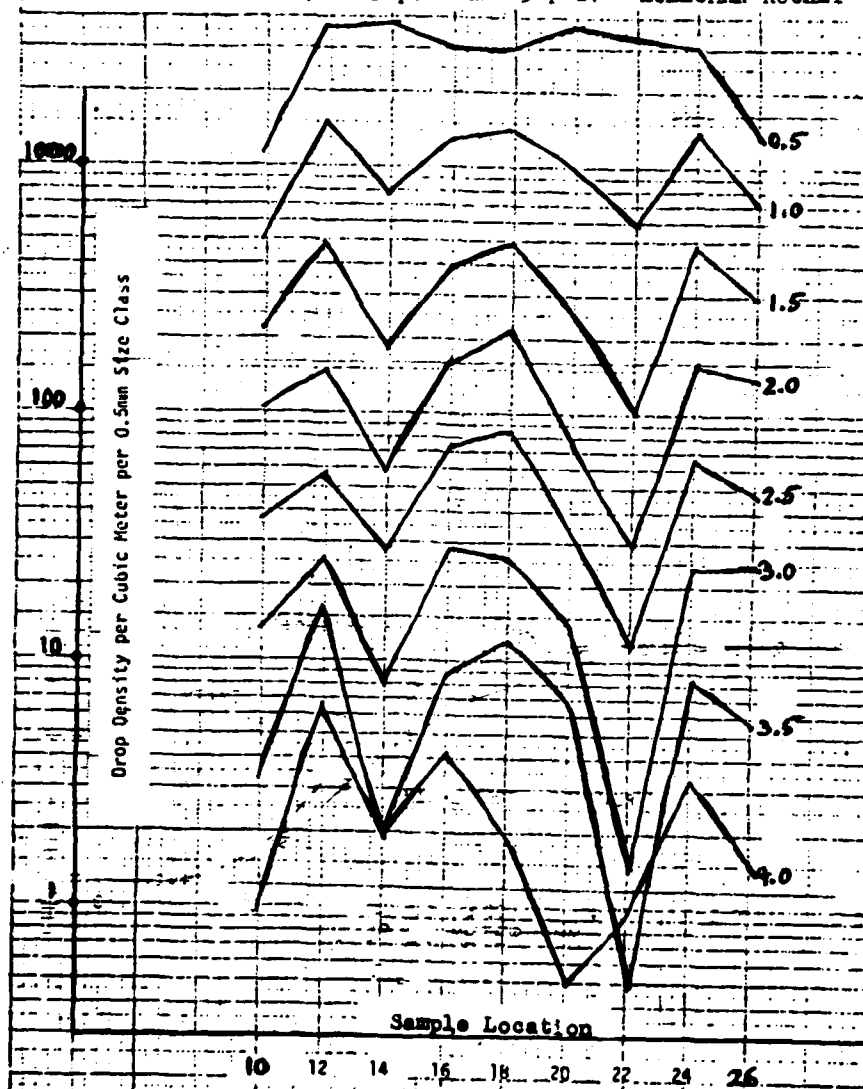
MMD - median diameter (mm)

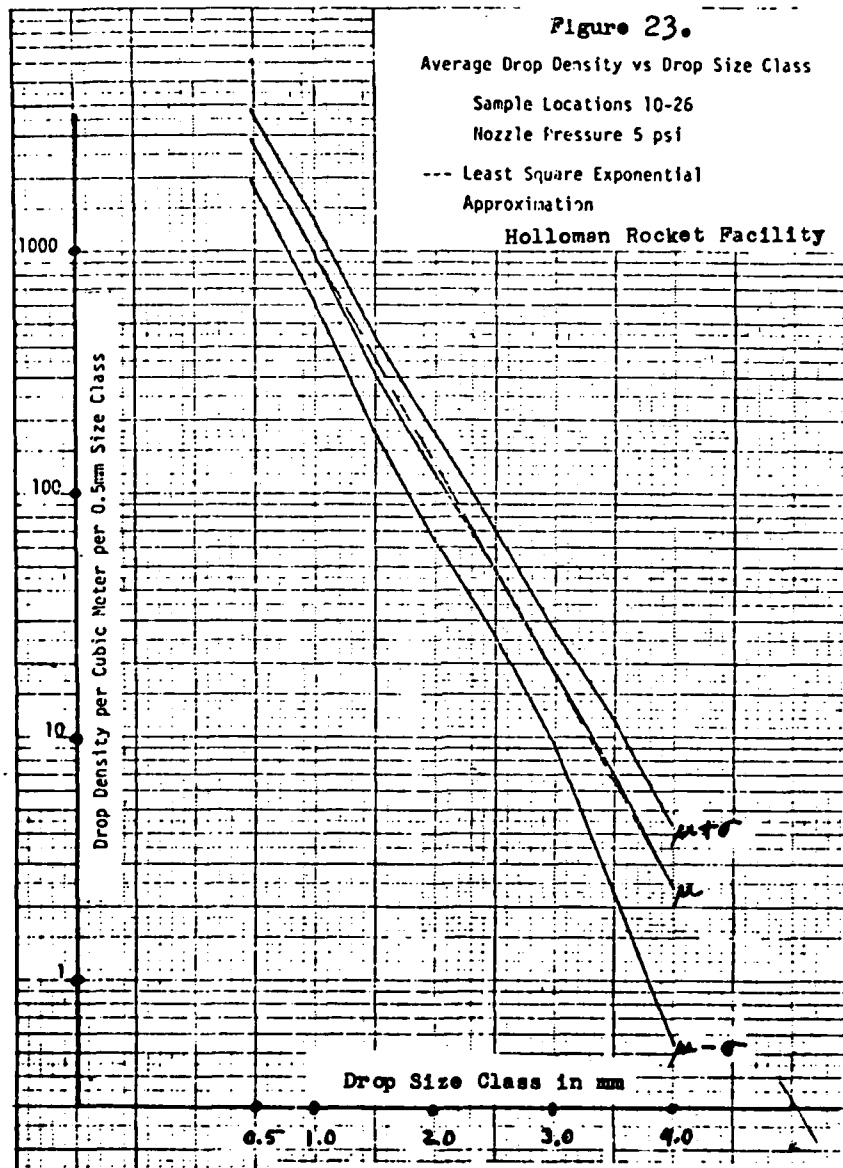
N(D) - number drops/cubic meter, of diameter D for $\Delta D \leq 0.5 \text{ mm}$

Figure 22 plots the number of drops/m³, for each drop size, as a function of the nine locations along the repeating 8 foot spray section.

Figure 23 plots the average number of all the drops, with an estimate of its variation, as a function of the drop size.

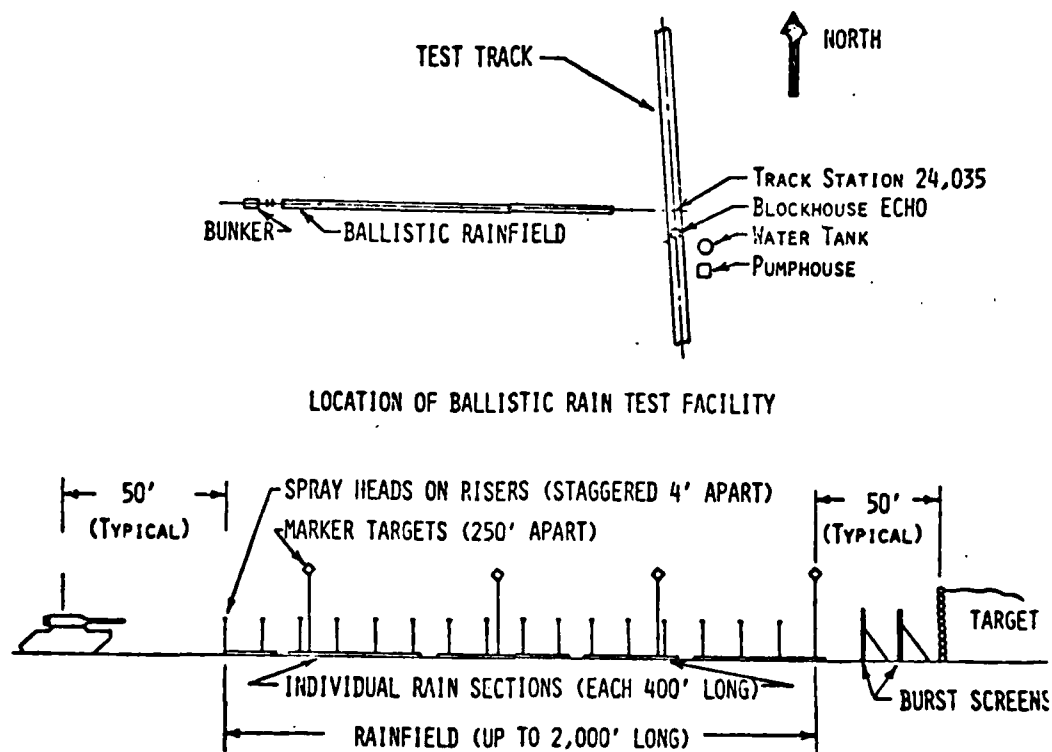
Figure 22. Average Drop number at locations 10-26
for Drop Size Classes 0.5 to 4 mm
(Water pressure 5 psi) HOLLOMAN ROCKET





Artillery (Ballistic) Test Facility

This test site called the Hay Draw Test site is 2000 feet long, and shells are stopped by a bunker. Sprays are positioned on opposite sides of the shell trajectory. Figures 24 and 25 illustrate the layout. Data on this field was generated with the deluge nozzle, 80200.



LOCATION OF BALLISTIC RAIN TEST FACILITY

Figure 24. Layout of Ballistic Rain Test Facility

Update to the ballistic range

Nozzles were replaced to produce a rate from 3 to 7 in/hr by changing pressure. There is no information on

the drop size distribution with these nozzles. Newly developed instruments are expected to scan shadows produced by the drops in a small volume with a laser beam.

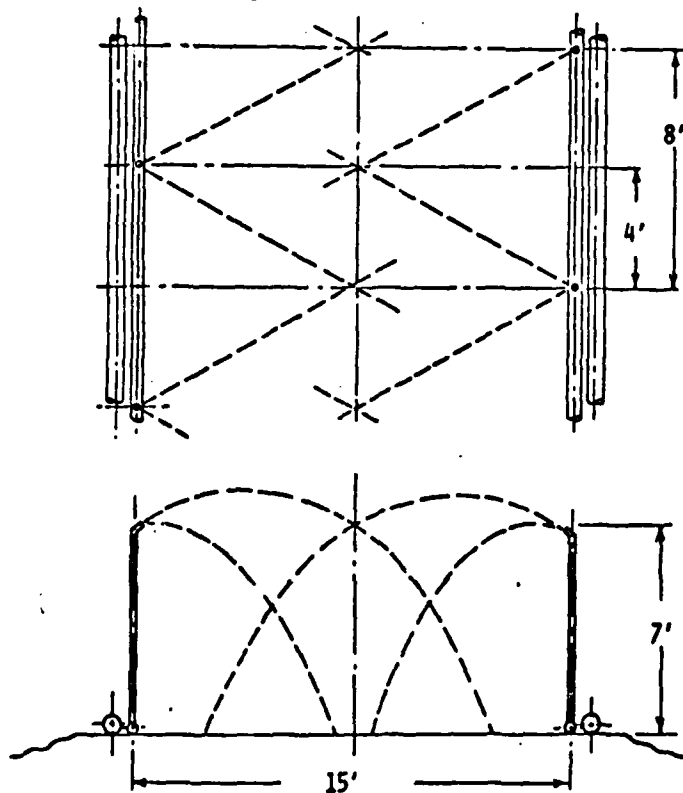
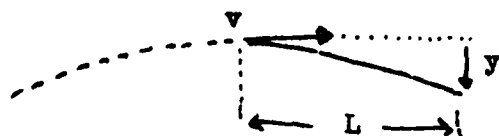


Figure 25. Ballistic rainfield cross section

A practical consideration is shell drop under gravity along the rainfield length. With air drag neglected, the drop from the trajectory top is:



$$y = g t^2 / 2 = \frac{g}{2} \left(\frac{L}{v} \right)^2$$

v(fps)	L(ft)	y (ft)
1500	500	1.8
1500	1000	7.1
2000	500	1.0
2000	1000	4.0

FUZE ENCOUNTER THROUGH RAIN

Mechanical and Electronic Fuzing

A partial lists of Army fuzes is given. Several have been tested in rainfields (references 10, 11).

<u>Artillery</u>	<u>Mortar</u>	<u>Recoilless/Tank</u>	
M557 PD	M524A6 PD	M91A2 BD	
M564 PD	M525 PD	M503A3 PD	
M577 MT	M567 PD	M509A1 PIBD	
M732 PROX	M734 MOP	M530A1	
		M534A1	
		M539	
		M578	
<u>Rocket</u>	<u>Missile</u>	<u>Small Caliber</u>	
M412E1	M805	M505	M579
M423	M812	M533	M594
M427	M815	M549	M714
M431		M550	MK 27
M433		M551	
M438			

Nominal velocities (fps): Mortar - 800
 Recoilless - 1200
 Artillery - 1950
 Tank - 4500

Apart from the frontal erosion effect, which is partially treated in appendix B, fuzes are structurally affected in three ways in high velocity rain flight:

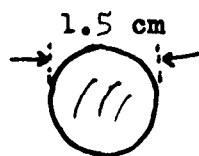
1. Single impact. Momentum transfer generally depends on the cube of the drop diameter and linearly with the shell speed. Larger drops are effective in producing high stress levels through the fuze, depending on fuze component stiffness.
2. Multiple impact (cumulative effect) occurs as in a progressive crushing or subsequent effective impacts before the fuze has sufficiently relaxed. This occurs usually after some critical drop diameter, and if the drops are too closely spaced as might occur in an accelerated test.

3. Resonance effect in small supported structures, and microphonics in proximity and electronic fuzes. If there is some periodicity in the rainfield (or if a driving oscillation is from some aerodynamic effect alone), the fuze components will react at this frequency, with a larger amplitude if the periodicity is near the resonant frequency of the fuze components.

Fuzes are too complex generally in their reaction to permit a detailed analytical look by way of structural response to all possible reactions to impulsive frontal impact.

Specific Case with Tropical Rainfield

As an example, consider a fuze with an effective frontal diameter of 1.5 centimeters, and that drops hitting this area of 1.767 cm² will affect the fuze. Momentum transfer to the lateral surface of the ogive is degraded and is not considered. The shell travels in a 100 meter rainfield, with a velocity of 1000 meters/sec.



$$A = \text{area} = 1.767 \text{ cm}^2$$

$$L = \text{rainfield length} = 100 \text{ m} = 328 \text{ ft}$$

$$v = \text{shell velocity} = 1000 \text{ m/sec} = 3280 \text{ fps}$$

ACTUAL
SIZE

Consider three AVERAGE parameters of this encounter:

1. l_i : the distance in meters the shell moves, ON THE AVERAGE, before it impacts one such raindrop:

$$l_i = \frac{1}{A N_1}$$

2. P_1 the number of impacts with these drops made ON THE AVERAGE in shell travel through 100 meters:

$$P_1 = L A N_1$$

3. ΔT_1 the time (seconds) between impacts ON THE AVERAGE of such size drops on the fuze frontal area:

$$\Delta T_1 = \frac{L_i}{v} = \frac{1}{A v N_1}$$

For this example, the TROPICAL field of 132 mm/hr (5.3 in/hr) is used. N_1 is the number of drops of diameter D_1 ($\Delta D = 0.5$ mm) per cubic meter. Table 11 lists the AVERAGE encounter values.

Table 11. AVERAGE encounter values in TROPICAL FIELD (5.3 in/hr):

D_1 (mm)	N_1 (/m ³)	$L_i = \frac{1}{A N_1}$ Distance (meters) before one drop encountered	$P_i = L A N_i$ Number impacts for 100 meter travel	$\Delta T_i = \frac{1}{A v N_i}$ Time (seconds) between drop impacts
1.5	360	16	6	0.016
2.0	250	23	4	0.023
2.5	135	42	2.4	0.042
3.0	65	87	1.1	0.087
3.5	25	226	0.44	0.226
4.0	10	566	0.18	0.57
4.5	3	1890	0.053	1.9
5.0	1.25	4530	0.022	4.5
5.5	0.5	11300	0.009	11.0
6.0	0.25	22600	0.004	23.0

Observations on this simple example:

1. P_i , the number of impacts, depends on the field length. Field length increase is done at the expense of shell drop and maintaining uniformity of rain over the trajectory. For a 1000 foot field, multiply these impacts by 3.

2. In all three parameters, L_i , P_i , ΔT_i , the actual rain distribution, N_1 , is present. For fuse response, it is not sufficient to just specify rain rate, but the rain DISTRIBUTION,

to ascertain the average number of large size drops present.

3. The important factor is ΔT . For a given fuze and velocity, how intense can the field be made? Statistics can readily be used, but for now consider average values of ΔT .

Figure 26 shows this TROPICAL distribution increased by a factor of 4 and 8. The average time ΔT becomes divided by these factors. For a factor of 4 (about 20 in/hr), the average

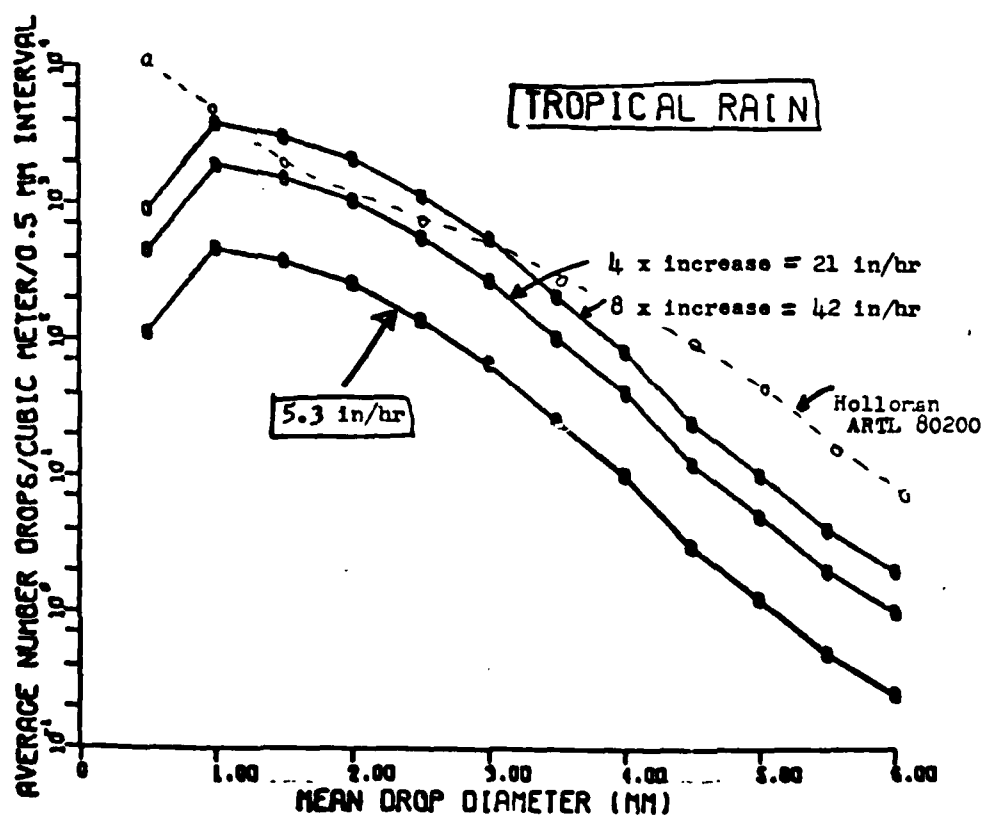


Figure 26. Increase of TROPICAL distribution by factors of 4 and 8.

time between collisions for drops greater than 3 mm is not less than 20 milliseconds. This may be a sufficient time for fuze response relaxation.

Again, with this TROPICAL field increased by an intensity of 4 to about 20 in/hr, for a 4.5 mm drop (0.5 mm interval), with the average time between collisions for these drops now about 470 milliseconds, about 1500 feet of such a 20 in/hr rate would have to be traversed for the 1.5 cm diameter fuze tip to engage ONE such drop (on the AVERAGE).

The point is: Are a few larger or many smaller (or both) drops more detrimental to the fuze? If the larger ones, then increase the rain rate as high as possible, and even bias it with one with many large drops.

RAIN WEB FOR FUZE RAIN TESTING

Introduction

Some evident handicaps of rain testing for PD fuzes are 1) wind gusts, 2) elaborate physical layout, 3) uncertainty of type of drops intercepted in any firing with the need of many firings to lend credibility to the fuze response. Effect of aerodynamic heating must necessarily be missing. These capricious aspects suggest the use of a rain web approach as a compromising solution.

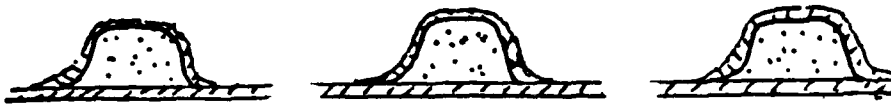
The UK has experimented with plastic spheres in excess of 5 mm diameter and with captive rain drops suspended in a crosshatch web system. Gun firings have been done.

Outlined here is an example of a "rain web" which is meant to obviate these handicaps. While the essential feature of rain encounter is preserved, this is accomplished in an arrangement that is convenient, easy to implement, and has a predictable distribution of drops intercepted for any firing.

Since larger diameter drops from 4 to 6 mm are important for impact, a planar array of 5 mm diameter drops will be used for this study as an illustration.

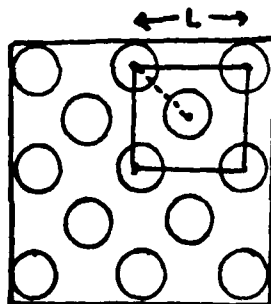
Fabrication of the Drops

In some manner the drops are held in a stationary pattern. They can be gelatinous blobs, with additives to prevent freezing, and contained between thin sheets of plastic perhaps sealed by heat. If possible, to keep weight down, the drops might be sealed individually or sprayed. Depending on the substrate



strength, holes might be initiated between drops. Details depend on material properties.

If all the drops are the same size, one repeating pattern is established with 13 drops, where the horizontal center to center spacing is a distance L , so there are two drops within



a cell L^2 in area. (Actual closest center to center distance is $L \sin 45^\circ$).

A water drop of 5 mm diameter has a volume: $\pi D^3/6 = 0.0655 \text{ cm}^3$.

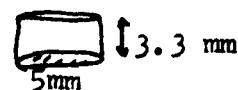
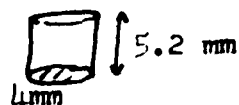
Consider for this example a fuze with an effective frontal diameter, D_F of

1.5 cm. If a plastic sheet supporting the web is 0.002 inch thick, (assume a density of water for the plastic), the volume of sheet intercepted by the fuze front is:

$$\frac{\pi D_F^2 (0.002) (2.54)}{4} = 0.009 \text{ cm}^3$$

In this example, this plastic portion intercepted by the fuze tip represents 14% of the volume of one of the drops and stresses the need of keeping the supporting web weight low, as this delivers a momentum over the entire frontal area, not particularly representative of rain encounter.

If the volume in a 5 mm drop were transferred to an ideal cylinder of base either 4 or 5 mm, the height would be:



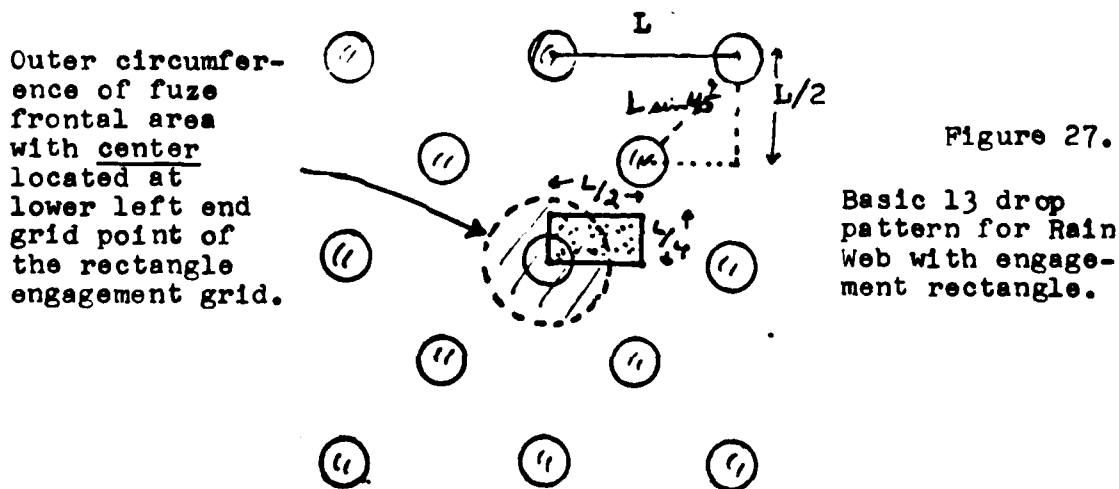
Though refinements to the computer program can include the effect of the weight of the sheet, and of non-uniform drop cylinder forms, this simulation will consider 5 mm drops as 4.5 mm diameter cylinders, 4.1 mm high, with a weightless support.

It is well to estimate the water weight (not including the weight of the supporting web) of a 3x3 foot web structure for 5 mm diameter drops with a spacing $L = 15$ mm (closest center-to-center distance would be $L \sin 45^\circ = 10.6$ mm).

$$\begin{aligned} \text{Weight(lb)} &= \frac{W^2 (2.54)^2 \pi D^3}{60 L^2 (453.6)} \quad 2 \quad (12)^2 \\ &= \frac{0.2145 (W \text{ ft})^2 (D \text{ mm})^3}{(L \text{ mm})^2} = 1.07 \text{ lb of water.} \end{aligned}$$

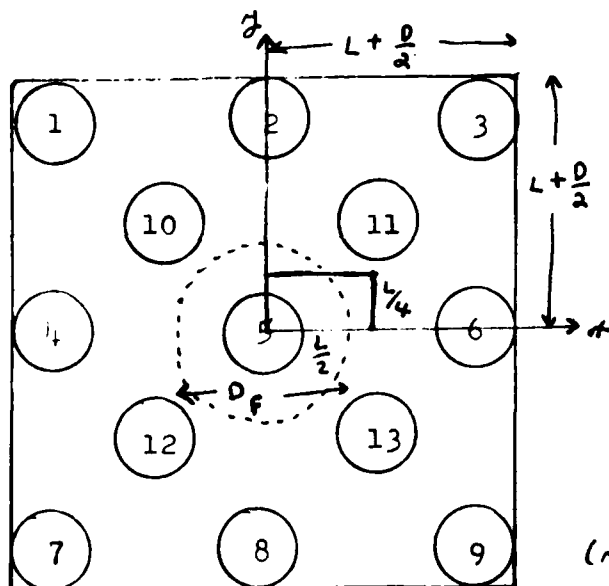
Frequency Distribution of the Encounter

In the example, all possible orientations of the fuze with the web are considered if the center of the fuze frontal area goes through a random selection of points within the rectangle of area $L/4 \times L/2$ defined in Figure 27:



The basic supposition is that the approaching center of the fuze tip can pass through any point on the rain web. The grid pattern for both the rain web and the approaching fuze was done in the following manner:

1. A repeating 13 drop pattern was represented by a 161x 161 point grid, or 25921 grid points. Zeros at the points represented locations of no drops, and 1's where the drop areas were present. An x-y coordinate system has its origin at the center of drop number 5.



The distances involved are:

$D = 4.5$ mm (representing 5 mm diameter drop).

$D_F = 15$ mm (fuze diameter).

L varies from 11 to 23 mm.

2. Locations of the boundary and inner grid points of the 13 circles were determined by the inequality:

$$(x - A_i)^2 + (y - B_i)^2 \leq \left(\frac{D}{2}\right)^2$$

where the centers of the 13 circles are located at A and B:

	A	B		A	B		A	B
1	-L	L	6	L	0	10	-L/2	L/2
2	0	L	7	-L	-L	11	L/2	L/2
3	L	L	8	0	-L	12	-L/2	-L/2
4	-L	0	9	L	-L	13	L/2	-L/2
5	0	0						

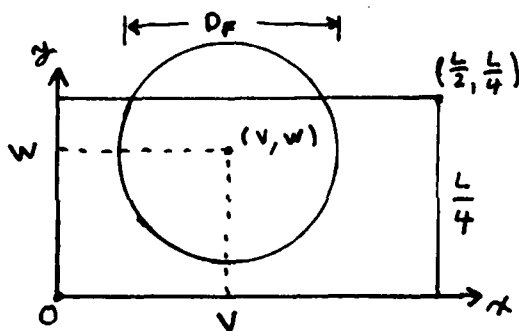
In the simulation, each of these 13 equations was interrogated by sweeping through the 25921 combinations of x and y

values. When this inequality was satisfied, that particular grid point (x,y) represented a region inside the drop.

3. The number of distinct encounters or collision orientations of the fuze with the web is the number of grid points inside the collision rectangle, which is essentially the area ratio of this rectangle to that of the entire square:

$$\begin{aligned} \text{Number of distinct} \\ \text{grid encounters} &= 161 \times 161 \left[\frac{(L/2)(L/4)}{[2(L + \frac{D}{2})]^2} \right] = \begin{array}{ll} 558 & \text{for } L = 11 \text{ mm.} \\ 612 & \text{for } L = 15 \text{ mm.} \\ 648 & \text{for } L = 19 \text{ mm.} \\ 672 & \text{for } L = 23 \text{ mm.} \end{array} \end{aligned}$$

4. The fuze tip is presented as a circle with the center located at the coordinates V and W . As the fuze engages the



web, the center of the fuze tip located at V, W can be at any of the 648 grid points in the rectangular array (for $L=19$ mm spacing). The location of the fuze area then is determined by interrogating

the entire 161×161 grid points of x and y for specific cases of V and W . Those values of x and y which satisfy:

$$(x - V_i)^2 + (y - W_i)^2 \leq (D_F/2)^2$$

are grid points where the fuze tip has cast its profile on the rain web.

5. Counting raindrop-fuze tip overlaps:

Consider the $L=19$ mm spacing. For the possible 648 encounters, the background 161×161 grid was interrogated for both the drops and the fuze tip. Where an overlap occurred with the fuze tip and any portion of a drop, a 1 was assigned to this grid point.

For each encounter, the drop-fuze overlap was counted and divided by the number of 1's which constituted one of the drops in the grid, to obtain the effective number of 5 mm drops encountered. Fractions of drops were summed to obtain the effective number of drops.

For example, for one orientation, 520 overlapping 1's were counted between the fuze and the drops it overshadowed. In this case, 341 grid points represented a cylindrical drop. This constituted hitting $520/341 = 1.525$ drops of diameter 5 mm.

To find the probability of encounter with 1.525 drops, the total number of times that 520 overlapping 1's occurred for the 648 possible orientations was calculated. The final sum indicated this occurred 7 times, and the probability

$$\text{became: } P_{D1} = 1.525 = \frac{N_i}{\sum N_i} = \frac{7}{648} = 0.0108$$

Four examples are given with uniformly distributed 5 mm drops (here represented as 4.5 mm diameter cylinders), as the drop center separation L , as defined in Figure 27, varied as 11, 15, 19, 23 mm. The fuze diameter remained at 15 mm.

Figure 28 shows this array with $L = 11$ mm (a rather close drop spacing), and the contour of the fuze diameter centered at the lower left end of the $L/4 \times L/2$ encounter rectangle.

After sweeping the entire rectangle, the program generated the frequency distribution for intersecting the number of 5 mm drops on any firing. This is Figure 29, where the frequency distribution is normalized to one. (Without normalization, the area under this curve is one). In any firing with $L = 11$ mm,

there is a high probability of intercepting 2.5 drops, with none below this number. The distribution goes to zero just before 4 drops. The probability of interception for a number range is estimated from this plot by taking some width along the horizontal axis, and noting the area above this width relative to the area under the entire curve.

The frequency distribution was somewhat grainy from the 181 x 181 grid, so a least square polynomial matrix smoothing was used with a linear fit over several grid points to obtain the representative distribution of Figure 29. An excessive number of points was avoided to prevent distorting the distribution.

Figure 30 is the $L = 15$ mm separation of drops, with Figure 31 as the resulting frequency distribution of interception. The range is now from one to two drops, in a rather unique distribution.

Figure 32 is for $L = 19$ mm separation, and Figure 33 shows a rather convenient distribution peaked at one drop, decreasing to zero, with the other side going to 1.35 drops.

The actual physical size of this seemingly optimum array is given at the right.

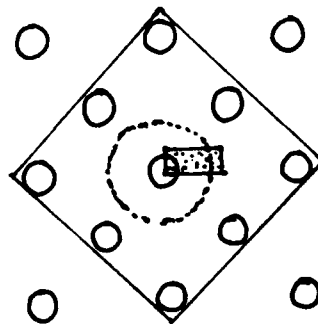


Figure 34 is the distribution with L increased to 23 mm. The peak occurs at one effective drop intercepted, but now the probability of collision with less than one and even no partial collision at all increases.

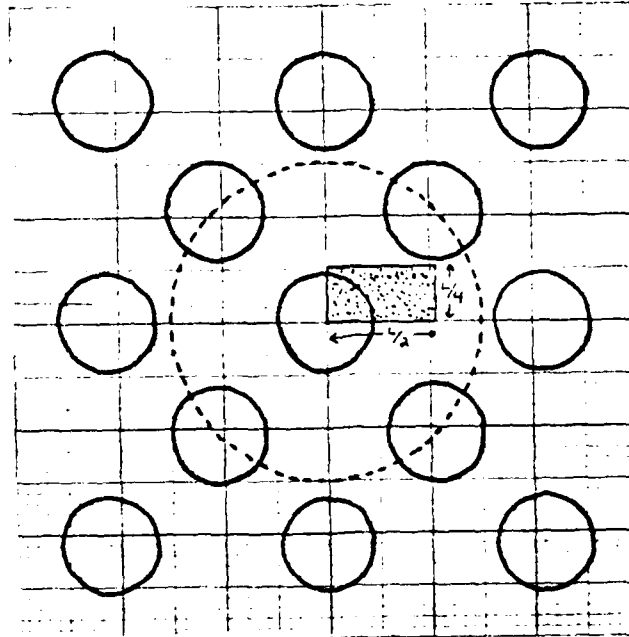


Figure 28. Web-fuze configuration for $L = 11$ mm.

Dashed circle represents circumference of 15mm diameter fuze.
Dotted rectangle represents encounter points with fuze cater.
(This drop configuration is very dense).

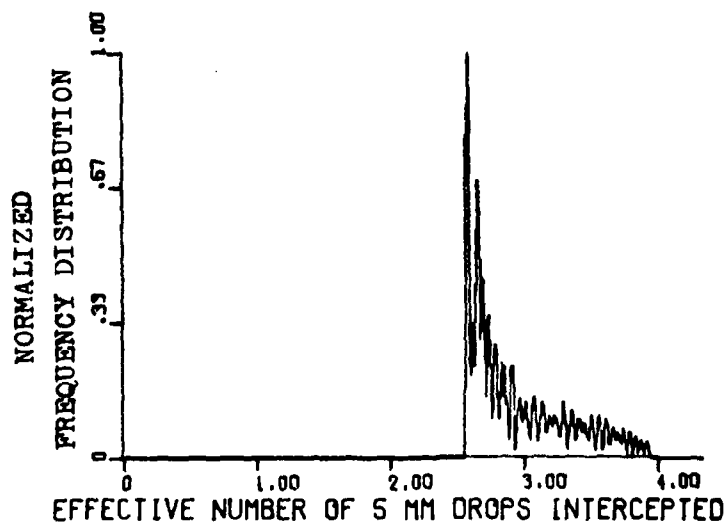


Figure 29. Calculated drop interception distribution ($L = 11$ mm).

(Portions of drops are summed to the effective number intercepted).

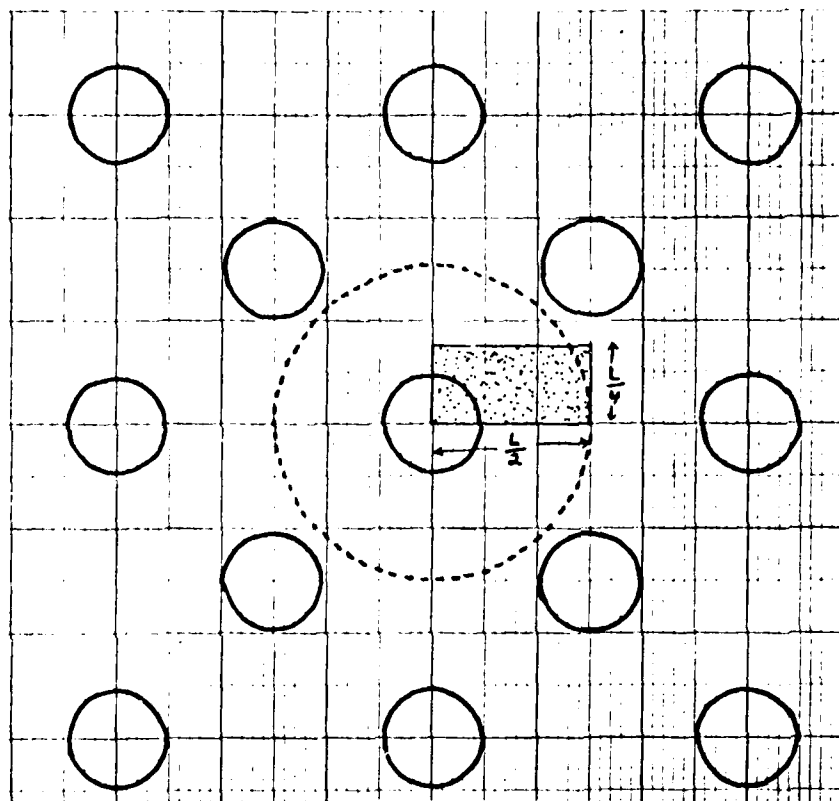


Figure 30. Web-fuze configuration for $L=15$ mm.
 Circles: 4.5 mm cylinders (5mm drops)
 Dashed circle: 15 mm fuze front
 Dotted rectangle: Sample space of collision orientations.

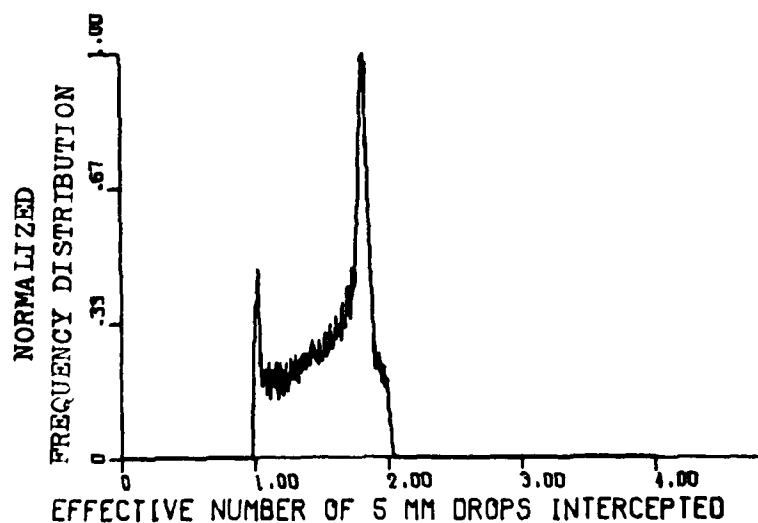


Figure 31. Calculated drop interception distribution ($L=15$ mm)

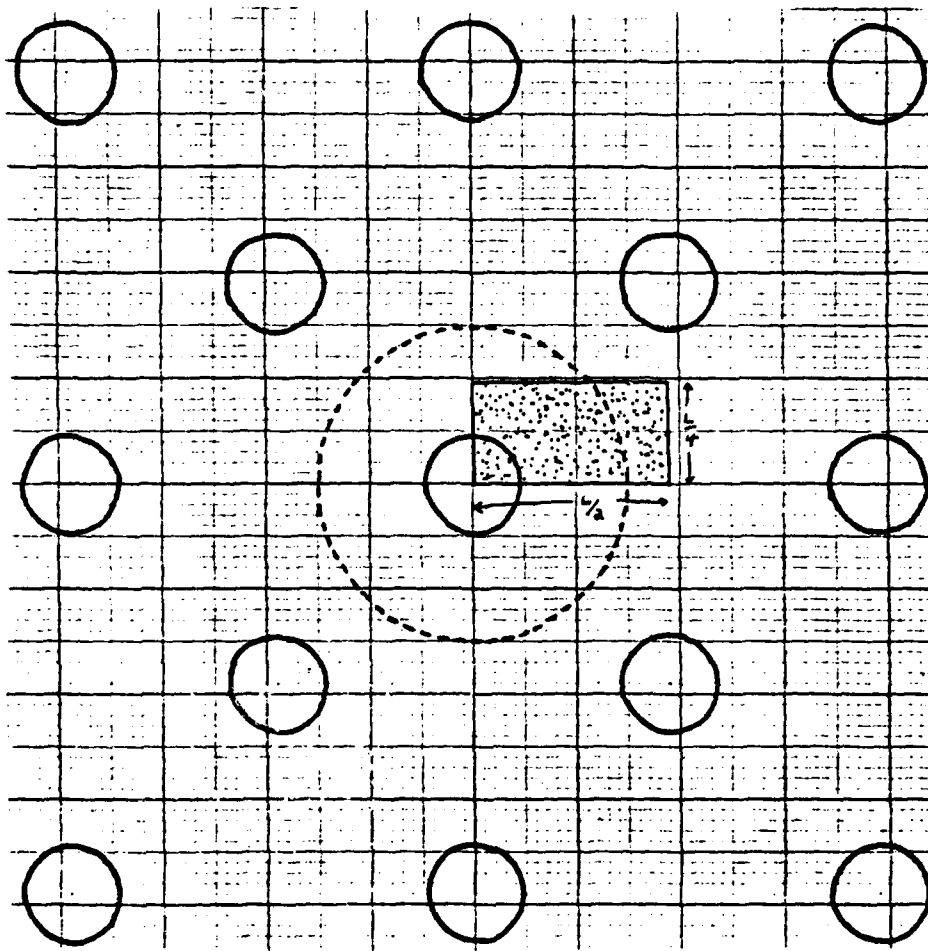


Figure 32. Web-fuze configuration for $L = 19$ mm.
 Circles: 4.5 mm cylinders (5mm drops)
 Dashed circle: 15mm fuze front

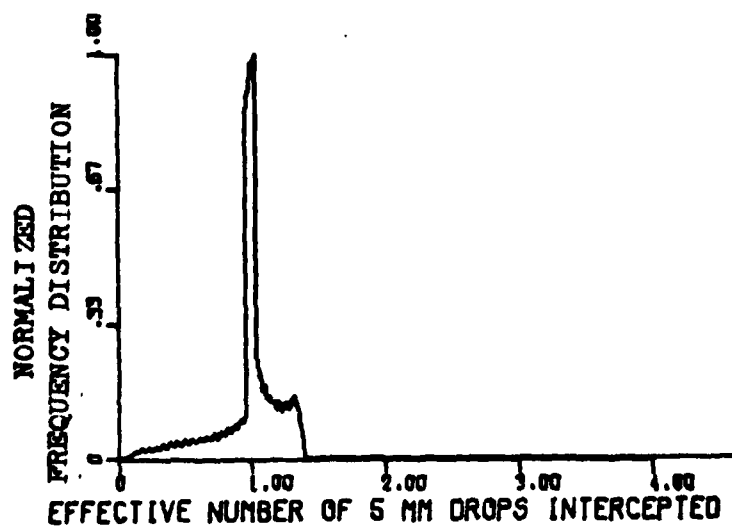


Figure 33. Calculated drop interception distribution ($L = 19$ mm)

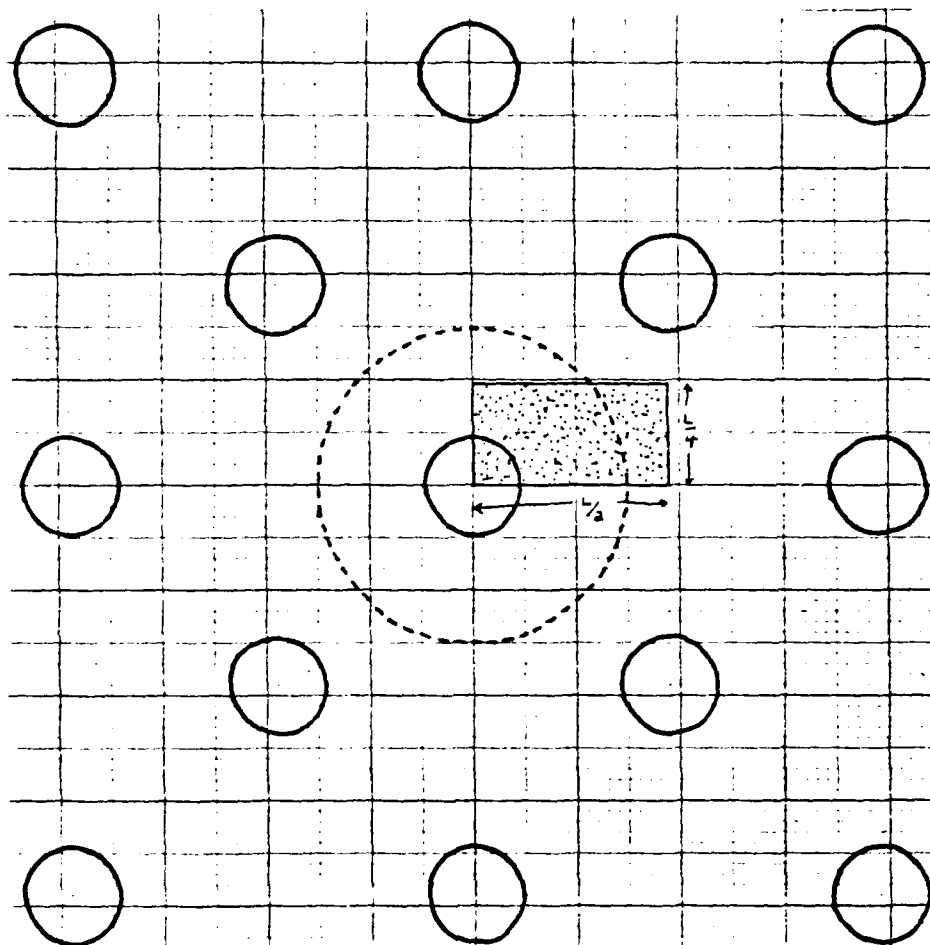


Figure 32. Web-fuze configuration for $L = 19$ mm.
 Circles: 4.5 mm cylinders (5mm drops)
 Dashed circle: 15mm fuze front

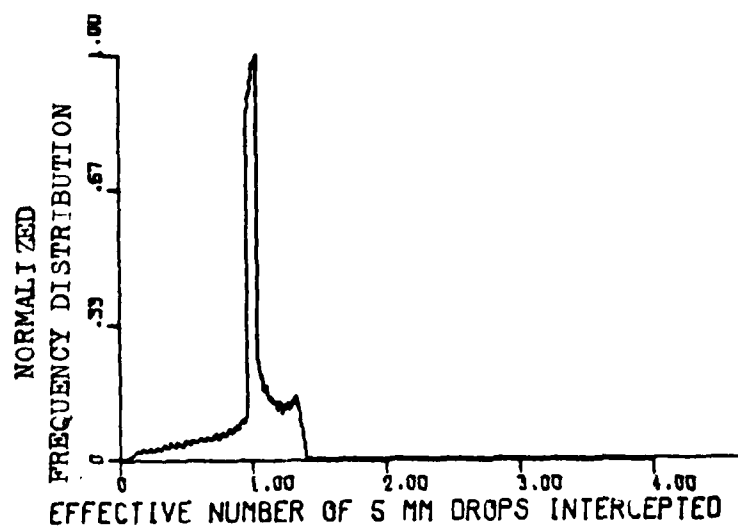


Figure 33. Calculated drop interception distribution ($L = 19$ mm)

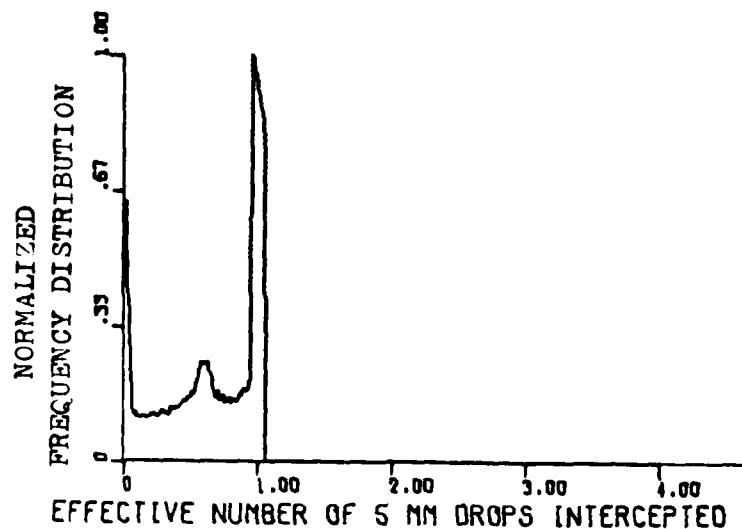
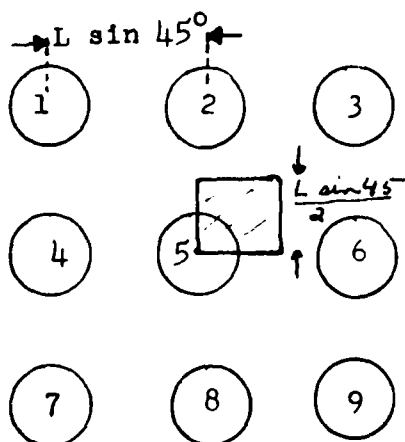


Figure 34. Calculated drop interception distribution ($L = 23$ mm)
(Increased drop spacing has increased the probability
of no partial collisions.)

Fractional drops intercepted and Water Content

The same results should be obtained (and were) for a simple
9 drop square array, where the collision encounter square is
now $(L \sin 45^\circ/2)$ on a side: $\text{Area} = \left(\frac{L \sin 45^\circ}{2} \right)^2 = \frac{L^2}{8}$



The analysis was extended one
step further to find the distri-
bution of fragments of drops and
how much of the drop encounter
comes from impacting an integral
drop, and how much of the encounter
comes from adding sums of several
drops impacted to sum to one drop.

The drops were numbered and for any collision orientation, the
1's for each drop were relegated to a histogram of drop portions

in 0.025 volume segments of a drop.

Only 9 drops are needed for the range of parameters used in this example. The encounter square now had $(161)^2 \left[\frac{\frac{L \sin 45}{2}}{2(L \sin 45 + \frac{D}{2})} \right]^2$
 $= 35 \times 35 = 1188$ collision orientations for the $L = 19$ mm spacing.

Figure 35 plots the normalized volume of water expected for any encounter, when $L = 19$ mm, as a function of portions of a drop up to an integral drop. The graph is saying that though in a collision, an integral drop is expected, there is still a low level of many fractions of drop fragments that may be expected in any firing. The high amplitude line for the integral drop is displaced one increment to the right because of plotting routines.

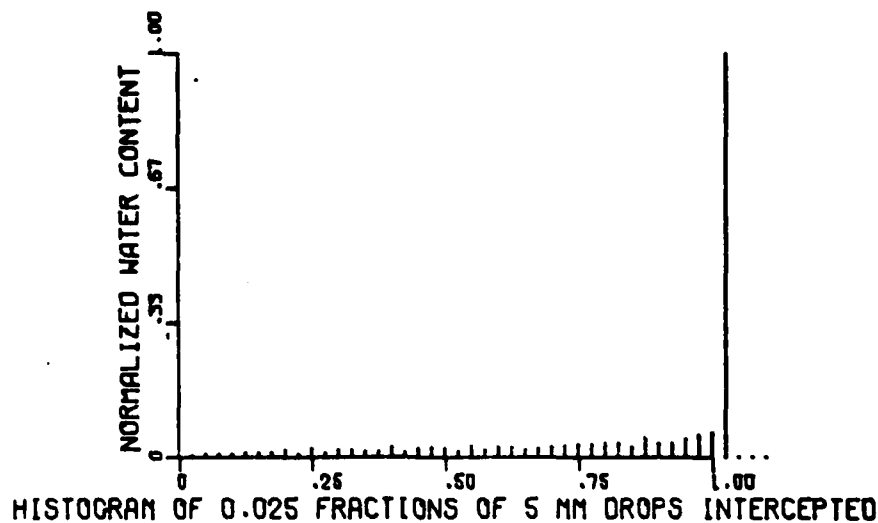


Figure 35. Water content for fractions of 5 mm intercepted drops. ($L = 19$ mm)
 (The same general histogram occurs for other L values).

Figure 36 is the associated cumulative water content for Figure 35 ($L = 19$ mm). Again, normalization is used instead of absolute units. All the fractions, from very minute to almost

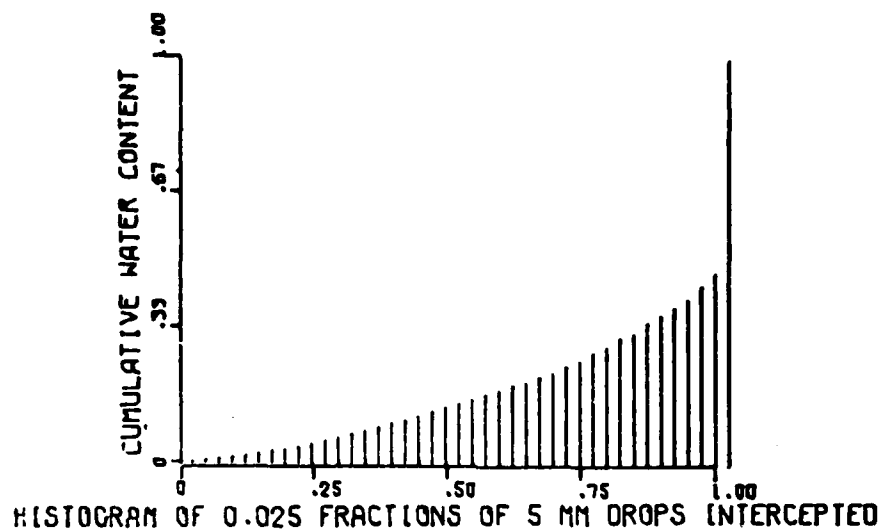


Figure 36. Cumulative water content for fractions of 5 mm diameter intercepted drops for 15 mm diameter fuze front. ($L = 19$ mm)
(Same general histogram occurs for other L values).

the entire drop, on the average, contributed to almost half of the water content intercepted in any firing. About 70% of water content comes from drops intercepted that range from $3/4$ to a complete drop. Other values of L spacing gave the same general plot with some small amplitude change.

The above approach is a purely geometrical analysis of the encounter. The actual encounter would involve some smoothing from the interaction of the drops at the periphery of the fuze tip boundary.

Even though in rainfields half of the water content (or equivalently half of the impulse imparted to the fuze) comes from drops below the median diameter, which is in the vicinity of 2 mm, fuze response should not be considered from the aspect of total momentum transferred, but rather from a subtle combination of the larger drops and repeated impacts that would cause a large amplitude response for those fuzes that are more susceptible to a spring type response. Also it is not expected that for each firing the drops will be at their average spacing to produce a predictable resonance driving load.

A direct approach for the facility would be to design in a periodicity or frequency important for the type of fuze considered. More important, whatever impacts do occur, the larger drops should be used for maximum response at any impact. Five mm drops appear convenient.

As a specific case, consider once more the example of a shell at 3280 ft/sec in tropical rain at 5.3 in/hr rate where the median diameter is 2.3 mm. The range is taken as 1000 feet, and the effective fuze frontal diameter is 15 mm. The frequency of impact is: Shell velocity/separation of web stations. For a shell at 3280 ft/sec and a 50 foot spacing of webs, this is a driving frequency of 66 HZ, or a time interval of 15 milliseconds. Engineering knowledge of a specific fuze would dictate what spacing to use for the moveable web stations.

However, as the expected frequency goes down, only a few stations may be possible along a 1000 foot range to accomplish this aspect of resonance producing multi-impacts.

To pursue this example further, the list below shows how many drops ON THE AVERAGE would be intercepted by this fuze at the cited drop diameter (ΔD here is 0.5 mm).

Size of drop (mm)	Number intercepted ON AVERAGE in 1000 foot range in tropical rain.	Frequency of impact (HZ) for 3280 ft/sec and fuze diameter of 15 mm.
1.5	20	62
2.0	13	43
2.5	7	23
3.0	3.5	12
3.5	1.35	4.4
4.0	0.54	1.7
4.5	0.16	0.52
5.0	0.067	0.22
5.5	0.027	0.09
6.0	0.013	0.04

In this case the driving frequency of the rain from drops 4mm and larger is very low and might not even be pertinent for resonant or multi-impact driving.

The drops in the range 2 to 3 mm give lower momentum transfer at each encounter, and if these drops are uniformly spaced, they may be at some important frequency of the fuze. If all these elements are present, then smaller drops may be pertinent. From this uncertainty comes the recommendation

for a confirmatory test at a facility as Holloman. This issue may still be resolved by a rain web system.

If this frequency aspect is set aside, physically it is a question of whether many low amplitude impulses, or wider spaced higher ones are more detrimental. Physically the latter appears more detrimental from the aspect of some minimum impulse needed to appreciably disturb the fuze mechanism.

From an applications aspect, there is the need to drive down the range and replace the web frames after each firing.

The lateral area of the fuze has not been discussed, as the momentum transfer here is degraded by the ogive contour. As the ogive passes through the web, the lateral impacts would be more severe than in ordinary rain because of the higher matrix density of the web drops.

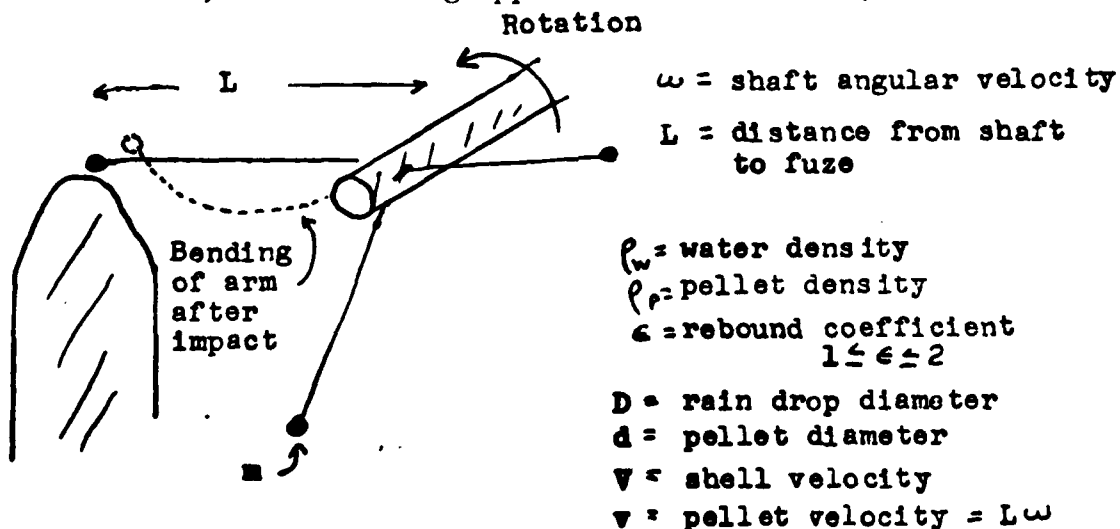
MECHANICAL SYSTEM FOR RAIN IMPACT SIMULATION

For single and even multiple rain impacts, a mechanical system such as a rotating flexible mechanical arm end weighted, or a rapid fire gun offer a degree of simulation.

There are dissimilarities. Rain impact with high velocity shells is an impulsive encounter lasting no more than about ten microseconds. Its erosive character is due to high pressure created at the surface and by radial flow.

The surface pressure profile will not be the same with a metallic impact. There is no radial flow and the impact duration (depending on the stiffness of the pellet and the fuze frontal configuration) may be an appreciable number of microseconds. This still merits some consideration. The air gun approach is straightforward, but it would be more convenient in a laboratory if the energy were obtained from a mechanical rotating system.

If lightweight, flexible arms were rigidly attached to a rotating shaft, with a spherical metal pellet attached to the arm end, the following approach could be used:



As a first approximation, neglect the weight of the flexible arm (this may be a serious neglect). Estimate the rotor speed, arm length L, and pellet properties to simulate rain impact. First have an equivalence of momentum transfer:

$$\frac{\rho_w \pi D^3 v}{6} = \frac{\rho_r \pi d^3 v \epsilon}{6}$$

$$\boxed{L \omega = \left(\frac{D}{d}\right)^3 \frac{v}{\epsilon} \left(\frac{\rho_w}{\rho_r}\right)} \quad \text{RPM} = \frac{30 \omega}{\pi} \quad (18)$$

Consider a specific case:

$$\begin{aligned} \rho_r &= 7.6 \text{ (steel pellet) g/cc} \\ \epsilon &= 1.2 \text{ (coefficient of restitution)} \\ L &= 0.83 \text{ ft (10 inches)} \\ D &= 4 \text{ mm (0.0131 ft) drop} \\ v &= 1900 \text{ fps} \end{aligned}$$

$$(\text{RPM}) d^3 = \frac{30}{\pi} \left(\frac{1}{7.6}\right) \frac{D^3 v}{\epsilon L}$$

$$(\text{RPM}) d^3 = \frac{30 (0.0131)^3 1900}{\pi (7.6) 1.2 0.83} = 0.00539$$

Consider a 1000 RPM shaft:

$$d^3 = 5.39 \times 10^{-6} \text{ (ft}^3\text{)}$$

$$\boxed{d = 5.3 \text{ mm}} \text{ steel pellet}$$

Steady state operating conditions depend on the mounting and stiffness of the rotating system, and experimentation is needed.

Duration of the collision is obtained by monitoring electrical contact between the fuze (assume a metallic cover) and the metal pellet system.

If the three pellets are so mounted as in the sketch, the time between collisions is:

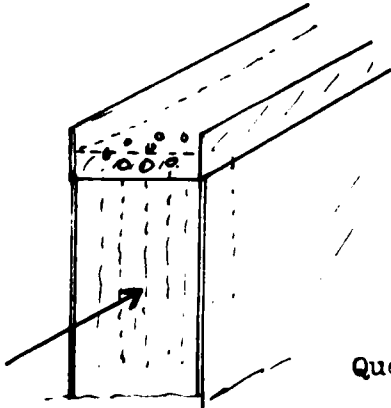
$$\frac{60}{3 \text{ (RPM)}} = 20 \text{ milliseconds.}$$

In the literature are examples of water and pellet type impact machines.

EXPERIMENTAL-PHOTOGRAPHIC STUDY OF O-C-O SYSTEM

Concept

The feasibility of an O-C-O (overhead-channel-orifice) system was briefly considered, both in theory and in a simple

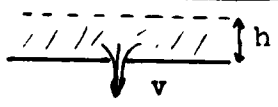


photographic experiment. To produce a more consistent drop distribution, the approach of orifice flow for a thin plate was used. Water is in an overhead channel at a liquid level with holes of various sizes drilled into the channel.

Questions:

What size holes should be used?
How uniform are the emerging drops?
What height is needed for drop formation?
What is the drop spatial separation?
Is such a system maintainable?

The velocity at which water emerges as a stream from a fluid height, h , is close to ideal gravity fall:


$$v \approx 0.99 \sqrt{2gh}$$

The amount (discharge rate Q) of water depends on the orifice configuration, as the effective exit area is not the geometrical area. For a thin plate and straight orifice, the discharge coefficient, f , is cited about 0.6 (dimensionless).

The discharge rate Q (ft³/sec) through the orifice is:
 $Q = f A \sqrt{2gh}$, where A = geometric orifice area.

Consider that at some distance down from the orifice, a stable drop pattern has been produced. Assume all the drops are of the same size, and are equally spaced. These are poor assumptions, but give an initial insight.

The drop diameter D is not expected to be the same as the orifice diameter d . Some function should exist, and



consider this as linear with C as the slope:

$D = C d$. At some region below the channel, a steady state exists. Mass rate balance between the number of drops, n , passing this location per unit time, and the efflux from the orifice is the same:

$$n \pi D^3 / 6 = f A \sqrt{2 g h} = f \pi d^2 \sqrt{2 g h} / 4 \quad (19)$$

The number of drops/sec passing this region becomes:

$$n = \frac{3}{2} \frac{f \sqrt{2 g h}}{C^2 D}$$

Or conversely, the discharge coefficient is: $f = \frac{2}{3} \frac{n D C^2}{\sqrt{2 g h}}$

Single flash photography:

- This could obtain the coefficient C and n :
- L = length of section in stabilized drop formation
- N = number of drops in this distance L
- v = velocity of drops in this section L
- Number of drops passing per unit time:
- $n = N / \Delta t = N v / L$
- Inspection of the drop size should give the slope C .

Of concern is the spacing between the drops, which will be too close: S = separation of the drops:

$$S = \frac{L}{N} = \frac{L v}{n L} = \frac{2 v C^2 D}{3 f \sqrt{2 g h}}$$

For: $v = 15$ fps
 $C = 1.2$
 $f = 0.6$
 $h = 6$ inches

$$S = 4.23 D$$

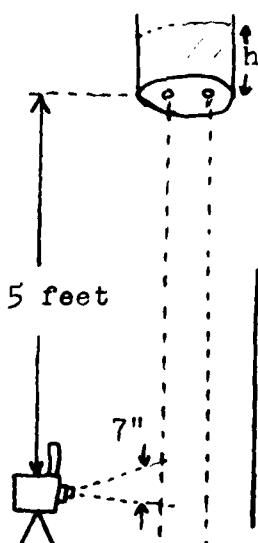
D(mm)	S(centimeters)
2	0.85
4	1.7

The conclusion is that unless the drops are scattered horizontally, they are too closely spaced vertically. Their speed is too slow.

Experiment and Tabulation of Results

A simple photographic setup to observe drop formation from a channel-orifice system consisted of four large cans, with carefully drilled orifices. Five feet below the bottom of the can, a 35mm flash camera observed the drop formation against a black background.

Skim milk had to be used for clear identification of the drops. The flash duration was less than 20 microseconds (no visible distortion from motion could be seen). Appendix A has several samples of the 60 SINGLE flash pictures taken.



Four different cans were used:

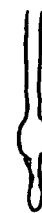
Can	Number of holes	Hole diameter		
		inch	inch	mm
1	2	1/16	.063	1.6
2	2	3/32	.094	2.38
3	2	1/8	.125	3.1
4	1	3/16	.188	4.76

The liquid level, h , was maintained at either 3 or 6 inches, representing exit velocities of 4 and 5.7 fps. The experiment was done under quiet conditions in the fluid. With rotational motion in the fluid, the stream was scattered sideways in what appeared a random manner. Unfortunately, no pictures were taken of this situation.

Experimental results:

1. An upper limit liquid drop size is created by the orifice. This appeared independent of the liquid level used.
2. A sharp peaked bimodal drop size distribution was

created. This could be seen in a picture of the stream about a foot below the orifice where the drop formation was essentially completed. The larger size drop is larger than the orifice diameter.



3. Drops are not in uniform vertical formation, and are too closely spaced vertically in some pictures. Some swirling motion in the fluid might be desirable for horizontal spreading of the drops.



4. Drops were photographed in a vertical distance of 7 inches, at a location 5 feet from the orifices. The drops from the largest orifice were not very spherical, and it was difficult to estimate their diameter.

Table 12 lists the holes, drop diameters (measured with a ruler from 8x10" pictures), and the average number and standard deviation of the number of drops seen over these 7 inch intervals. These are averages for all experiments, both 6 and 3 inch channel fluid height.

Table 12. Drop sizes, number, liquid content from orifice flow experiment

Hole (mm)	Drop diameter (mm)			Number drops over 7" drop, 5 feet below orifices			Grams (G)	
	Large	Med	Small	Large	Med	Small	3"-6"	6"
				\bar{x} sD	\bar{x} sD	\bar{x} sD		
1 1.6	2.27	--	1.14	9.1 2.0	-- --	8.3 1.6	.058	.066
2 2.38	3.18	--	1.6	7.1 1.4	-- --	5.4 1.3	.129	.135
3 3.1	3.52	--	1.8	7.2 1.3	-- --	5.5 1.0	.182	.184
4 4.76	5.5	3.6	1.7	6.5 2.0	3.3 1.4	3.8 1.5	.656	.713

The last two columns in table 12 give the average number of GRAMS of liquid seen in this 7 inch interval for two conditions:

(1) For all the data, both 3 and 6 inch heights. For the four type orifices, the mean fluid height was:

Orifice	Mean fluid height (in)
1	4.8
2	5.3
3	5.3
4	3.8

(2) Data for only the 6 inch fluid height.

To test the consistency of the data, the discharge coefficient, f , was calculated for the orifices, which theoretically should be 0.6. Since the drop velocity could not be determined experimentally, a velocity of 17 fps was used for these drops. See the section on Reynolds number and figure 3.

(1) Calculate liquid flow through seven inch window:

$$\boxed{R \text{ (cc/sec)}} = \left[\frac{G \text{ (grams)}}{7'' \text{ window}} \right] \left[\frac{17 \text{ ft}}{\text{sec}} \right] \left[\frac{12 \text{ in}}{\text{ft}} \right] = \boxed{29 G \text{ (grams)}} \quad (21)$$

(2) Calculate the liquid flow from the orifices:

$$Q \text{ (cc/sec)} = f A \sqrt{2gh} = f \frac{\pi}{4} d^2 (\text{in}) \sqrt{64.4 \sqrt{h(\text{ft})} \left[\frac{12 \text{ in}}{\text{ft}} \right] \left[\frac{2.54 \text{ cm}}{\text{in}} \right]^3}$$

$$\boxed{Q \text{ (cc/sec)}} = \boxed{1240 d^2 (\text{in}) \sqrt{h (\text{ft})}} f = \boxed{W f} \quad (22)$$

d - orifice diameter (in)

h - fluid height in

channel (ft)

f - discharge coefficient

Find f :

$$\boxed{f = \frac{29 G}{W}}$$

The coefficient W is calculated for the various conditions. Mean height \bar{h} is used for the combined 3 and 6 inch heights.

Hole	d(in)	$\frac{W}{(h)}$	$\frac{W}{(h=0.5)}$	$\frac{f}{(h)}$	$\frac{f}{(h=0.5 \text{ ft})}$
1	0.063	3.11	3.48	0.54	0.55
2	0.094	7.28	7.75	0.51	0.51
3	0.125	12.9	13.7	0.41	0.39
4	0.188	24.7	31.	0.77	0.67

There is crude agreement with the theoretical value $f=0.6$. The value is lower for the third hole; and it was difficult to estimate the drop diameter for the fourth size hole.

Application to outdoor test

1. A specific drop size distribution can be created. The rain rate can be controlled to a degree, and is proportional to the square root of fluid height in the channel.
2. The vertical drop separation is too close (at times the drops are almost binary and would be equivalent to a very large drop on a fuze). Some swirling motion in the channel may change this.
3. To prevent clogging of the orifices, a covered and filtered channel system would be needed.
4. For an intense, calibrated rainfield of short length, this O-C-O system may be suitable.

REFERENCES

1. J. Domen, Raindrop Impact on PD Fuzes, Fuze Environment and Characterization Symposium (1972), Dover, NJ, has a summary of rain distributions, literature survey, and fuze application. (This paper is reprinted as Appendix B).
2. E. Mueller and A. Sims, Calibration and Comparison of Simulated Rain Fields with Natural Rains, Illinois State Water Survey, 1971.
3. J. Lynn, Investigation of a Simulated Rain Test for Fuzes, 1955 report from Franklin Institute, TR FV-1804, prepared for Picatinny Arsenal, Fuze Development Laboratory (Standardized Rain). This is an early investigation of pertinent aspects of rain simulation.
4. M. Skolnik, Radar Handbook, McGraw-Hill, 1970, 24-24.
5. N. Sissenwine, Synopsis of Background Material for MIL STD 210B, Climatic Extremes for Military Equipment, AFCL-TR-74-0052, 24 Jan 1974.
6. P. Tattelman, Extremes of Hydrometeors at Altitude for MIL STD 210B, Supplement-Drop-Size Distributions, ARCL-TR-73-0008, Air Force Systems Command, Hanscom Field, Bedford, Mass, 9 Jan 1973.
7. F. Ehni, Layout and Calibration of the Rain Simulation Facility at the Holloman Test Track (Test Track Division, Nov. 1975). Update measurements (to only 4 mm) at the rocket test facility.
8. The Holloman Track, Facilities and Capabilities, Armament Development and Test Center, 6585th Test Group, Test Track Division, Holloman Air Force Base, NM, 1974.
9. MIL STD 331A, Proposed Test, Rain erosion/Sensitivity (Gun-Fired Projectiles), 15 Oct. 1977. Essentially covers the report of Ehni of 1975.
10. Fuze Impact Response Catalog, Brennan et al., June 1978, LCWSL, ARRADCOM, Dover, NJ. Reviews 35 fuzes which are currently fielded.
11. Technical Manual 43-0001-28, Dec. 1978, Artillery, Ammunition, Guns, Howitzers, Mortars, Recoilless Rifles, Grenade Launchers, and Artillery Fuzes.
12. R. Gunn and G. Kinzer, "The Terminal Velocity of Fall of Water Droplets," Journal of Meteorology, August 1949.

APPENDIX A. Photos from study of O-C-O system.

Of the sixty photos taken for the overhead-channel-orifice system, only five are included here. The liquid height in the channel for these photos was six inches.

A centimeter ruler is referenced with each photo.

Figure	Number on photo	Hole size number	Hole Orifice (mm)	Large drop diameter(mm)
37	1	1	1.6 (note "binary" drops)	2.27
38	50	1	1.6	2.27
39	59	2	2.38	3.18
40	22	3	3.1	3.52
41	39	4	4.76 (drops unstable)	~(5.5)

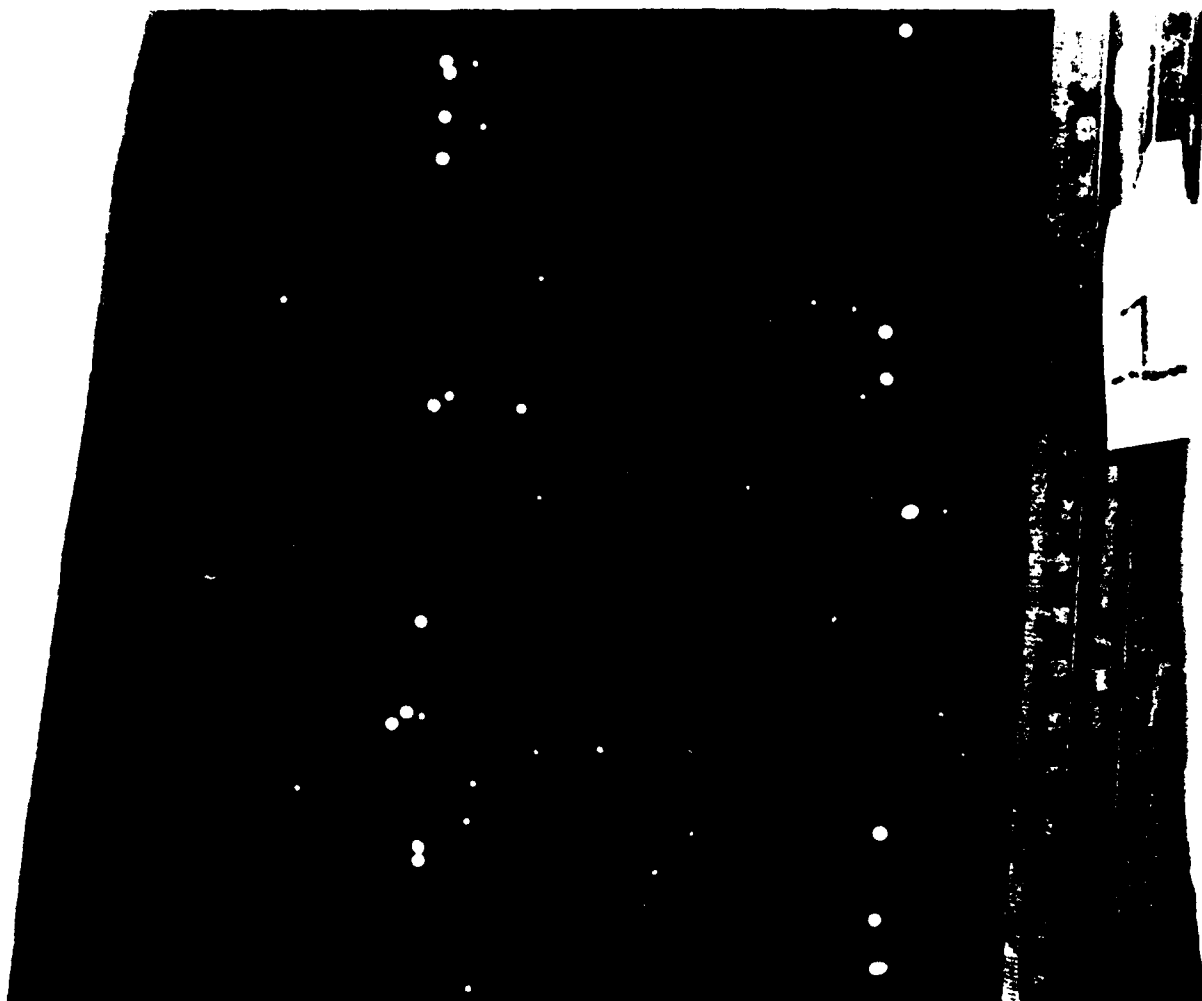


Figure 37. Drops from 1.6 mm orifice.

(Large drop diameter approximately 2.27 mm)

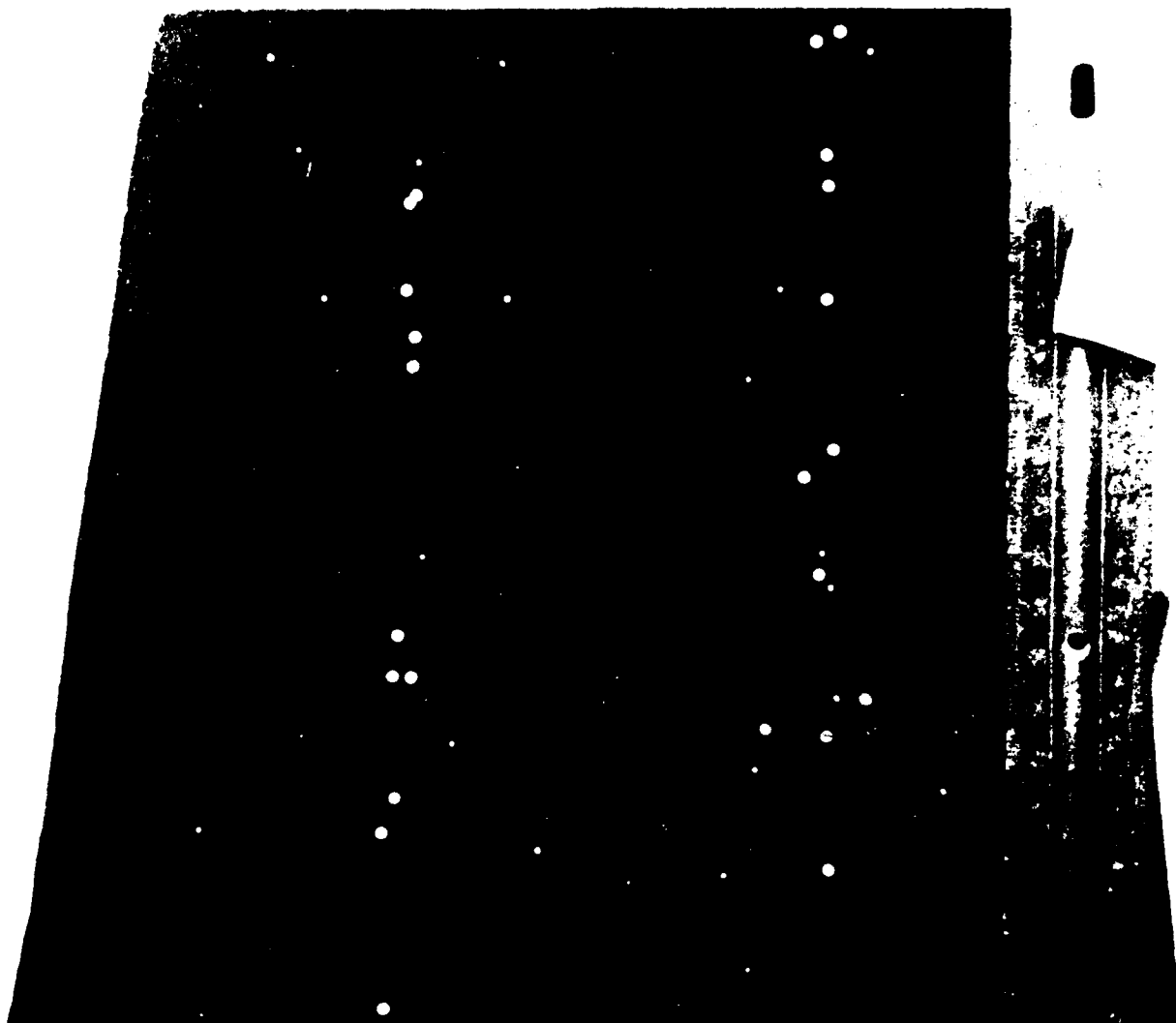


Figure 38. Drops from 1.6 mm orifice.

(Large drop diameter approximately 2.27 mm)

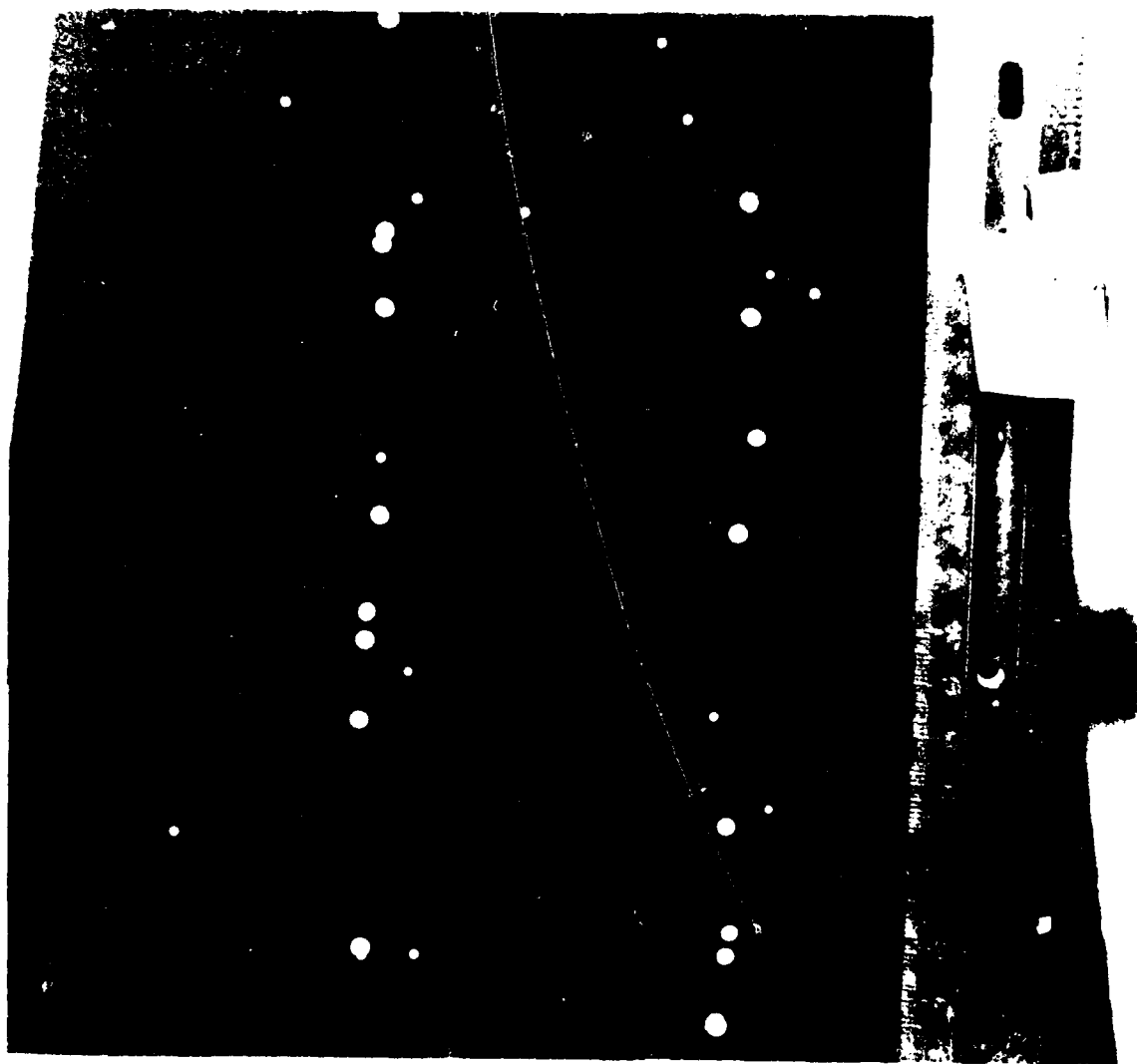


Figure 39. Drops from 2.38 mm orifice.

(Large drop diameter approximately 3.18 mm)

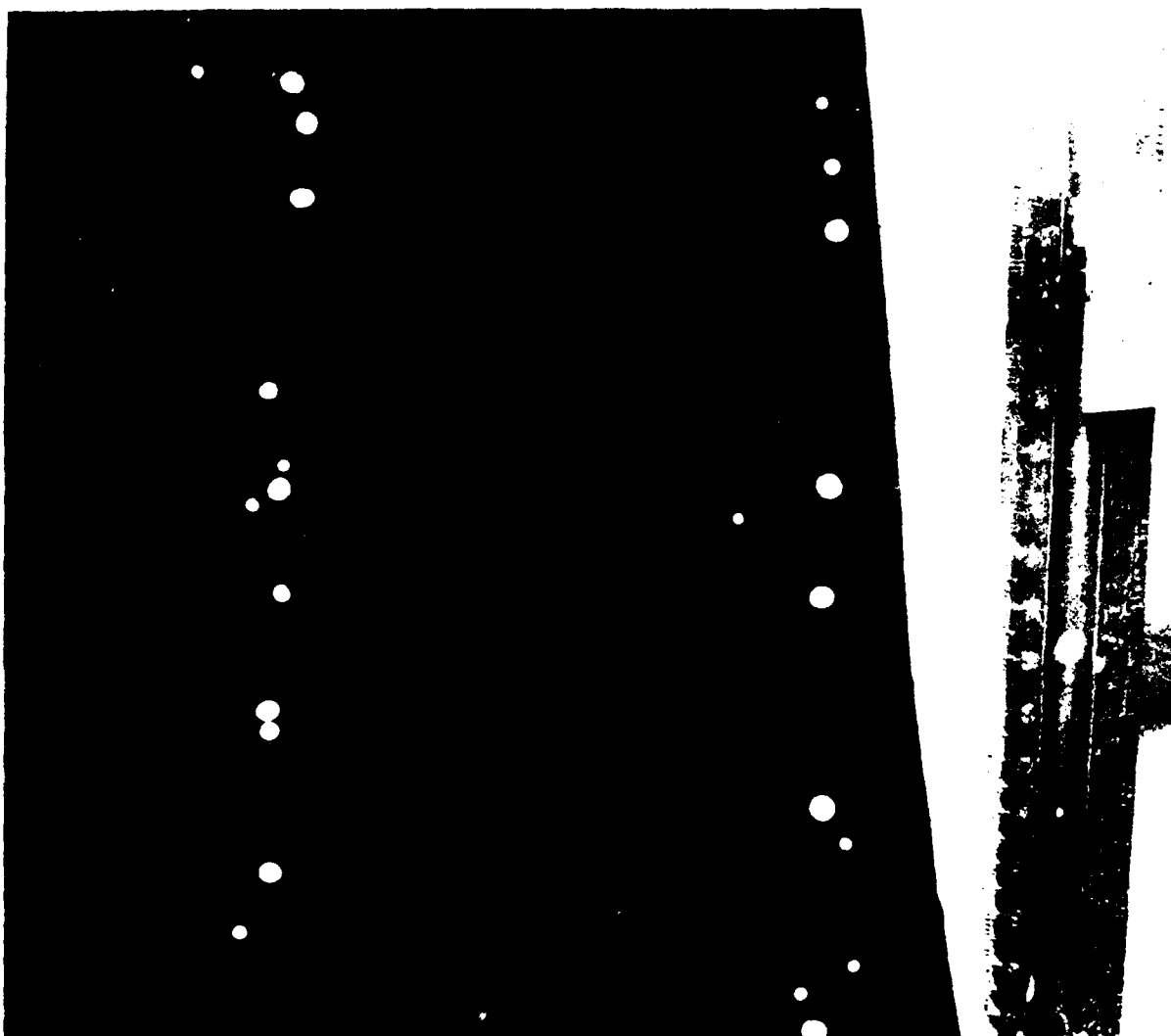


Figure 40. Drops from 3.10 mm orifice.

(Large drop diameter approximately 3.52 mm)

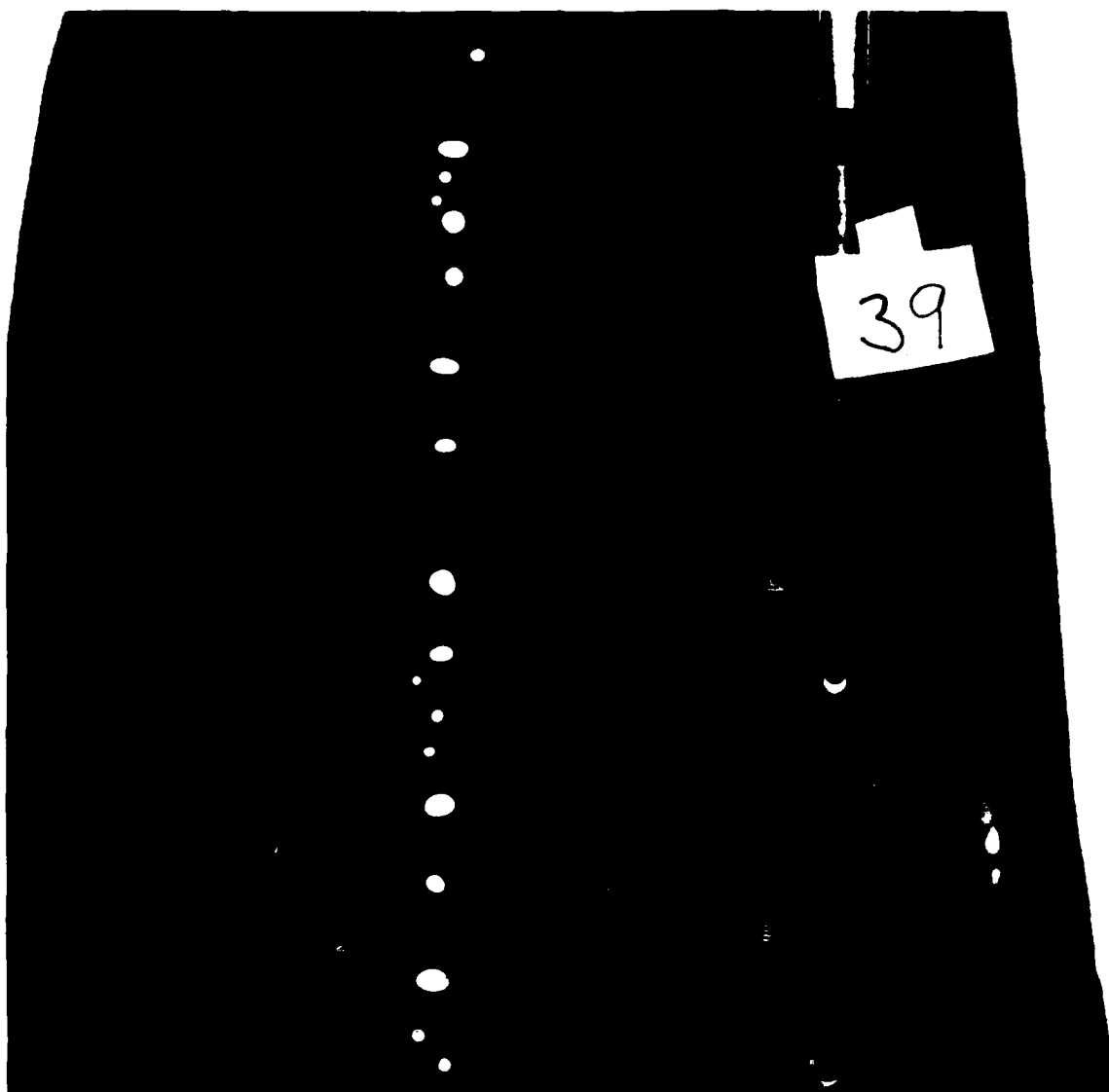


Figure 41. Drops from 4.76 mm orifice.

(Large drop diameter approximately 5.5 mm)

APPENDIX B. Raindrop Impact on Point Detonating Fuzes

Paper from

**PROCEEDINGS
of the
FUZE/MUNITIONS ENVIRONMENT
CHARACTERIZATION SYMPOSIUM (U)
(Volume 2: Sessions IV-VI)**

**Sponsored by
U.S. ARMY MUNITIONS COMMAND
PICATINNY ARSENAL**

**at
Picatinny Arsenal, Dover, N.J.
November 28 & 29, 1972**

RAINDROP IMPACT ON PD FUZES
(UNCLASSIFIED)

by

J. K. Domen

Picatinny Arsenal
Dover, New Jersey 07801

ABSTRACT

A summary is given of analytical expressions related to rainfields, and of specific information (graphs, tables) of reported rain drop size distributions per unit volume for various natural rains and artificial rains at testing facilities. A review is made of rather diverging analytical approaches to ascertain the pressure and force time pulse imparted by drops on rather rigid surfaces.

A computer simulation which employed momentum conservation is presented for a specific point detonating artillery fuze nose (spring-mass) response to high velocity flight in heavy natural and excessive artificial rainfall, with corresponding experimental results at Holloman Air Force Base.

A pertinent summary is given of experimental results of erosion of rain impacted surfaces, the basic phenomenon involved, methods employed for erosion abatement, and analytical considerations for erosion process.

RAINFIELD CHARACTERISTICS

For both naturally occurring and artificially produced rains, raindrop diameters range from a fraction of a millimeter to rarely over six millimeters. The liquid water content L (g/m^3) of rain is defined as water mass M for some given volume V where the sum is taken over all drops in the volume:

$$L = M/V = \frac{\pi \rho}{6V} \sum_{i=1}^F N_i D_i^3 \quad (\text{g}/\text{m}^3) \quad (1)$$

where F = Final group of drops.

N_i = Number of drops with average diameter D_i per volume V .

ρ = Water mass density ($1 \text{ g}/\text{cc}$).

The rainfall accumulation rate R (in/hr) is then given as:

$$R = x/t = \frac{\pi}{6V} \sum v_i N_i D_i^3 \quad (\text{mm/hr}) \quad (2)$$



where t = Time

v_i = Terminal velocity of drop of diameter D_i

x = Accumulation depth

For quiet conditions, all drops attain their terminal velocity⁽¹⁾ after a fall of about 50 feet, and this speed can be expressed approximately as:

$$v \text{ (ft/sec)} = 16 \sqrt[3]{D(\text{mm})} + 2 \quad (3)$$

for drops in the diameter range of 1 to 6 millimeters. A droplet of 1.5 mm diameter requires about 20 foot free fall to attain an 18 ft/sec terminal velocity. Table 1 lists the reported terminal velocity of drops.⁽²⁾

TABLE 1. WATER DROP TERMINAL VELOCITY

$D(\text{mm})$	$v \text{ (ft/sec)}$	$D(\text{mm})$	$v \text{ (ft/sec)}$
1.25	15.9	3.25	27.2
1.50	18.1	3.50	28.
1.75	20.	3.75	28.6
2.00	21.6	4.00	29.
2.25	23.	4.50	29.8
2.50	24.3	5.00	30.3
2.75	25.5	5.55	30.5
3.00	26.4	6.00	30.5

Water drops in an artificial field generally have a lower terminal velocity because of the small drop height, and consequently a higher drop concentration. An equivalent rate for the artificial field is defined as the rain rate obtained if the drops were travelling at their terminal velocity, and is higher than the usual accumulation rate.

The mean diameter ranges from 1.4 to 2.1 mm for natural rain and is that diameter drop having a mass equal to the mass content M divided by the total number of drops N per unit volume:

$$MD = \sqrt[3]{\frac{\sum N_i D_i^3}{N}} \quad (D \rightarrow \frac{M}{N}) \quad (4)$$

where $N = \sum N_i$ = Total number of drops in volume V .

The median diameter ranges from 1.2 to 2 mm for natural rain and is that diameter drop for which half the total mass M is above this diameter and half below. It occurs when during the summation from either spectrum end the equality occurs:

$$\sum N_i D_i^3 = \frac{1}{2} \sum_{i=1}^F N_i D_i^3 \quad (D \rightarrow M \dots) \quad (5)$$

An empirical logarithmic relation appears to exist between rainfall rate and liquid content. (3) Data for the range from moderate rain ($R = 3$ mm/hr) to cloudburst ($R = 100$ mm/hr) can be expressed as:

$$L(\text{g/m}^3) = 0.075 R^{0.864} \quad (\text{mm/hr}) \quad (6)$$

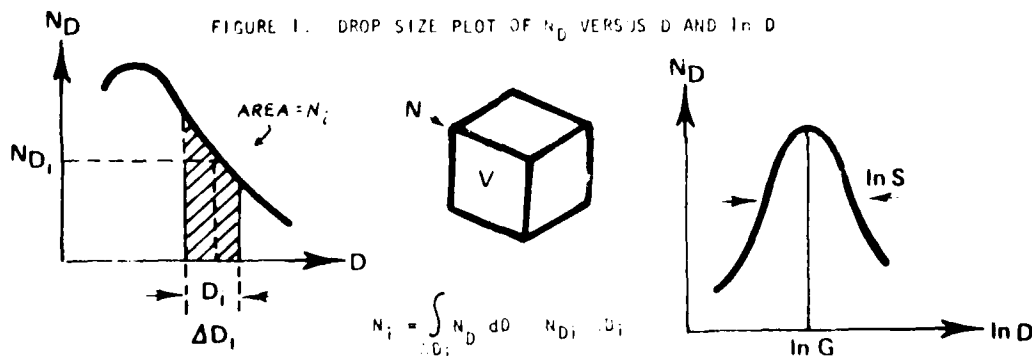
Logarithmic least squares fit for Miami, Florida data has been reported as: (4)

$$L(\text{g/m}^3) = 0.0525 R^{0.95} \quad (\text{mm/hr}) \quad (7)$$

Natural rain data indicates that the median or maximum drop diameter (mm) is proportional to the cube root of the rain rate (mm/hr). (4)

Natural rain spectrum of frequency of occurrence of drop diameter usually has a peak between 0.7 and 2 mm. If the frequency of drop size for natural rain is plotted versus the log of the drop diameter, the curve appears Gaussian normal (Figure 1). (5) Natural rainfall appears to plot well with the expression:

$$N_D dD = \frac{N}{\ln S \sqrt{2\pi}} e^{-\frac{1}{2} \left[\frac{\ln(D/G)}{\ln S} \right]^2} \quad d(\ln D) \quad (8)$$



where N = Total number drops per unit volume (area under either curve) = $\sum N_i$
 N_D = Number drops per unit volume per diameter interval
 N_i = Number drops in diameter interval ΔD_i centered at diameter D_i

G = Geometric mean diameter

$$\ln G = \frac{1}{N} \sum_i N_i \ln D_i$$

S = Geometric standard deviation

$$(\ln S)^2 = \frac{1}{N} \sum_i N_i (\ln D_i)^2 - (\ln G)^2$$

For a cited distribution of 114 mm/hr at the Canal Zone, these values are:

$$\begin{array}{ll} \ln G = .3414 & \ln S = .414 \\ G = 1.407 \text{ mm} & S = 1.513 \text{ mm} \\ \text{Mean Diameter} = 1.81 \text{ mm} & \text{Median Diameter} = 2.4 \text{ mm} \end{array}$$

Except for small diameter drops, another form has been used for N_D (drops per cubic centimeter per centimeter diameter) but has had limited success:⁽⁶⁾

$$N_D = 0.08 \text{ cm}^{-4} e^{-\lambda D} \quad (9)$$

where $\lambda(\text{cm}^{-1}) = 41 R^{-.21} (\text{mm/hr})$.

Natural Rainfall

Rain drops usually occur below 20,000 feet but may be found as high as 50,000 feet. They seldom appear above 35,000 feet.⁽⁷⁾ Drop size distributions are ordinarily reported and plotted in histogram form as the number of drops N_i per volume V within a certain diameter interval ΔD near a diameter D_i versus diameter D . A "standard" rainfall (Table 2) has been reported with 90% confidence that in 95% of the area-month combinations of the U.S., 99% of all rainfall intensities will be equal to or less than this standard of 2 in/hr.⁽⁸⁾

TABLE 2. DROP SIZE DISTRIBUTION OF "STANDARD" RAIN ($\Delta D = .25 \text{ mm}$)

$D_i (\text{mm})$	$N_i (\text{Drops}/\text{m}^3)$	$D_i (\text{mm})$	$N_i (\text{Drops}/\text{m}^3)$
.125	0	3.375	5.13
.375	1026	3.625	3.07
.625	452	3.875	1.84
.875	227	4.125	1.23
1.125	145	4.375	0.67
1.375	107	4.625	0.41
1.625	76	4.875	0.25
1.875	50	5.125	0.17
2.125	43	5.375	0.11

TABLE 2. DROP SIZE DISTRIBUTION OF "STANDARD" RAIN ($\Delta D = .25$ mm) - CONT'D

D_i (mm)	N_i (Drops/m ³)	D_i (mm)	N_i (Drops/m ³)
2.375	29	5.625	0.08
2.625	20	5.875	0.04
2.875	12	6.125	0.02
3.125	7.69	6.375	0.02
		$N = 2207.7$	

In Figure 2 is summarized for various world locations, the rainfall rate equalled or exceeded for an indicated percentage of total time in that location, not just during the time it is actually raining.⁽⁹⁾ This data is based on approximately one year, except Panama is exaggerated as data here is taken during the wet season from June to November. Table 3⁽⁹⁾ lists the rates not for just the percentage of total time (Figure 2) but also for the percent of time given that it is raining. Table 3 includes rates for desert and temperate-tropical regions. Specific data of natural rain drop sizes for the Canal Zone (Table 4 and Figure 3)⁽¹⁰⁾, Miami Table 5)⁽¹¹⁾, Marshall Islands (Table 6)⁽¹¹⁾ and North Carolina (Figure 4)⁽⁵⁾ was obtained by continuously photographing a small volume and obtaining the number and drop size per volume (m³). The average distributions for all major climatic zones are made from data at nine locations around the world with rates within $\pm 12\%$ of the average rate, and are plotted in Figure 5. Here, 927 samples were used for the 5.2 mm/hr rate and 154 for the 95.6 mm/hr.

TABLE 3. RAINFALL RATE (mm/hr) EQUALLED OR EXCEEDED FOR INDICATED PERCENTAGE OF

	RAIN AND NON-RAIN TIME				ONLY RAIN TIME			
	.01%	.1%	.5%	1%	.01%	.1%	.5%	1%
Arctic (Alaska)	9.	5.4	3.7	3.0	15.	8.2	5.8	4.8
Temperate (N.J.)	55.2	15.2	4.8	3.3	140.	72.	37.	24.
Tropical (Panama)	132.0	84.0	27.0	8.4	218.	139.	115.	98.
Desert (Arizona)	64.0	31.0	7.9	3.6	130.	80.	59.	40.
Temperate - Tropical (N.J., Florida, Panama, etc.)	95.6	45.6	13.3	5.2	189.	121.	87.	69.

Spacial Distribution of Raindrops

Quantitative information is not readily available for the spacial distribution between drops. Photographs do indicate non-uniform spacing and for simulation purposes a Poisson distribution might be reasonably assumed. For example, for a PD Fuze with a nose of effective frontal normal area A at high velocity v through a rainfield of N drops per volume V, consideration of the cylindrical volume swept out by the nose gives the average time between collisions (TBCOL):

$$TBCOL = 1/(NAv) \quad (10)$$

and the average distance between drops for a uniform drop spacing is $1/(NA)$. If $N = 10,000$ drops/m³, and the nose is 0.5" in diameter, the average distance becomes 0.787 m = 2.58 ft/per impact. With the Poisson term $NA = 0.387$ fraction drop impacted/foot travel, the probability of M impacts in one foot of travel becomes:

$$P(M) = \frac{e^{-NA} (NA)^M}{M!} \quad (11)$$

P(0) = .6791
P(1) = .2628
P(2) = .05085 (Probability of 2 drops in one foot travel = 5.1%)
P(3) = .00656

Artificial Rainfall

Data is reported for two facilities at Holloman Air Force Base, New Mexico:

(1) An artillery range where H - 1/2 U 80200 (deluge) nozzles are usually employed at 3 1/2 psi with each nozzle discharging 5.9 gal/min. The pipe supported nozzles stand on the ground, alternating on opposite sides, and spray at about 65 degrees above the horizontal. The accumulation rate from the nozzles is from about 20 to 36 in/hr. The drop intensity is nine times as heavy as tropical rain of 132 mm/hr. (2) Rocket mono-rail sled track, 35,000 feet long of which 6000 feet is through a rainfield produced ordinarily by the standard nozzle H - 1/4 U 8070 which gives a smaller number of drops and fewer large drops. Sled velocity up to Mach 5 is possible. If the deluge nozzles are employed, only about 2000 feet of the track can be used because of the high delivery rate.

The nozzles produce an excessive number of small drops (about 0.5 mm diameter) and there is insufficient drop height (especially for smaller size) to attain terminal velocity. The average drop size spectra for these facilities with their standard nozzles are listed in Table 7.⁽⁹⁾ Other reported "deluge" nozzle (M 1/2 U80200) distributions are in Table 8.^(12,13) The average standard artillery range and rocket track rainfields are plotted in Figure 6 and compared with tropical rain of 132 mm/hr. The natural rain falls between the two distributions for diameters greater than 2.6 mm. Figure shows scatter for the rocket track. More information is contained in reference 9.

Table 9 is a Sandia distribution.⁽¹⁴⁾

FIGURE 2. THE FREQUENCIES OF OCCURRENCES OF ONE-MINUTE RAINFALL RATES AT VARIOUS LOCATIONS IN TERMS OF PERCENTAGE OF TOTAL TIME

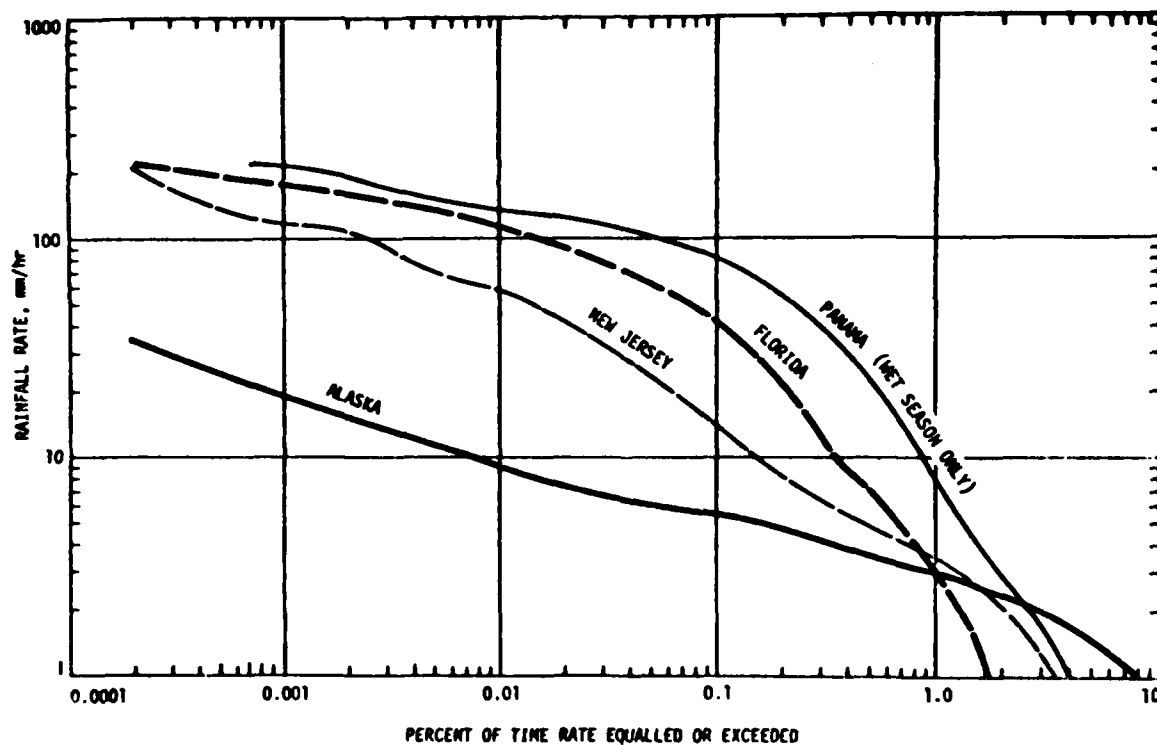


FIGURE 3. AVERAGE RAINDROP DISTRIBUTIONS FOR DATA TAKEN AT THE PINA RANGE, CANAL ZONE, JUNE 27 to JULY 19, 1968

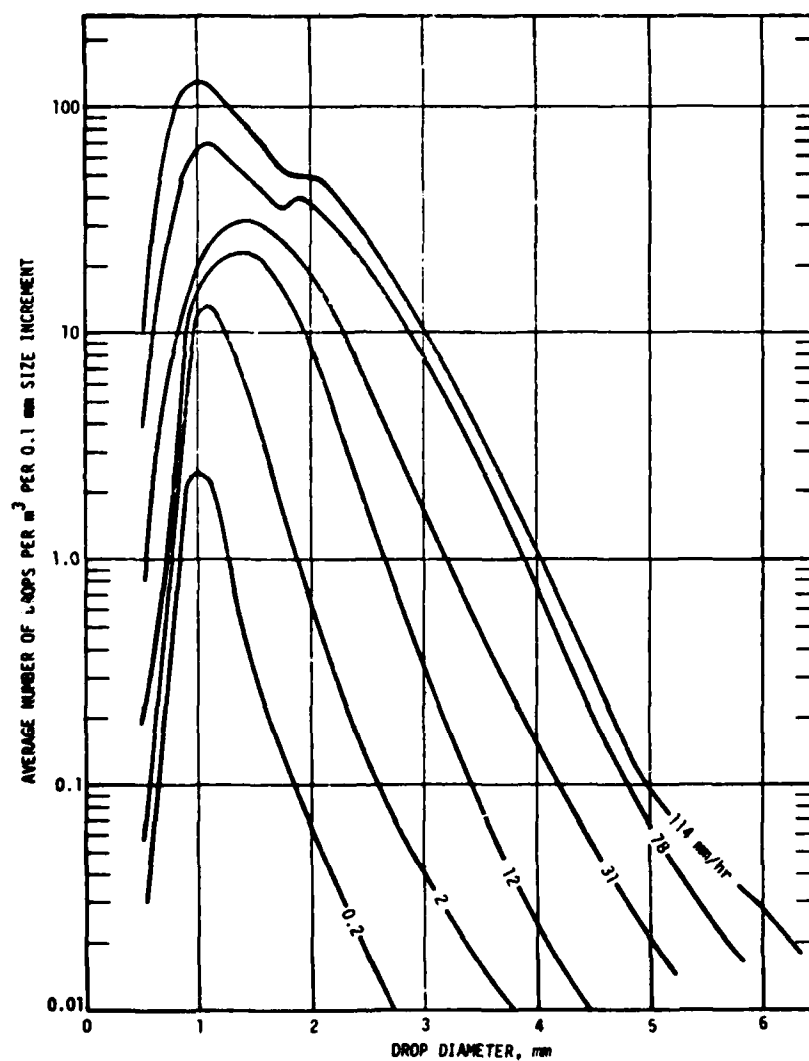


FIGURE 4. AVERAGE DROP SIZE DISTRIBUTIONS FROM NORTH CAROLINA
FOR VARIOUS RAINFALL RATES, MM/HR

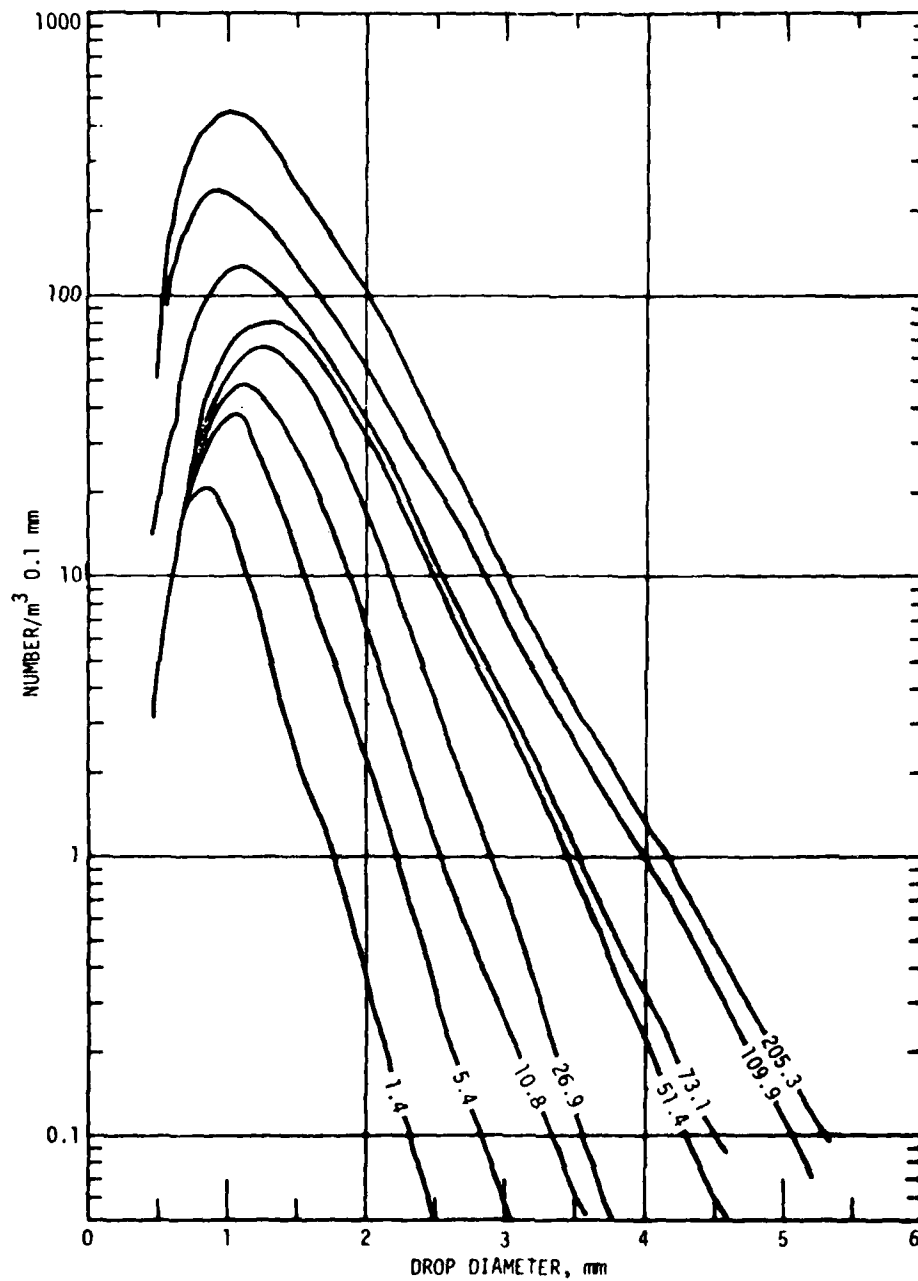


FIGURE 5. AVERAGE DROP-SIZE SPECTRA FOR NATURAL RAINFALL RATES OCCURRING 0.01, 0.1, 0.5 and 1.0% OF THE TIME (These curves are for all available data from nine locations in all major climatic zones around the world.)

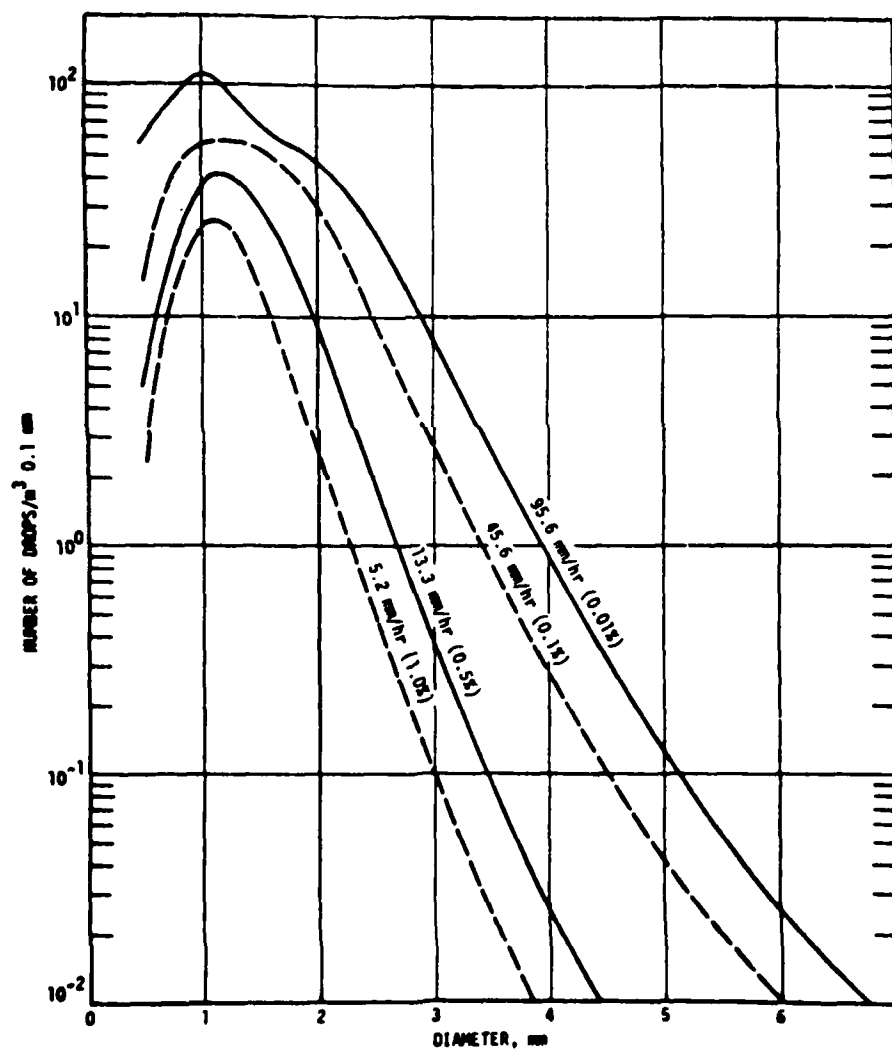


FIGURE 6. DROP-SIZE SPECTRA FOR THE ARTILLERY RAINFIELD, THE STANDARD TRACK RAINFIELD, AND FOR THE 132 MM/HR TROPICAL RAIN

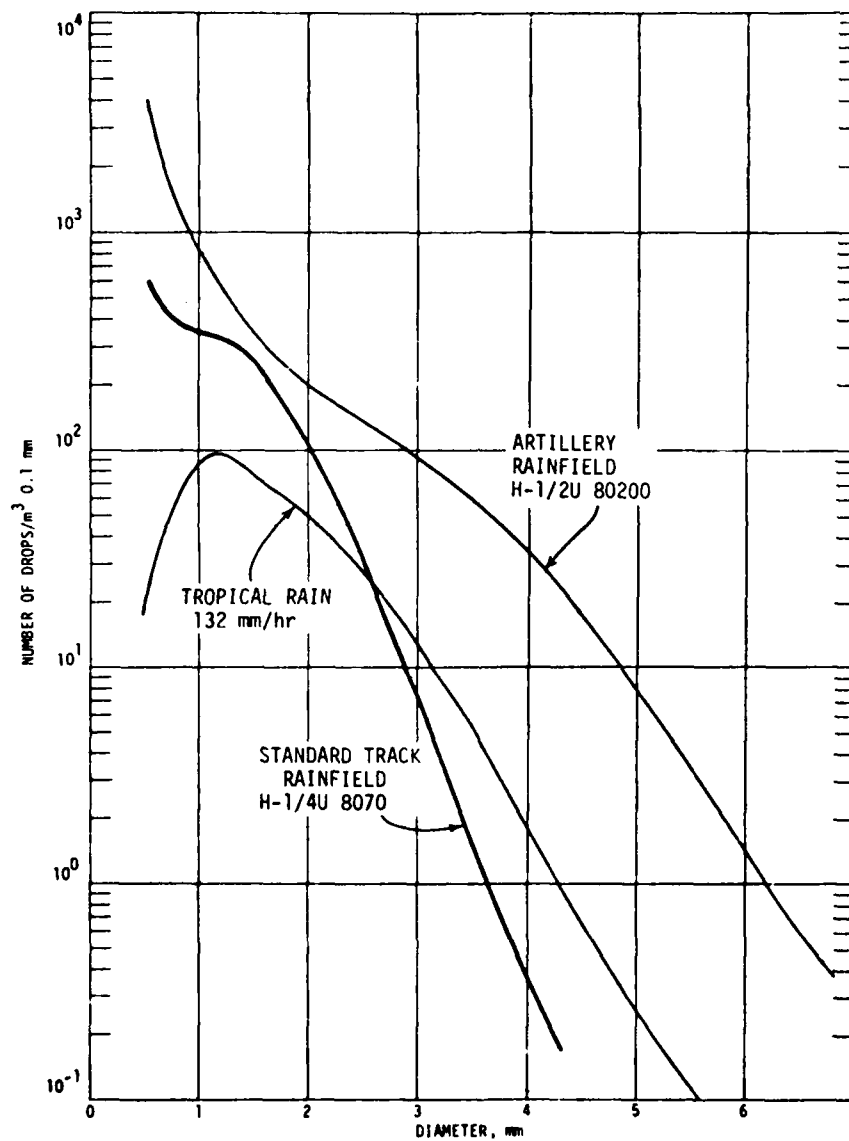


FIGURE 7. THE AVERAGE SPECTRUM FOR THE STANDARD ROCKET TEST TRACK RAINFIELD BASED ON FOUR NO-WIND TEST RUNS
(The vertical bars show the range of measurements from the four runs.)

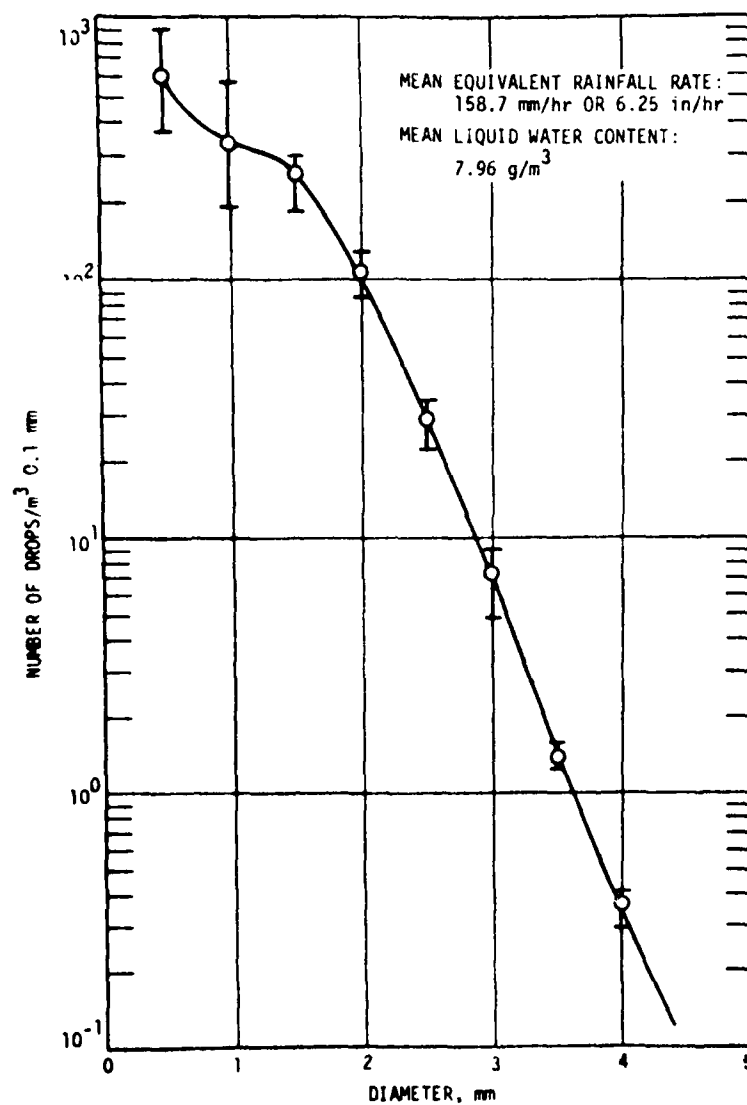


TABLE 4. AVERAGE RAINDROP DISTRIBUTIONS
CANAL ZONE (JUNE-JULY 1968)

($\Delta D = 0.2\text{mm}$)

	R(mm/hr) Rate			NS Number m ³ samples		
	L(g/m ³) Liquid Content			N Drops/m ³		
	DM(mm) Median Diameter					
R	0.2	1.	1.9	2.9	4.4	7.2
L	.01	.06	.11	.17	.24	.37
DM	1.4	1.5	1.5	1.6	1.6	1.8
NS	85.	120.	115.	83.	125.	163.
N	12.4	44.6	77.4	109.6	141.	178.
<u>D_i (mm)</u>						
.55	.12	.1	.21	.3	.28	.49
.75	.97	1.55	1.76	2.3	2.35	2.86
.95	4.3	10.9	15.6	16.1	18.4	17.2
1.15	4.08	14.8	27.2	31.9	39.5	38.9
1.35	1.7	8.9	16.85	30.3	36.2	44.4
1.55	.6	4.6	8.2	16.6	23.2	33.3
1.75	.23	2.35	3.8	6.85	11.	19.75
1.95	.18	.64	2.	3.2	5.6	10.5
2.15	.11	.37	.72	1.1	2.3	5.1
2.35	.06	.16	.47	.46	1.2	2.5
2.55	.02	.05	.25	.32	.4	1.38
2.75	.01	.07	.16	.12	.22	.55
2.95		.07	.11	.05	.19	.42
3.15		.03	.06	.01	.1	.27
3.35					.03	.19
3.55			.02		.05	.13
3.95		.01				.03
4.15		.01		.01		.01
4.35						.01
4.55					.01	
4.75						.01

TABLE 4. (CONT'D) AVERAGE RAINDROP DISTRIBUTIONS
CANAL ZONE (JUNE-JULY 1968)

($\Delta D = 0.2\text{mm}$)

R(mm/hr) Rate		NS Number m ³ Samples				
L(g/m ³) Liquid Content		N Drops/m ³				
DM(mm) Median Diameter						
R	11.7	18.8	30.5	49.4	77.9	114.
L	.57	.86	1.35	2.1	3.3	4.86
DM	1.9	2.1	2.2	2.4	2.5	2.4
NS	145.	82.	73.	64.	59.	15.
N	224.5	274.9	380.1	538.4	883.9	1461.2
<u>D_i (mm)</u>						
.55	.76	1.12	2.	4.9	14.2	24.7
.75	4.3	7.15	11.	25.9	60.2	124.2
.95	18.2	20.3	30.2	55.5	120.6	247.4
1.15	35.7	34.7	46.8	69.2	124.1	226.3
1.35	46.1	46.15	57.75	69.3	104.6	181.
1.55	43.2	48.2	58.2	65.2	85.6	136.2
1.75	31.9	40.8	51.6	62.05	76.9	112.5
1.95	19.7	29.4	42.9	55.1	77.3	102.
2.15	11.7	19.5	28.7	43.06	65.9	90.
2.35	6.03	11.3	18.6	29.3	51.	68.6
2.55	2.86	6.8	12.6	19.4	35.1	49.2
2.75	1.62	4.1	7.04	12.6	24.	32.4
2.95	.88	2.43	5.	8.9	15.7	24.3
3.15	.52	1.17	3.17	6.	10.5	14.5
3.35	.32	.68	1.5	4.16	7.1	10.2
3.55	.11	.45	1.35	3.14	4.5	7.6
3.75	.08	.24	.7	1.67	2.71	4.
3.95	.04	.22	.44	1.04	1.35	2.68
4.15	.02	.09	.24	.91	.89	1.4
4.35	.02	.04	.13	.34	.62	.84
4.55		.02	.04	.24	.27	.49
4.75	.01		.04	.2	.25	.21
4.95			.04	.13	.09	.14
5.15				.06	.2	.07
5.35			.01	.05		.14
5.55			.01	.02	.2	.07
5.75			.01	.02		
6.35	.01	.01			.02	.07
6.75				.02		

TABLE 5. RAINDROP SIZE DISTRIBUTION
MIAMI, FLORIDA

TH = Thunderstorm

CR = Continuous Rain

RS = Rain Showers

R = Rain

D(mm)	Wet Season			Dry Season		
	TH	CR	RS	TH	RS	R
.5	185	0	2	85	0	0
.6	220	4	0	252	1	0
.7	387	12	0	673	4	0
.8	589	29	1	1032	6	2
.9	1029	101	6	1883	6	4
1.0	1393	210	41	1426	13	29
1.1	1670	365	124	1843	25	102
1.2	1966	407	238	1778	40	171
1.3	2087	516	561	2121	41	292
1.4	2111	612	1107	2188	59	407
1.5	2072	736	1837	2303	68	454
1.6	2081	803	2482	2223	102	429
1.7	1882	611	2316	2240	111	522
1.8	1551	546	2005	2129	133	605
1.9	1517	492	1785	1646	115	584
2.0	1280	425	1352	1363	109	474
2.1	999	309	719	1411	79	348
2.2	891	202	460	933	37	225
2.3	696	191	399	767	41	194
2.4	658	159	325	586	25	154
2.5	540	157	237	557	28	100
2.6	433	159	192	516	16	63
2.7	342	108	104	441	23	55
2.8	296	113	52	215	18	47
2.9	281	65	41	172	20	25
3.0	218	64	24	107	11	16
3.1	187	47	7	100	6	13
3.2	163	32	2	87	8	14
3.3	101	14	3	66	5	7
3.4	98	17	1	41	2	5
3.5	87	19	2	50	2	4
3.6	96	9		28	1	1
3.7	55	6		25	0	4
3.8	68	7		12	2	4
3.9	64	3		8	0	4
4.0	49	1		16	2	2
4.1	50	4		17		1
4.2	39	1		7		1
4.3	23	1		11		
4.4	19	2		5		
4.5	13	0		6		
4.6	15	0		4		
4.7	5	0		3		
4.8	10	1		4		
4.9	7			1		
5.0	9			2		
5.1	3			2		
5.2	7			2		
5.3	6			0		
5.5	4			2		
5.6	3			2		
5.7	1					

TABLE 6. AVERAGE RAINDROP SIZE DISTRIBUTION
MARSHALL ISLANDS

R(mm/hr) N(/m ³)	1	2	4	7.1	12.6	24.8	47.3	94.8	170.5
D(mm)	94.87	169.54	252.4	370.33	615.32	869.44	1212.66	2120.22	2420.17
.5	5.61	8.61	4.03	2.59	7.77	6.6	16.67	128.53	25.
.6	7.29	12.37	8.07	7.06	21.32	13.12	37.11	90.3	63.13
.7	10.14	17.33	15.35	16.17	33.42	21.96	56.94	167.59	59.62
.8	12.76	21.33	24.56	32.08	49.49	41.18	79.73	158.6	120.68
.9	13.32	22.	28.64	36.95	49.4	42.13	81.88	195.89	125.84
1.0	15.02	26.25	45.98	62.17	85.	99.85	113.42	183.81	233.4
1.1	10.69	19.34	35.59	54.51	79.52	104.27	96.66	135.45	222.45
1.2	7.22	14.43	28.	46.52	70.95	98.3	95.26	111.69	187.22
1.3	4.67	9.22	19.71	34.78	58.5	97.18	91.44	106.52	152.5
1.4	2.88	6.17	13.23	24.23	48.77	83.89	87.91	94.95	133.8
1.5	1.92	3.97	9.77	16.85	34.45	68.42	79.1	98.15	112.52
1.6	1.15	2.55	6.45	11.3	25.2	53.41	74.56	90.3	119.85
1.7	.76	1.71	4.05	7.4	17.33	42.1	63.91	86.17	118.71
1.8	.54	1.37	2.95	5.69	11.37	35.1	59.38	93.3	123.47
1.9	.31	.88	1.87	3.52	7.75	20.38	45.55	65.09	82.45
2.0	.24	.65	1.29	2.42	5.51	16.04	37.8	72.12	96.91
2.1	.13	.39	.78	1.82	3.12	8.81	25.83	45.25	72.53
2.2	.07	.29	.57	1.08	1.95	6.29	21.32	42.15	49.08
2.3	.05	.22	.43	.83	1.25	3.64	13.49	30.79	53.73
2.4	.05	.16	.4	.63	.78	2.55	10.16	30.79	56.72
2.5	.02	.07	.23	.51	.42	1.61	6.63	20.77	38.33
2.6	.02	.07	.12	.38	.47	1.	5.11	21.39	37.92
2.7	.01	.04	.09	.19	.28	.37	3.19	14.88	29.86
2.8	.01	.03	.05	.23	.29	.52	2.81	9.71	22.94
2.9	.01	.02	.03	.11	.25	.26	1.64	7.44	18.29
3.0		.01	.05	.05	.18	.03	1.21	6.3	15.7
3.1		.03	.01	.07	.1	.06	1.18	3.2	10.02
3.2		.00	.03	.07	.18	.09	.86	2.58	8.47
3.3		.01	.01	.01	.11	.03	.57	2.17	6.82
3.4		.01	.01	.00	.05	.09	.23	1.03	3.62
3.5		.01	.01	.02	.01	.06	.32	.72	2.89
3.6				.00	.01	.00	.26	.62	2.89
3.7				.01	.05	.06	.14	.31	3.
3.8					.00		.09	.21	2.17
3.9					.03		.09	.31	1.65
4.0					.00		.03	.21	.93
4.1					.01		.00		1.14
4.2							.00		1.34
4.3				.02			.03		.52
4.4				.01	.01		.03		.52
4.5				.01			.03	.21	.21
4.6					.01		.03		.21
4.7							.00		.00
4.8						.03	.00		.41
4.9						.03	.03		.31
5.0					.01				.1
5.3								.1	.1
5.4								.21	.1
5.5				.01				.00	.00
5.6				.00				.00	.1
5.7				.01				.21	

TABLE 7. HOLLOMAN AVERAGE DROP SIZE SPECTRUM
ARTILLERY RANGE (STANDARD NOZZLE H-1/2 U 80200)

D(mm)	No./m ³ 0.1 mm	No. Drops/m ³ ≤ D	Water in Drops ≤ D (g/m ³)
0.5	4059	4059	.36
0.7	1650	7584	.98
1.0	820	11089	2.51
1.5	340	13463	5.49
2.0	210	14743	9.70
2.5	140	15573	15.28
3.0	96	16150	22.18
3.5	60	16517	29.32
4.0	33	16726	35.47
4.5	17	16840	40.29
5.0	7.9	16897	43.68
5.5	2.4	16922	45.60
6.0	1.4	16932	46.65
6.5	0.5	16936	47.12
All Sizes		16941	47.68

ROCKET TEST TRACK (STANDARD NOZZLE H-1/4 U 8070)
(NEGLECT DROP < 0.5MM IN DIAMETER)

D(mm)	No. Drops/m ³ ≤ D	Water in Drops ≤ D (g/m ³)
0.75	1450	0.209
1.25	3110	1.256
1.75	4345	3.617
2.25	4882	5.938
2.75	5032	7.165
3.25	5068.9	7.687
3.75	5076.6	7.860
4.25	5078.6	7.927
4.75	5079.2	7.958

	Artillery Range	Rocket Track
L(g/m ³)	47.7	7.96
Equivalent Rainfall Rate	1257mm (49.5 in)/hr	158.7mm (6.25 in)/hr
Mean Volume Diameter (mm)	1.75	1.44
Median Volume Diameter (mm)	3.21	1.8

TABLE 8. HOLLOWMAN DROP SIZE SPECTRUM
(H 1/2 U 80200 NOZZLES AT 6 PSI MANIFOLD PRESSURE)

A. Reference 12.		$\Delta D = 0.5\text{mm}$
Di	Average Ni (Drops/m ³)	Range of Ni
0.5	18000	
1.0	7500	6900 - 2900
1.5	3200	6900 - 1200
2.0	1400	2300 - 650
2.5	600	790 - 220
3.0	250	460 - 150
3.5	100	240 - 12
4.0	50	81 - 12
4.5	19	
5.	8	

B. Reference 13. - [Flour Pellet Sampling Method (33.1 in/hr fall). Two extreme samples.]

No. Drops/m ³		
Diameter (mm)	Sample 2	Sample 4
0.5 - 1.0	5910	4400
1.0 - 1.4	1279	891
1.4 - 2.0	1247	883
2.0 - 2.4	519	407
2.4 - 2.8	477	419
2.8 - 3.3	317	316
3.3 - 4.0	127	139
4.0 - 4.7	44	71
4.7 +	18	40
	N = 9938.	7566.

TABLE 9. SANDIA FACILITY DROP DISTRIBUTION
(TERMINAL VELOCITY NOT ATTAINED) FOR RATE ABOUT 5.5 IN/HR
(DROPS PHOTOGRAPHED AT OIL INTERFACE)

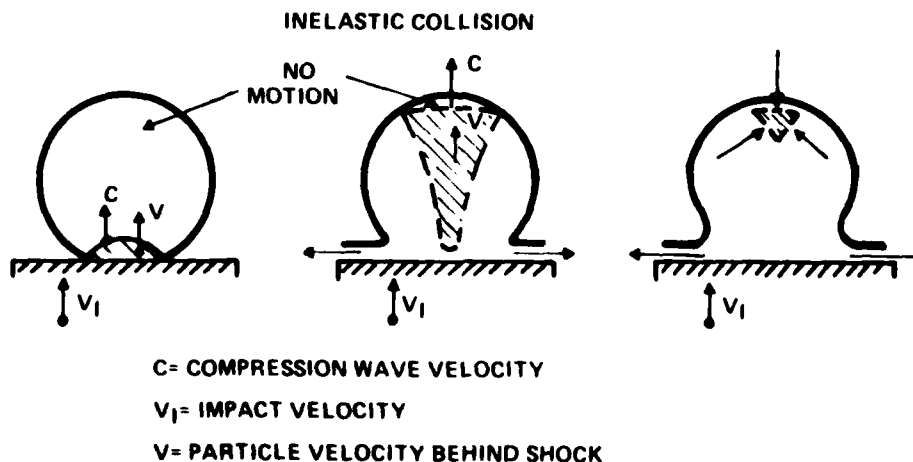
Di (mm)	Ni (Drops/ft ³)	Weight Grams (10 ⁻³)
0.5	48	3.23
1.0	90.7	47.6
1.5	70.6	125.
2.0	14.5	60.8
2.5	0.7	5.9
3.0	0.7	10.2
3.5	0.7	16.4
	N = 226/ft ³	

FORCE-PRESSURE-TIME PROFILE OF IMPACTING WATER DROPS

From a practical aspect, knowledge of the dynamic interaction of a water drop with a finite solid surface system at any impact velocity appears incomplete, both analytically and experimentally. The situation appears worse when the "surface" is a system which has significant gross motion during the interaction. Hydrodynamic codes are being employed for hypersonic collisions of solid targets with solid and liquid particle projectiles⁽¹⁵⁾ and experiments with piezoelectric transducers for determining force-time from supersonic impacts in heavy rainfall are continuing.⁽¹⁶⁾ Several complications arise in the general question of the specific force-pressure-time profile between drop and system:

- a) The drop is not always spherical in a rainfield.
- b) The bow shock preceding a supersonic system offers some degree of acceleration and deformation of the drop before system collision.
- c) Complicated by geometry and system and drop compressibility, a pattern of pressure and tension waves traverse the drop as partially illustrated in Figure 8.⁽¹²⁾

FIGURE 8. QUALITATIVE PROFILES OF INITIAL WAVES IN LIQUID DROP



At first, as a rigid mass at velocity V_1 strikes a stationary drop, a shock wave originates at the interface, moves with velocity C into the drop, accelerating the water traversed to some average speed V . As the shock propagates, reflected tension release waves at speeds generally less than C are reflected from the free boundary and penetrate the shocked fluid. A rarefaction shock cannot exist in a liquid. A pressure gradient induces radial flow while water above the shock front remains at zero velocity. Some spalling at the back of the drop might be expected as the reverse tension wave is initiated. It appears that the drop encounter is essentially inelastic (or plastic) as the mass of the drop is splashed in a direction along the surface such that for a normal encounter as illustrated, the momentum imparted to the system = mV_1 . No experimental references cite a significant rebound of the drop mass on a rigid surface. Photographs of a 2 mm diameter drop on a hard smooth magnesium alloy at 1000 ft/sec revealed negligible spalling.⁽¹⁷⁾ Correlation of energy required to statically deform a honeycomb crush type PD fuze with raindrop energy available from high velocity sled tests at Holloman Air Force Base indicated a plastic type collision.⁽¹²⁾

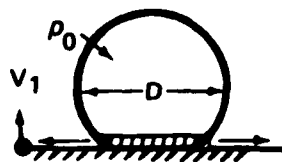
d) The net axial force at any time is the integral of pressure over the effective contact area; but pressure appears as some function of radial distance along the contact area, increasing during the earlier stages, and decreasing during the later stages of the encounter.

Some liberty will be used in interpreting four chosen experimental-analytical models to arrive at the magnitude of pressure expected on PD fuzes.

Model 1. Incompressible Drop-Incremental Momentum Transfer

An unrealistic model of the encounter takes no consideration of shock wave propagation into the drop, with the drop imparting forward momentum to the system in incremental mass slices dm as the system surface with velocity V_1 sweeps over the drop (Figure 9). If the system is very massive and rigid:

FIGURE 9. INCREMENTAL MASS MODEL



$$dm = \pi R_0 V_1^2 (D-r) dt \quad (12)$$

$$\text{Force } F = V_1 \frac{dm}{dt} = \pi R_0 V_1^3 t (D - V_1 t) \quad (13)$$

$$\text{for } 0 < t < D/V_1$$

where m - Drop mass

r - Distance into drop

R_0 - Density of uncompressed water

t - Time

The drag coefficient force expression with the dynamic pressure is:

$$F = C_d R_0 V_1^2 A/2 \quad (14)$$

This is identical to expression (13) with drag coefficient $C_d = 2$ for plastic encounter, and the contact area interface $A = \pi V_1 t (D - V_1 t)$. Such an encounter implies a constant pressure $R_0 V_1^2$ throughout the collision and a parabolic profile of the contact force (Figure 10).

Representative values are in Table 10.

FIGURE 10. INCOMPRESSIBLE DROP FORCE-TIME PROFILE

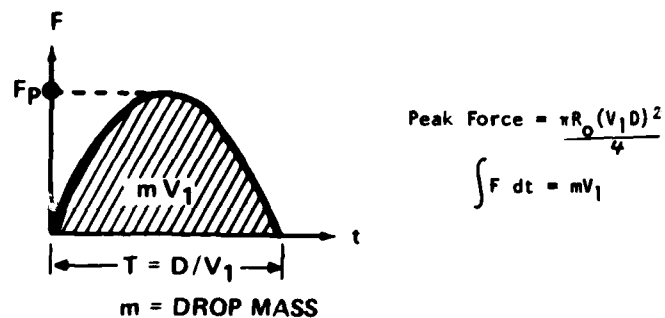


TABLE 10. REPRESENTATIVE VALUES IN INCOMPRESSIBLE DROP MODEL

D(mm)	V_1 (Ft/Sec)	Pressure (KSI)	Peak (Lb)	T (Microsec)
2	2000	54.	262.	3.28
	3000	121.	590.	2.18
	4000	216.	1050.	1.64
3	2000	54.	590.	4.92
	3000	121.	1330.	3.28
	4000	216.	2360.	2.46
6	2000	54.	2360.	9.84
	3000	121.	5310.	6.56
	4000	216.	9450.	4.92

Model 2. Colliding-Compressible Cylinders, Laterally Constrained

Though neglecting the geometry of drop and system, a more realistic approach for interpreting initial stages of contact is the usual column of height H of compressible water, constrained laterally to avoid pressure release effect, struck by a similar infinitely wide elastic solid surface system with the generation of planar pressure waves. Figure 11 shows a cross section cut out of an infinite width of the process.

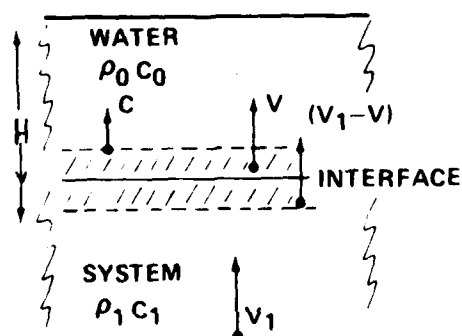
FIGURE 11. INFINITE PLANE COMPRESSIBLE WATER-SOLID SYSTEM

PRESSURE BALANCE:

$$P = \rho_1 C_1 (V_1 - V) = \rho_0 C V$$

$$P = \frac{\rho_0 C V_1}{1 + \frac{\rho_0 C}{\rho_1 C_1}} \rightarrow \rho_0 C V_1$$

(WATERHAMMER)



- where
- C_0 - Acoustic velocity in water (4800 ft/sec at 20°C)
 - C_1 - Acoustic velocity in solid system
 - C - Shock pressure wave velocity in water
 - H - Height of water column initially at rest
 - ρ_0 - Density of uncompressed water
 - ρ_1 - Density of solid system
 - V_1 - Impact velocity of solid system
 - V - Particle velocity in water, or interface velocity during impact
 - $(V_1 - V)$ - Particle velocity in system surface
 - Z_0 - Impedance of water = $\rho_0 C_0$
 - Z_1 - Impedance of solid system = $\rho_1 C_1$
 - Z - $\rho_0 C$

For pressure balance at interface:

$$P = R_1 C_1 (V_1 - V) = R_0 C V = \frac{Z V_1}{1 + Z/Z_1} \quad (15)$$

In Z, the wave speed corresponding to the pressure rise created by the wave must be used and not the acoustic speed of the undisturbed liquid. An empirical expression has been reported for the shock wave velocity C at which the pressure wave propagates upstream through the fluid: (18)

$$C = C_0 + kV \quad k = 2 \text{ for } 0 < V/C_0 < 1.2 \quad (16)$$

$$k = 1.33 \text{ for } 1.2 < V/C_0 < 2$$

where V is the particle velocity in water and is approximately expressed as:

$$V = V_1 \left[\frac{Z_1/Z_0 + k(V_1/C_0)}{1 + (Z_1/Z_0) + 2k(V_1/C_0)} \right] \cong V_1 B \quad (17)$$

on the condition that:

$$k(V_1/C_0) [1 + k(V_1/C_0)] \ll [1 + (Z_1/Z_0) + 2k(V_1/C_0)]^2 \quad (18)$$

A more approximate expression for V is:

$$V = V_1 \left[\frac{1}{1 + Z_0/Z_1} \right] \cong V_1 B' \quad (19)$$

Thus, the pressure becomes:

$$P = R_0 (C_0 V + kV^2) \quad (20)$$

The impedance ratios for B' for aluminum, steel-water interfaces, with B and C (ft/sec) for various impact velocities V_1 are listed in Table 11.

TABLE 11. IMPEDANCE RATIOS, PARTICLE VELOCITIES, SHOCK VELOCITIES FOR ALUMINUM, STEEL-WATER INTERFACES

Z_1/Z_0	Aluminum-Water		Steel-Water	
	9.4		26.7	
B'	0.9		0.96	
V_1 (Ft/Sec)	B	C	B	C
100	.9	4980	.96	5000
1000	.874	6500	.95	6700
2000	.85	8200	.94	8560
3000	.83	9780	.93	10400
4000	.81	11280	.91	12100
6000	.77	14000	.89	15500

This approach indicates shock wave velocity much higher than acoustic velocity in water with water molecules accelerated close to the initial impingement velocity V_1 . The force exerted at the interface area A would be a constant: $F = AP$. If the surface system is taken to be incompressible, Z_1 goes to infinity, and the usual waterhammer expression results:

$$P = R_0 CV_1 \quad (21)$$

as the pressure existing, e.g., at a valve when suddenly closed to water moving at velocity V_1 in a pipe. If the water is of height H , this pressure exists for approximately $2H/C$, when the reflected pressure release wave begins arriving at the valve, resulting in a negative pressure contribution there. Dissipation dampens these reflections.

A momentum approach results in the same waterhammer expression: If a slab of liquid of area A , thickness x , is accelerated to a velocity V_1 during the time t it takes a stress wave at speed C to move over x , then the force on the slab is $F = R_0 ACV_1$. The pressure is $R_0 CV_1$. Deviation from reality of the compressible cylinder approach:

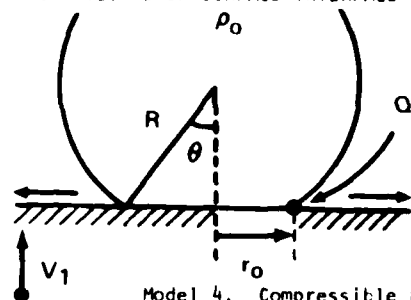
1. The surface system is a finite solid acted on over a small area, with corresponding smaller system particle velocity ($V_1 - V$) than is implied.

2. The pressure gradient between the inside where waterhammer pressure exists and the free boundary causes radial flow at velocity V_r . Initially, regardless of geometry, the radial flow stagnation pressure ($R_0 V_r^2/2$) should grossly equal the waterhammer pressure ($R_0 CV_1$) or $V_r = \sqrt{2CV_1}$. V_r becomes several times the impact velocity but only for a small portion of the drop mass flow. For a flat ended, free boundary liquid cylinder of radius R , the impact interface area over which the waterhammer pressure acts is released in about the time R/C_0 after impact. The drop is not a flat-ended cylinder, but offers changing contact area as collision progresses.

Model 3. Hydrodynamic Incompressible Drop and Rigid Solid Surface

This treatment⁽¹⁹⁾ concluded that maximum pressure occurs in an outer ring of the circle of contact (Figure 12), with pressure increasing with the radial distance along the plane of contact up to this ring. When the ring of contact is about $0.6R$, this ring of maximum pressure vanishes and maximum pressure, now the dynamic pressure $R_0 V_1^2/2$, exists at the center with pressure decreasing across the contact area from the center to the periphery of the circle of contact (Table 12).

FIGURE 12. DROP-SURFACE INTERFACE



Model 4. Compressible Drop on Flat Solid Surface (Engel)

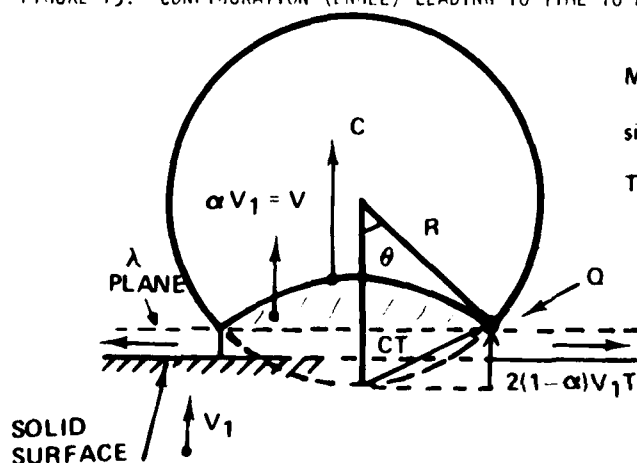
TABLE 12.

MAXIMUM PRESSURE = $a\rho_0 V_1^2$
AT Q

r_0	a	θ°
0.1R	3.0	6
0.2R	1.5	11
0.3R	1.0	17
~ 0.6R	0.5	37

An approach, still not without disconcerting features, allows for the compressibility of a spherical drop in that the waves are not all started simultaneously, but employs some planar wave assumptions. (20,21,22) In a region traversed by the compression wave, αV_1 is defined as the average axial velocity acquired by the water molecules. α , thus, is a measure of what fraction of impact velocity V_1 is imparted to the water molecules on the average from the compression wave traveling through the drop. ($\alpha = 0$ would imply no compression wave; $\alpha = 1$, that the wave brings water molecules up to the striking surface velocity.) α is said to be governed mainly by divergence of the wave as it spreads through the drop. As collision continues, shock waves are initiated at contact points of the sphere and the λ plane (upper) boundary of radial flow (see Figure 13). Maximum pressure may be expected at region Q where water is being accelerated both by the shock wave arrival and by the effective (λ plane) solid surface front. As velocity V_1 increases, wave divergence decreases and α approaches unity.

FIGURE 13. CONFIGURATION (ENGEL) LEADING TO TIME TO MAXIMUM PRESSURE AT OUTER RING



MAX PRESSURE AT Q:

$$\sin \frac{\theta}{2} = \frac{2(1-\alpha)V_1}{c} = \frac{CT}{2R} \quad (22)$$

T = TIME TO REACH MAX PRESSURE

With 0.9 taken arbitrarily for α , and C from equation 16 for aluminum-water, values for this approach are listed in Table 13.

TABLE 13. TIME T TO MAXIMUM RING PRESSURE ($\alpha = 0.9$, ALUMINUM-WATER)

D(mm)	V_1 (Ft/Sec)	θ (Deg)	T(Microsec)	C(Ft/Sec)
2	1000	.9	.03	6500
	3000	1.8	.09	9780
5	1000	.9	.08	6500
	3000	1.8	.10	9780

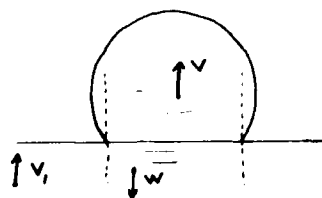
However, it has been reported⁽²³⁾ that high speed lateral flow begins when $\theta = 17^\circ$ independent of impact velocity; and that maximum impact force is approximately proportional to impact velocity, implying constant effective impact area.

It is stated that the (average) maximum pressure created during the compression wave period is:

$$P = \alpha R_0 C V_1 / 2 \quad (23)$$

This expression relates to the time averaged impact pressure over the entire collision rather than to the maximum pressure which occurs at the edges of the contact area, and which decays rapidly because of radial flow. Values for α were determined from pit-depth equation which involved the time for the entire process. Some inferences about α were derived by considering that particle velocity imparted to the drop should be some fraction α (to maintain contact at the interface) of the velocity change in the solid system. The usual constrained cylinder intersects the periphery of the drop (Figure 14).

FIGURE 14. CONFIGURATION FOR α DERIVATION

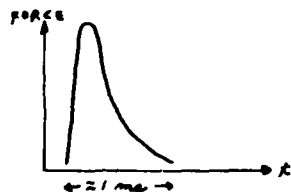


$$\begin{aligned}
 V &< (V_1 - W) \\
 V &= \alpha(V_1 - W) \\
 (1 - \alpha) V_1 &= V_1 - V - \alpha W \approx V_1 - V \text{ (for rigid surface)} \\
 V &\approx \alpha V_1
 \end{aligned} \quad (24)$$

where V - Particle velocity in compressed water
 V_1 - Initial impact velocity of solid on stationary drop
 W - Particle velocity in compressed solid

$(1-\alpha)V_1$ becomes the velocity at which the surface moves through the drop. This appears to effectively lengthen the collision duration by a factor $1/(1-\alpha)$ longer than D/V_1 . In an experiment with a 5.7 mm diameter drop at its $V_1 = 26.9$ ft/sec terminal velocity, the value of α was determined by observing the radial flow velocity and using the Bernoulli relation $V_r = \sqrt{\alpha CV_1}$ to determine α as 0.4. A barium titanate disk coated with silver, lacquered and cemented with polystyrene adhesive to a metal base showed the force for a 40 foot fall of this drop rose very rapidly and underwent a rapid decay to zero in about one millisecond (Figure 15). The interaction time appeared extended from 0.7 ms (D/V_1) to about 1.2 ms.

FIGURE 15. FORCE PROFILE FROM LOW VELOCITY DROP



It appears difficult to set up force and pressure time curves for any of the last three models. Calculated comparison pressure magnitudes for the four models are listed in Table 14.

TABLE 14. COMPARISON OF ESTIMATED INTERFACE PRESSURE (KSI) OF VARIOUS MODELS FOR 5 MM DIAMETER WATER DROP

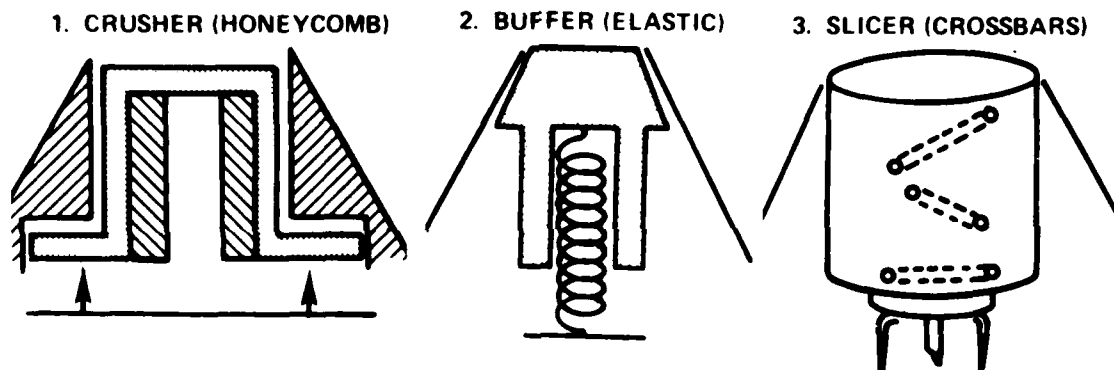
Impact Velocity V_1 (Ft/Sec)	Aluminum-Water		Steel-Water	
	1500	3000	1500	3000
1. $R_0 V_1^2$ (Momentum Transfer)	30	121	30	121
2. a. $\frac{R_0 C V_1}{1 + \frac{R_0 C}{R_1 C_1}}$ (Modified Waterhammer)	128	324	145	386
b. $R_0 C V_1$ (Waterhammer)	149	394	154	418
3. $3 R_0 V_1^2$ (Hydrodynamic)	91	364	91	364
4. $R_0 C V_1 / 2$ (Engel)	75	197	77	209

Water shock velocity C calculated from (15). α (Engel) taken as 1. Momentum transfer model pressure constant for entire collision. Other pressures are pertinent for "initial" stages of collision.

SIMULATION OF SPRING-MASS PD AT HIGH VELOCITY IN RAIN

For an analytical description, the system impacted appears as an involved mechanical system. Three common rain PD desensitizers (Figure 16) are illustrated: (1) Crusher with a honeycomb fixture supporting the PD for absorbing the kinetic energy of drops; (2) Buffer with some effective spring mass system which buffers momentum onto the shell, continuously restoring itself to initial position; (3) Slicer⁽²⁴⁾ employing some recessed cavity with, e.g., crossbars of sufficient strength to shatter the drops into smaller size and simultaneously buffer some momentum onto the shell. Soft target sensitivity and erosion dictate limits on such designs.

FIGURE 16. PD RAIN DESENSITIZING DESIGNS



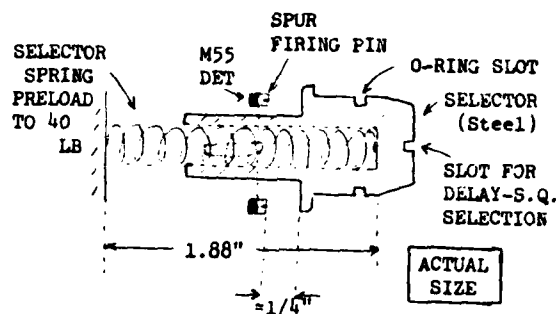
Simulation Procedure for Buffer System

In an elementary approach, the conservation of momentum mv_i (m = drop mass, v_i = impingement velocity) can be used with certainty, and the initial energy with reservation because of its uncertain distribution between consequent gross system motion and heat dissipation; but neither is of immediate assistance in the time domain. The response of a spring-mass PD (Figure 17) in a proposed artillery fuze to high velocity flight in heavy rainfall was simulated by a straight-forward approach employing conservation of momentum and ordinary harmonic motion for the time between raindrop impacts. A spring, loosely positioned in a confining channel in the steel PD nose, places the system under a 40 pound nominal compressional load, and a further compression of 0.26 inches is needed to bring the firing pins in a

position to begin initiating sensitive M55 stab detonators. If the mass and spring were attached and free, the natural period $2\pi\sqrt{(M + m_s/3)/K}$ would be 14.5 ms. For velocities of interest in the range 1000 to 3000 ft/sec, the expected force contact with any drop is in the order of several microseconds; and, therefore, the force-time curve (unknown) was avoided and the momentum I transferred or area under the force-time curve was employed.

$$I = \int F dt = mv = MV \quad (25)$$

FIGURE 17. MASS-SPRING PD DESIGN



System Parameters:

- A - Area of flat front end = .001364 ft² (1/2" diameter)
- D - Drop diameter
- K - Spring constant (40 lb/in nominal)
- m - Mass of raindrop
- m_s - Mass of spring = .00054 slug (0.28 oz)
- M - Mass of steel PD nose = .00235 slug (1.21 oz)
- S - Compressional static load (40 lb nominal)
- v - Velocity of shell relative to ground (ft/sec)
- V - Velocity of PD nose relative to shell body (ft/sec) = \dot{x}
- w - Natural frequency of free system = 435 rad/sec
- x - Position of PD relative to shell body

With harmonic motion between impacts and neglect of all friction, especially in the O ring area, the equation of motion and conditions are simply:

$$\begin{aligned} x(0) &= x_{i1} \\ (M + m_s/3) \ddot{x} &= -Kx \quad \dot{x}(0) = V(0) = V_{i1} \quad \text{Constraint: } 1'' < x \leq 1.26'' \end{aligned} \quad (26)$$

with position x and velocity V of the PD nose:

$$x(t) = \frac{V_{i1}}{w} \sin wt + x_{i1} \cos wt \quad (27)$$

$$V(t) = V_{i1} \cos wt - w x_{i1} \sin wt \quad (28)$$

$$\left. \begin{aligned} x_{\max} &= x_i \sqrt{1 + (V_{i1}/w x_{i1})^2} \\ \text{TVELO} &= \frac{1}{w} \tan^{-1} (V_{i1}/w x_{i1}) \end{aligned} \right\} \begin{aligned} &\text{Valid for } + V_{i1} \\ &\text{(Motion toward detonators)} \end{aligned} \quad (29) \quad (30)$$

x_i - PD position just BEFORE encounter with i th drop.

x_{i1} - PD position just AFTER encounter with i th drop $= x_i + V_i D_i / v$.

V_i - PD velocity just BEFORE encounter with i th drop.

V_{i1} - PD velocity just AFTER encounter with i th drop $= V_i + m_i v / M$.

x_{\max} - Maximum possible excursion after any impact.

TVELO - Time for x_{\max} to occur.

Calculated values for the PD design for single drop encounters are listed in Table 15.

TABLE 15. PARAMETERS FOR SINGLE DROP ENCOUNTER FOR SYSTEM ($S=40$ lb; $K=40$ lb/in)

Drop Diameter D (mm)	Shell Velocity v (ft/sec)	Impulse I (oz-sec)	PD Velocity V (ft/sec)	x_{\max} (mm)	TVELO(ms)
2	2000	0.0071	0.19	~ 0	-
	3000	0.0122	0.33	~ 0	-
3	2000	0.027	0.73	0.005	0.05
	3000	0.044	1.18	0.013	0.07
5	2000	0.138	3.68	0.13	0.23
	3000	0.212	5.63	0.30	0.35
6	2000	0.237	6.31	0.38	0.39
	3000	0.368	9.78	0.91	0.60
7	2000	0.386	10.3	1.0	0.63
	3000	0.586	15.6	2.25	0.93
8	4000	1.16	31.0	8.0	1.62

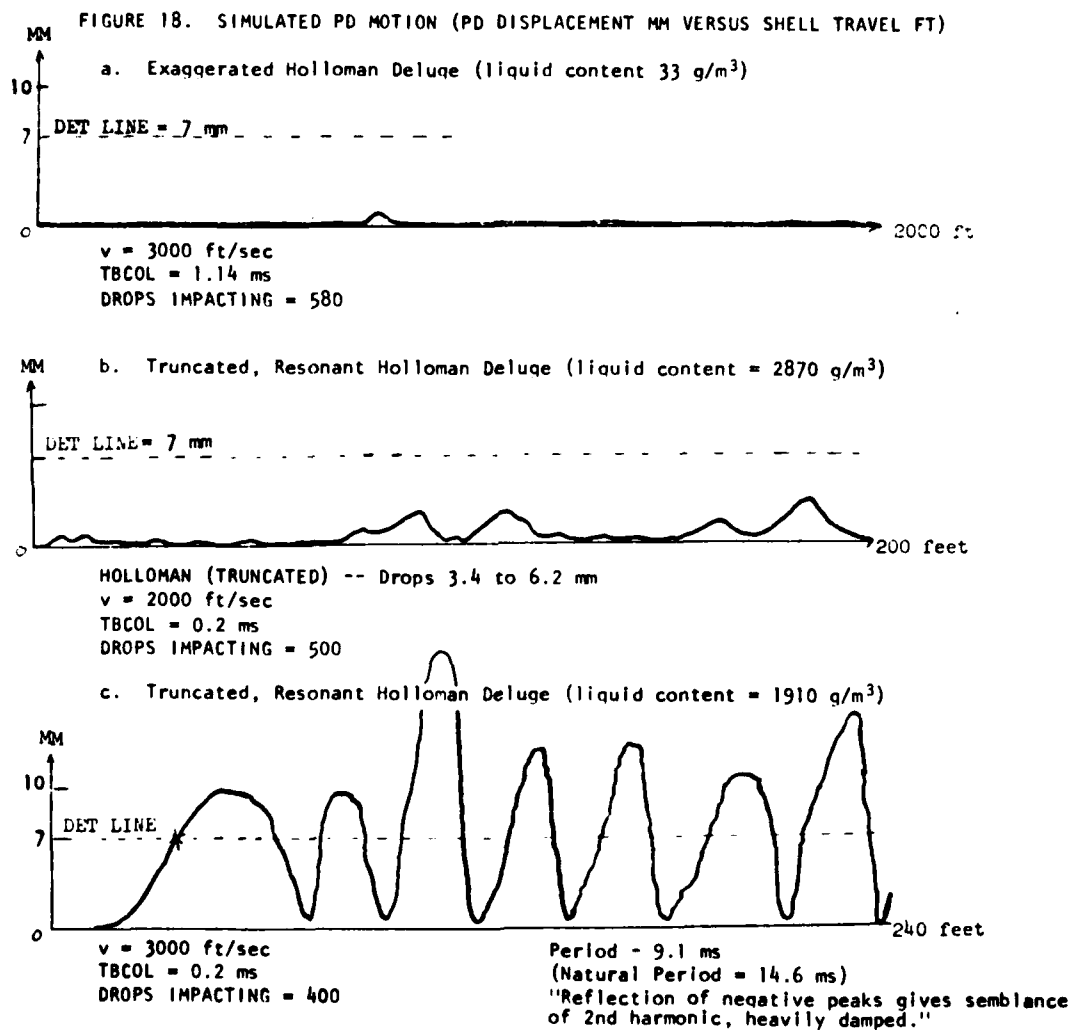
It was assumed drops were uniformly distributed in space, and the time between collisions (TBCOL) was determined by the volume swept out by the PD area A, with a shell velocity v , in rain density N . $TBCOL = 1/(NAv)$. Two distributions were used: 1) the cited Canal Zone 114 mm/hr (4.5 in/hr) equivalent to a cloudburst (liquid content 4.5 g/m³); and 2) Holloman "deluge" rainfield of about 28 in/hr accumulation rate (liquid content 25 g/m³) from a flour pellet measurement with the number of drops at the large diameter end arbitrarily increased to exaggerate (liquid content 33 g/m³) this deluge rainfield for a more pessimistic response. Each successive drop was chosen randomly from the drop size distributions (Table 16).

TABLE 16. RAIN FIELDS USED IN SIMULATION

Canal Zone (Table 4; 114 mm/hr)			Exaggerated Holloman Deluge		
N_i/m^3	% Total Drops	D(mm)	N_i/m^3	% Total Drops	D(mm)
141	9.7	.7	4400	58	.73
373	25.8	1	891	12	1.26
281	19.3	1.3	883	12	1.77
204	14.0	1.6	407	5.1	2.31
147	10.1	1.9	419	5.5	2.7
128	8.8	2.2	316	4.2	3.42 (3.1)
80	5.5	2.5	139	1.8	4.32 (3.7)
46	3.2	2.8	71	.9	5.04 (4.4)
25	1.7	3.1	40	.5	6.2 (4.7+)
14	.96	3.4	$N = 7566$ 100 (Values in parenthesis for Holloman were 'average' diameter values for actual 4th sample in Table 8.)		
7.5	.52	3.7			
3.5	.24	4			
1.4	.1	4.3			
0.6	.04	4.6			
0.3	.02	4.9			
0.3	.02	6			
$N = 1452.6$	100				

In the simulation procedure, final conditions of position and velocity of the PD just before another drop impacted, along with an impulsive velocity from the next drop, became the initial conditions for harmonic motion in the next TBCOL. Whenever $x_i \leq 0.2$ mm, printout occurred of x_i and V_i at each T_i ($T_i = TBCOL/5$). All drop sizes were printed. Ordinary shell velocity trajectories were employed, and also velocities at 4000 ft/sec. For the realistic case of 3000 ft/sec, simulation indicated negligible PD motion for the Canal Zone distribution, and excursions up to about one mm for the exaggerated Holloman deluge distribution. Figure 18a

is a typical computer plot of PD displacement toward the detonators (about 7 mm needed) versus distance travel (2000 ft) in the rainfield and shows the recovery feature of the nose. Subsequent to the simulation, prototype fuzes were built and tested (December 1969) at Holloman AFB in the deluge rain (≈ 28 in/hr) with an entrance rocket sled velocity of about 2750 ft/sec into the 2000 ft of rain. Inspection of fuzes revealed negligible maximum motion (small fraction of millimeter) of the PD nose.



Disregarding the surge wave problem, the above approach was employed for a "truncated" Holloman field by disregarding small size drops, then increasing this distribution for a "resonant" condition of drops impacting the PD every 0.2 ms. This effectively increased the liquid content of the Holloman deluge by about 100. At this intensity, the total water content is still only a fraction of one percent of the total volume. Table 17 lists these values. Figures 18b and c are typical computer outputs for these bizarre type rainfields.

TABLE 17. ARBITRARY LARGE DROP, HIGH DENSITY RAINFIELDS

D(mm)	Truncated Holloman	"Resonant" Holloman (TBCOL = 0.2 millisec)	
	N_1/m^3	$N_1/m^3 (v=2000)$	$N_1/m^3 (v=3000 \text{ ft/sec})$
3.42	193	28,230	18,000
4.32	139	20,330	13,550
5.04	71	10,360	6,900
6.2	40	5,830	3,880
N	443	64,750	42,330
Liquid Content (g/m ³)	19.7	2870.	1910.

Criticisms of this Method

1. The assumptions of simple harmonic motion between impacts, and of conservation of energy in the PD mass from the plastic drop encounters until the PD mass strikes its mechanical stop at $x = \text{one inch}$, at which all acquired momentum and energy is taken as transferred to the shell itself, take no account of wave propagation effects along the spring. There is room for a variety of alternate approaches. The approach of stress wave propagation in the metal nose, the boundary conditions on the spring ends and nose, with momentum buffering onto the shell system, the standard coupled differential equations for the spring with associated masses and constants, implies its own inherent assumptions and offers an interesting approach of much greater complexity for computer solution. For a spring constrained at both ends, surge waves⁽²⁵⁾ occur if force loading occurs at frequencies f_n (Table 18) for this design.

$$f_n = \frac{nd}{2\pi D^2 N} \sqrt{\frac{Gq}{2w}} \quad n = 1, 2, 3 \dots \quad (31)$$

d - Diameter wire = .065"
 D - Diameter of coil = .285"
 G - Torsion modulus = $1.1 \times 10^7 \text{ lb/in}^2$

N - Number active coils = 20
 w - Weight density = 0.286 lb/in^3

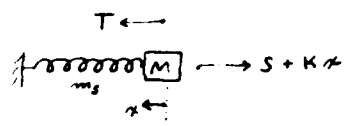
TABLE 18. SURGE WAVE FREQUENCIES

n	f_n (HZ)	Period (ms)
1	160	6.3
2	320	3.1
3	480	2.1

A reference⁽²⁶⁾ cites the time for a compressional wave to travel down and back along a spring compressed or extended to a length L as $2\sqrt{m_s/K} \approx 2.1$ ms. The propagation velocity for the design is $L\sqrt{K/m_s} = 150$ ft/sec for the $L = 1.88$ inch 40 lb load compression length.

2. The value of the aerodynamic force from air flow was not known. This force makes the PD more rain sensitive, subtracts from the 40 lb static load, and shifts the spring force-compression curve to a lower parallel line requiring direct use of equations of motion (Figure 19). (The dynamic air pressure term $R_0 v^2/2$ at 3000 ft/sec for this nose is about 13 lb.)

FIGURE 19. FORCES ON PD SYSTEM



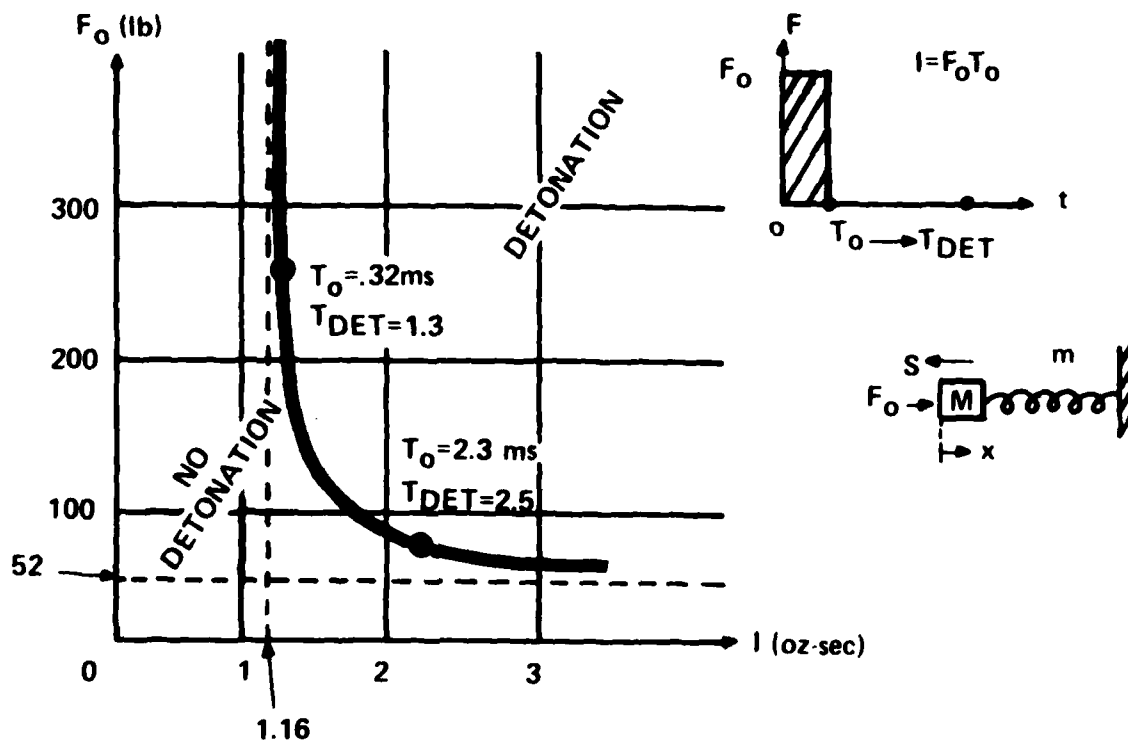
$$\begin{aligned}
 (M + m_s/3) \ddot{x} &= T - (S + Kx) \\
 x(0) &= 0 \quad 0 < x \leq 0.26'' \\
 \dot{x}(0) &= V_{il}
 \end{aligned}
 \tag{32}$$

T = Aerodynamic Force

Sensitivity Curve for the PD Fuze

The energy required to compress the spring another 0.26 inch (1.08 ft-lb) [spring enters slightly non-linear region], and to initiate the M55 detonators in this design (= .05 ft-lb), requires an impulse of 1.16 oz-sec, or impulsive PD velocity of 31 ft/sec. To obtain an indicative sensitivity curve (Figure 20), based on rectangular pulses, a plot of constant force level F_0 that must be maintained for time T_0 is plotted versus impulse $I_0 (= F_0 T_0)$ delivered. With the equation of motion $(M + m_s/3) \ddot{x} = F_0 - (40 + Kx)$, conditions for detonation are satisfied when at time TDET, the solution attained the values $x = 6.6$ mm and $\dot{x} = 6$ ft/sec. Aerodynamic loading will shift the asymptotes.

FIGURE 20. CONSTANT FORCE -- PD SPRING MASS SENSITIVITY CURVE



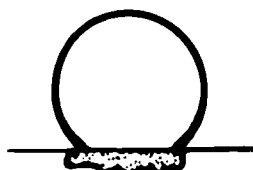
EROSION PHENOMENA

In the 1000 to 3000 ft/sec velocity range erosion, rather than cratering, is the dominant form of damage from raindrops⁽²⁷⁾ and all structural materials show erosion damage when exposed to nominal rain for sufficiently long time at velocities in excess of Mach 0.8. In 1961, an F106A airplane flown through thunderstorms from 15,000 to 40,000 ft from Mach 0.84 to 1.63 sustained severe erosion from water drops and/or tiny ice crystals at rivet heads and leading edge of wings, cockpit frame and plastic antenna covering. The principal causes cited for erosion damage are: (1) impact force; (2) radial flow; and (3) cavitation (Figure 21). However, there are almost as many mechanisms of erosion failure as there are classes of

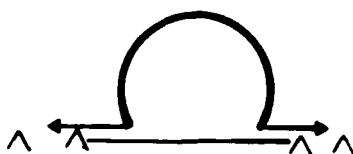
materials. Thin resilient coatings such as neoprenes and polyurethanes will transmit shear stress to the substrate causing failure in the adhesive bond. Additional impacts cause the coating to stretch, deform or burst. Plastic type materials and soft metals flow plastically resulting in cratering and pitting. Plastic laminated materials fail from erosion of upper layers of the fabric.

FIGURE 21. CITED CAUSES OF SURFACE EROSION

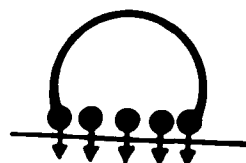
1. IMPACT FORCE



2. RADIAL FLOW



3. CAVITATION



Impact Force

During the early stages of collision of a drop with a planar solid surface, maximum pressure appears independent of drop diameter and is asserted to exist in a ring around the central point of collision. At supersonic velocities, local pressure of about 0.1 to 1 million psi is exerted on the target. Part of the impact energy from liquid impact radiates⁽²⁹⁾ into the solid by: (1) longitudinal compression wave; and (2) transverse or shear wave (at about half the longitudinal velocity) with particle motion perpendicular to propagation direction. If the waves reflect on a free surface of the solid, each incident wave generally produces two reflected waves, with a complicated stress pattern resulting. Large tensile stresses are produced when intersecting waves are in opposition, and lead to fractures especially in brittle materials, rather than in ductile metals. The spalling feature occurs when an initial compression wave is being reflected in the opposite surface as a tension wave. Fracture occurs a

little way in from the rear surface where the algebraic sum of reflected tensile stress and compressive stress associated with the tail end of the incident wave first reaches the solid tensile strength. The volume of material between fracture and rear surface still has high particle velocity in the outward direction and may fly off the back as a spall. The fracture surface created acts as a new reflecting surface for the remainder of the compression wave, and may lead to secondary fractures in toward the center of the plate. Fractures near the impact surface are caused by tensile stresses accompanying the release of the load. For angles other than normal incidence, the energy of the incident compression wave reflected in the rear surface is shared between a wave of tension and a shear wave.

Radial Flow

A solid sphere inflicts damage by exerting localized pressure; whereas a liquid drop can cause damage by its radial flow, exerting an erosive shear stress on the solid surface because of the liquid viscosity, and also at the base of any protrusion on the surface with a bending moment about the protrusion. As the impacting drop spreads out, the water radial velocity may be two to three times impact velocity. For a glass plate surface, flow velocity approaching ten times the impingement velocity for short times after impact has been found.

Table 19 lists some results of single impact studies with 8 million frames/sec camera rate of the radial velocity of 2 mm water drops at 987 ft/sec onto Perspex.

TABLE 19. 2 mm WATER DROPS ON PERSPEX (PLASTIC)

Impact Velocity (ft/sec)	Time from Impact (Microsec)	Radial Velocity (ft/sec)
987	0.8 - 2.9	3056
	2.9 - 3.9	2650
	3.9 - 5.6	2610
	5.6 - 12.9	1820

No spalling effect was observed at the back of the water drop. However, at low velocities and at 1000 ft/sec, there is evidence at the last stages of collision when the drop has been flattened into a radially flowing disk, that a spray of much smaller droplets at the periphery appears to rebound from the striking surface.

Hard spheres do not satisfactorily simulate water impact. Polytetrafluoroethylene (PTFE) and modeling clay (plasticine) most closely resemble water flow characteristics but have scouring action. Table 20 shows some results⁽³⁰⁾ with solid spheres which showed some permanent set, except for sapphire which had complete recovery.

TABLE 20. SOLID SPHERE COLLISION ON PERSPEX

Sphere Material	Impact Velocity (ft/sec)	Contact Duration (microsec)	Velocity Separation (ft/sec)	D (mm)
Polyethylene	1018	52.	115	4
Nylon	957	6.7	240	4
Cellulose Acetate	985	5.	250	4
Sapphire	1075	8.5	373	2

Cavitation

Cavitation is the formation of bubbles in a liquid, and occurs when pressure on a liquid, or in a small volume in a liquid, drops below the liquid vapor pressure at the temperature in question. When pressure on the liquid is raised, or when bubbles move out of a local low to a high pressure region, the bubble-cavities collapse. Collapse of cavities produces damage called cavitation erosion. During the duration of each impact, some bubbles will be collapsing on or near the impact surface. The bubble collapse lasts only a few microseconds and the collapse speeds are estimated to be greater than impact velocity. Shocks from implosion offer a small contribution to damage, while the main damage is caused by jet impact near the end of collapse of the spherical bubbles in an asymmetric mode such that high velocity microjets impinge on the surface. It appears cavitation microjet diameter is well less than one mil and with velocity up to several thousand ft/sec, and probably with large length to diameter ratio. (28,31,32,33)

There are theories⁽²⁰⁾ for the origin of this cavitation: (1) When the head of the drop has just disappeared into radial flow, the continuous outward flow of liquid under its own momentum produces a pressure drop at the center of the spreading liquid disk. If pressure at the center of the spreading liquid disk falls below the vapor pressure, cavitation results. (2) Alternating waves of compression and tension exist in the head of the liquid. The initial compression wave is reflected from the free liquid-to-air surface as tension or negative

pressure wave and moves down to the surface. Returning tension wave adds algebraically to the compression wave still being initiated at the impact surface, and as the impact pressure has been decreasing steadily, the net pressure may be negative. Repeated reflection of the wave may occur before the bubble grows to sufficient size.

Erosion Factors

Generally, erosion varies as the cosine of the angle of incidence. Slightly higher erosion rate was found at ten degrees from the normal⁽¹⁸⁾ for aluminum at Mach 1.2; and for neoprene coatings, most erosion occurred at impact angles between 25 and 30 degrees from the normal.⁽³⁴⁾ With drops of similar size, flattened droplets caused more severe erosion than oval shaped ones. If erosion E is defined:⁽¹⁸⁾

$$E = \frac{\text{Volume of material lost per unit area per unit time}}{\text{Volume of liquid impinged per unit area per unit time}}$$

an empirical formulation for E (Expression 33) shows the strong dependence on velocity. It is also reported that at velocities up to about 1300 ft/sec, weight loss from samples in rain is proportional to the fifth power of velocity.⁽³⁵⁾

$$E \approx V^3(V - V_c)/V_c^4 \quad \text{for } 1 < V/V_c \leq 3 \quad (33)$$

V - Velocity of impingement

V_c - Cut off velocity for erosion (e.g. ≈ 390 ft/sec for 0.66 mm drops)

Maximum impact stress generally is a function of material properties and impact velocity. Yet, erosion also depends on drop size and shape. Though contact area varies as D^2 for a sphere and as D for a cylinder jet, the force from cylindrical jets of water on barium titanate transducer showed loads rather linear with velocity, without a clear dependence on jet diameter.⁽¹⁸⁾

Impact stress alone is not a sole criterion for erosion. Larger drops increase the time of force, and materials with definite yield point in the static stress-strain curve have measurable time delay associated with the initiation of plastic deformation. Strain rate for the usual longitudinal impact test is particle velocity divided by specimen length. For impact on a semi-infinite body, length could be related to the depth of quasi-static stress fields,

small for smaller drops, resulting in high effective strain rate. If there is a strain rate effect, such that for a given strain the stress increases with strain rate, then maintaining the same total volume of impinging water, the total strain and relative energy transfer for a given impact velocity would be less with smaller drops.

Aerodynamic heating can reduce the strain-stress curve, resulting in damage.⁽³⁶⁾ Polyurethane was found to be about one-sixth as strong at 250°F than at 74°F.⁽³⁷⁾ If the impact stress does not exceed the coating tear strength, these temperature induced reductions of impedance may be beneficial.

Erosion Abatement

Various coatings and coverings are employed for rain protection. Nickel plating^(38,39) has extended life of the leading edge materials by about 40 times over neoprene. A thickness of at least 12 mil nickel on laminates extended life of leading edges on aircraft, helicopter rotor blades and jet engine compressor blades, and a 16 mil thickness has been employed on high strength-temperature plastic (polybenzimidazole PBI). An explanation for improved performance from a rough nickel surface asserts that rough (sandblasted) surface breaks the drop into minute particles and these minute particles produce less radial flow and lower shear stresses.

Limited data is available on rain erosion at velocities from 1000 to 3000 ft/sec.⁽⁴⁰⁾ Cushioning of the impact stresses only occurs once a critical thickness of coating is reached of several millimeters. As the impact pressure reduces, the velocity of radial flow is also reduced with accompanying shear surface stress. No known elastomeric coating or glass reinforced plastic can withstand erosive action of rain at velocities greater than 3000 ft/sec for more than a few seconds. Ceramic materials resist damage to 4000 ft/sec. Epoxy-glass nose-cones with radius of about 1.5 inches eroded after 85 seconds exposure at 1150 ft/sec; 8 seconds at 2200 ft/sec; and 3 seconds at 2600 ft/sec (Holloman AFB 6000 ft field). Unprotected ceramic nose cones shattered in the sled tests. Composite materials do not withstand liquid impact well because of the sharp stress peak caused by the initial compressible behavior of the material, and stress waves produced lead to interlaminar failure. A possible composite system advantage is the attenuation or dispersion of the stress waves by multiple reflection processes.

If the dynamic stress-strain curve is plotted for some material from data, the slope yields the elastic modulus E , and the elastic wave speed C is then $(E/R)^{0.5}$ where R is the density. Dynamic impedance $Z = RC$. Elastomer (several polyurethanes, neoprene) coatings have small impedances, and in effect give easily under raindrop impact. These materials can endure large, reversible amount of deformation without being damaged. Elastomeric materials resist erosion (at prescribed temperature, and except after extreme prolonged exposure) by minimizing stresses at impact area, provided the velocities are sufficiently below the level needed to fracture the elastomer. The material must recover fast enough, retaining its elastic properties. A random, high strain rate loading exists from rain impact. The dynamic response of a polyurethane at a strain rate of about 1000 sec^{-1} showed stresses three times higher (at comparable strains) than the stresses obtained statically. (37)

Experimental studies of polyurethanes have indicated that low modulus with good tensile strength and elongation gives the most erosion resistant coatings. (41) Polymeric materials (epoxies, silicones, polyimides and teflon) with thermal capability do not exhibit properties of tensile strength, elongation and tear strength required for resistance to dynamic forces of impact. Of elastomeric coatings, polyurethane on aluminum and epoxy laminate substrates was found to be up to 5 times as resistant to subsonic rain impact than neoprene. Urethanes in which the polyol molecular weight is about 650 exhibit best resistance in simulated rain environment. Polyurethane coating was superior when exposed to rain and hail in flight conditions.

Of thermoplastics, polycarbonate polymer (Lexan) was superior; poorest was polytetrafluoroethylene (Teflon TFE). (42) Of metals, the stellite alloys (Co-Cr-W) demonstrated best erosion resistance. (43) Various rainheads of stainless steel, neoprene, solid polycarbonate, polyurethane and metal crossbar designs were tested for PD fuzes at various sled speeds at Holloman. For example, a stainless steel sheet 15 mil thick was punctured after 2200 ft/sec entry into the 2000 ft long Holloman deluge rainfield. (44) The forward rim surface of a stainless steel ogive section was chewed up for 4600 ft/sec entry. Metals are not markedly strain rate sensitive. Impact produces plastic deformation, dependent on liquid mass geometry, when the peak pressure exceeds the instantaneous flow stress in the metal. Polymers and glasses are

strain rate sensitive, and the tendency is to elastic deformation in the areas of compression and fracture in regions of tension. The area of impact is found relatively undamaged, but surrounded by well defined ring cracks.

Water which flows laterally forms a protecting liquid film.^(45,46) An increase in the density of drops increases the water film's protective role and reduces deformation from impact shock. If the film is too thin, multiple reflection in the thin film rapidly brings up pressure to full value for "dry" impact. A water layer comparable to half a cylinder jet radius acts as a useful cushion, reducing shock pressure by factor of one half.

In an investigation⁽⁴⁷⁾ of the splash envelope of raindrops at low impact velocity (terminal velocity from 40 ft tower), drops greater than about 2 or 3 mm diameter became measurably flattened on the bottom. Drops from 2.9 to 5.6 mm fell into water depths of 0.1 to 90 mm above a smooth plate glass. (A splash shape was not formed by impact on smooth, hard, dry, horizontal surface; rather the waterdrop merely spreads horizontally without forming the splash envelope and droplets above the surface.) The splash envelope increased to its greatest height when the water depth was about one-third the drop diameter, and decreased to constant size for depths greater than three drop diameters.

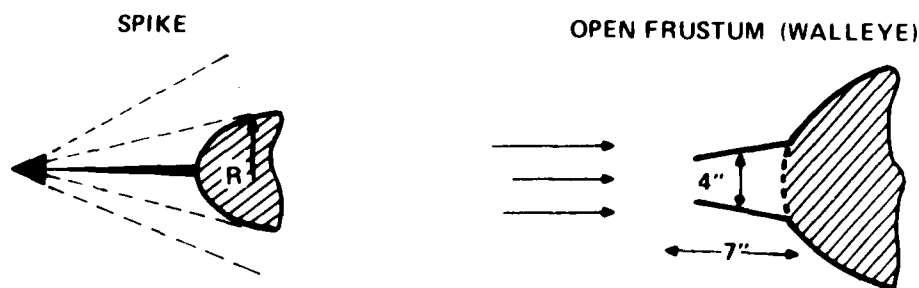
For ceramics and high hardness metals, it is thought that impact fatigue or work hardening causes small imperfections in the surface, to be removed with subsequent impacts. Velocities in excess of Mach 1.3 (1400 ft/sec) were needed to damage high density alumina (Al_2O_3) with 2 mm mercury drops.⁽²²⁾ However, it was reported⁽⁴⁸⁾ that as alumina density increases and porosity decreases, the bond to the reinforced laminate becomes weaker. A correct match is needed for the thermal expansions of laminate and coating. In general, the alumina coatings were about 2 1/2 times more rain erosion resistant than neoprene coating. It appears⁽⁴⁹⁾ it is not possible to predict rain erosion of particular ceramic materials at high Mach number because: (1) theory associated with prediction of forces from water drop impact on solid surfaces is insufficiently developed; (2) property data for ceramics is not available; and (3) behavior of ceramics under multiple impact (fatigue) is not understood. Despite the compressive strength of alumina ceramics, they were damaged by multiple impacts as low as 820 ft/sec. Pyroceram 9606 is reported superior to alumina 753.⁽⁴²⁾

Structures (Figure 22)

Investigations indicated that spikes^(50,51) placed on missile nosecones effectively protect radomes from erosion at velocities up to 3000 ft/sec by advancing the bow shock wave. To protect fragile windows,⁽⁷⁾ an open end frustrum of a cone was attached to the front of a missile to induce raindrop breakup. The captive "air cushion", moving at essentially flight speed, provided for protection up to Mach 2.5.

FIGURE 22. STRUCTURES FOR EROSION ABATEMENT

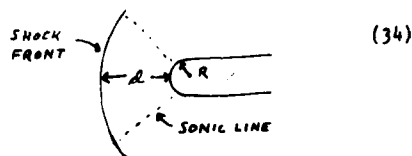
STRUCTURES: (LOW MACH #)



Shock Disintegration of Drops (Mach 3 - 12)

A projectile at supersonic velocity through air with a blunt nose has a detached shock wave front; a sharp point projectile has a shock attached to the point. The width of the shock itself is exceedingly small. A body with hemispherical nosecone of radius R (ft) traveling in air at velocities v (ft/sec) greater than the speed of sound (1090 ft/sec at 0°F) is preceded by a detached shock wave whose stand off distance d (ft) is given by:⁽⁴⁰⁾

$$d = R (0.129 + 7.61 \times 10^5 / v^2)$$



At 2000 ft/sec, the shock wave is 0.32, and at 6000 ft/sec is 0.13 of the radius away. For a body of revolution with a flat nose, the standoff distance is about $0.8R$ for Mach 2, and about $0.6R$ for Mach 6.⁽⁵²⁾

For one dimensional, compressible, isentropic perfect gas flow, the stagnation temperature T_2 ($^{\circ}\text{R}$) and gas density ρ_2 in the shock region is given by: ⁽⁵³⁾

$$T_2 = T_1 (1 + (k-1) M^2/2) = N T_1 \quad (35)$$

$$\rho_2 = D \rho_1$$

where k - Ratio of heat capacities (C_p/C_v) = 1.4

M - Mach number

ρ_1, T_1 - Atmospheric density, temperature ($^{\circ}\text{R}$)

TABLE 21. TEMPERATURE (N) AND DENSITY (D) RATIO FOR NORMAL SHOCKS

Mach Number M	N	D
1	1.	1.
2	1.69	2.67
3	2.68	3.86
5	5.8	5.00
10	20.4	5.71

The reduction of the drop by evaporation would be a function of rate of heat transfer and time required for the drop to traverse the shock region. This mass loss by heat transfer is negligible for ordinary rain droplets, but the cooling effect of rain helps reduce the ablation rate of missile material.

A projectile or missile, depending on its design, imparts some of its motion to the air around it. For high Mach number, up to a million G acceleration can be experienced by drops, and if the impact with the front air stream is applied far enough ahead of the surface to be protected, the drop may be shattered into droplets too small to cause damage. When the drop is exposed to an airstream, various competing forces determine whether the drop will be broken up, and if so, the time for the process. ⁽⁵⁴⁾ Forces that tear apart the drop scale approximately with dynamic pressure $\rho V^2/2$ and the tendency to maintain drop shape with inertia forces, surface tension, and to a lesser extent, viscous forces.

A criterion to predict whether or not a liquid drop would disintegrate under aerodynamic conditions is the Weber Number W (alternate definition has 2 in denominator): ratio of inertial energy of drop to its surface energy. Some find the critical Weber number between 6 and 14.

$$W = \rho_2 u_2^2 D/S \quad (36)$$

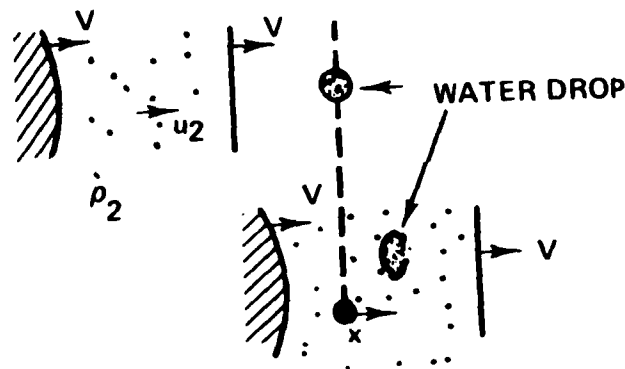
D - Drop diameter

S - Surface tension (.073 newtons/m for water at 20°C)

ρ_2, u_2 - Air density, speed relative to drop

Quantitative results of raindrop breakup effects (Figure 23) from a strong shock

FIGURE 23. SHOCK-WATERDROP COLLISION IN LAB COORDINATES



(Mach 3 to 12) were obtained in shock tubes^(55,56) with drop diameters from 0.5 to 2.5 mm with pressures from 140 to 760 torr. The displacement x after actual time t of shock front passage of an initially motionless drop following contact with a shock front is reported as:

$$x \approx 0.8 D T^2 \quad (37)$$

where D - Original drop diameter

T - Dimensionless time

ρ_2, ρ_L - Gas density in shock region, liquid density

u_2 - Flow velocity in shock region in lab coordinates

x - Distance traveled by drop in lab coordinates

Equation 37 corresponds to a constant acceleration path with an average drag coefficient of about 2.1 based on the original drop cross section. Table 22 lists standard (NACA

Report 1235) pressure-density-temperature values for various altitudes.

TABLE 22. PRESSURE-DENSITY-TEMPERATURE FOR VARIOUS ALTITUDES

Altitude (ft)	Atmospheres	Pressure (torr)	Pressure (lb/in ²)	Density (grams/cc) x 10 ⁻⁴	Temperature (°K)
0	1.	760	14.69	12.3	288.2
10,000	.687	523	10.1	9.07	268.3
20,000	.46	350	6.75	6.54	248.6
30,000	.297	226	4.36	4.58	228.7
40,000	.185	141	2.72	3.01	216.6
50,000	.114	87	1.68	1.86	216.1
60,000	.071	54	1.04	1.15	216.6
100,000	.011	8	0.158	0.174	216.6

The drop is always flattened initially by the pressure differential from air flow.

There are four descriptive modes for the disruption of the liquid drop by airstream impact:

(1) Drop oscillates until division in two, at low speeds; (2) At slightly higher speeds, the drop is severely distorted into parachute shape and soon shatters; (3) At still higher speed, continuous stripping mode of breakup occurs in which a spray is formed at the periphery of the drop and swept into the wake; (4) At extreme high speeds (catastrophic), drops shatter very rapidly in a distinct mode.

The transition from stripping to catastrophic mode occurs early in the shock tube tests at Mach 11, at intermediate time at Mach 6, and at later time (if at all) at Mach 3.

X-ray data suggested time for complete breakup due to stripping has a constant value $T \approx 3.5$ or $x \approx 10 D$, independent of Mach number. The mass m of the drop remaining of the initial mass m_0 as a function of time could be correlated roughly by the formula:

$$m = m_0 (1 + \cos(\pi T/3.5))/2 \quad (39)$$

When the critical Weber number is exceeded, the first mode occurs. For 1 to 2 mm diameter drops, the critical value ranges from about 4 to 13, corresponding to velocities of 40 to 200 ft/sec at sea level. (7) As W is increased, there is a small range of values for which the second mode occurs. For large values (about 3 times the critical), breakup occurs by flattening and stripping. For high velocity flight, the third mode is relevant wherein the creation of

small fragments leads to increase of surface to volume ratio, and sudden increase in acceleration. The dimensionless time T elapse between shock contact and drop breakup in the catastrophic mode is correlated by equation 40:

$$T = 45 W^{-0.25} \quad (40)$$

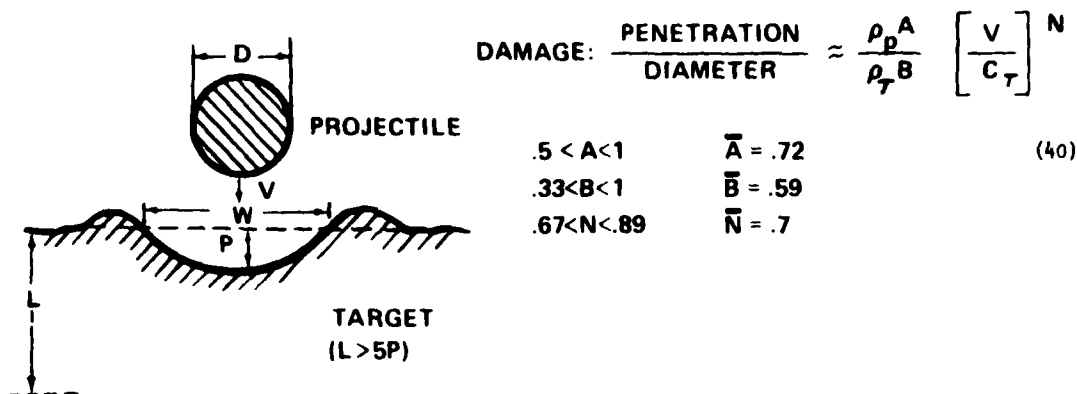
An investigation of a 2.7 mm diameter water drop at Mach 1.5 indicated substantial deformation several inches beyond the shock front passage. (14)

Waterdrops will be shattered as they pass through the bow shock region that precedes a body travelling at supersonic velocity only if the time of traversal in the shock region is greater than the break-up time. The traverse time is determined by the velocity and geometry of the leading surface of the body. Data indicates that raindrops of normal size will impact unshattered on the hemispherical nosecone of a missile at 1000 ft/sec if the nosecone radius is less than about 0.7 ft; at 2000 ft/sec if the radius is less than about 1.6 ft; and at 10,000 ft/sec if the radius is less than 2.8 ft. (40) It is expected that raindrops will not be shattered in passing through the bow shock layer of most missiles, and serious erosion would occur with most nosecone materials on missiles having nosecone radii less than 1.5 ft at velocities greater than about 3000 ft/sec, with greater damage caused by those drops striking normal to the surface.

Hypervelocity Impact

Rather than erosion, cratering from extreme compressive force of drops becomes the dominant form of damage at velocities above a few Mach numbers. As the velocity approaches Mach 10 to 20, water drops cause the same penetration damage as a ductile solid of the same density, as the only appreciable parameters are velocity and density. A jet of water at 5000 ft/sec has sufficient force to cut metal. Data for estimating drop damage at velocities greater than about 3000 ft/sec is obtained from impacts of single drops of liquids or solid particles on semi-infinite targets (with thickness at least five times penetration depth). Damage is normally reported as depth of penetration (P) divided by drop diameter (D). Figure 24 shows the crater profile, though the crater top has a jagged, peeled over edge.

FIGURE 24. CRATERING CHARACTERIZATION



Empirical expressions of such damage correlate satisfactorily with impingement of water, mercury, polyethylene pellets, lead, copper, iron and stainless steel on semi-infinite targets of most ductile metals. Penetration damage expressions based on data at velocities from 2000 to 30,000 ft/sec usually have the form of equation 40. (40)

- C_T - Velocity of sound in target (proportional to material strength)
- ρ - Density of projectile (P) or target (T) (lb/in³)
- S - Target shear strength (lb/in²)
- V - Impact velocity (ft/sec)

For a given raindrop depth of penetration into a target at 1000 ft/sec, penetration is 2.2 times at 3000 ft/sec, and 8 times at 20,000 ft/sec. No general expression appears available for thin or sandwich type target, or ablating targets.

Many empirical expressions are available for drop damage. The following equation (57) (in-lb/sec units) is found to explain 92 percent of total variance of indicial data in the velocity range of 0 to 15,000 ft/sec (V_p - Projectile volume, in³):

$$P = 0.172 (V_p)^{0.33} \frac{\rho_p^{.979} V^{.693}}{\rho_T^{.35} S^{.457}} \quad (41)$$

For velocities from 5000 to 35,000 ft/sec, the following equation⁽⁵⁷⁾ is proposed to explain 87 percent of total variance of data in this range:

$$P = 0.772 (V_p)^{0.33} \frac{\rho_p^{.673} V^{.449}}{\rho_T^{.426} S^{.275}} \quad (42)$$

Another equation⁽⁵⁸⁾ for hypervelocity impact that correlates a wide variety of metal-to-metal impact:

$$P = 0.311 D \left[\frac{\rho_p}{\rho_T} \right]^{.167} \left[\frac{\rho_p V^2}{S} \right]^{.282} \quad (43)$$

Calculations⁽¹⁵⁾ with HELP hydro code (multi-material Eulerian, compressible fluid, elastic-plastic flow, time and 2D space) with a 3.4 mm water drop onto 6061-T651 aluminum target indicated collision lasts approximately 5 microseconds, with some target rebound for the 4655 ft/sec encounter. Results are in Table 23 where Q is the distance P plus height of the deformation above the surface line, with some extrapolated results from a water-gelatin projectile experiment.

TABLE 23. HELP 2D CODE CALCULATIONS AND EXTRAPOLATED WATER-DROP (3.4 mm) EXPERIMENT

Velocity (ft/sec)	Crater Dimensions (Calculated) (Inch)			Extrapolated Experiment (Inch)	
	P	Q	W	P	W
4655	.018	.048	.194	.012	.18
9180	.072	.126	.278	--	--

Water produces a very shallow and flat-bottomed crater at 5000 ft/sec but the crater is nearly hemispherical at 10,000 ft/sec and has nearly the same depth as for an aluminum impact of the same energy.

Miscellanea

Initial studies⁽⁵⁹⁾ showed similarities in the behavior of hail to that of water drops during the impact phase. Hail, spherical and bullet shaped, in diameters from 12.7 to 25.4 mm were fired from a high pressure gas gun at speeds up to 3000 ft/sec onto aluminum alloy

(0.6 to 3 mm) and polymethylmethacrylate (6.35 to 25.4 mm) at an angle of 25° to the horizontal. Photographs showed that shortly after impact, a thin vertical layer of ice was formed. There were no signs of spalling from the rear surface of the projectile. The coefficient of friction was taken as 0.9. The shock wave velocity in ice is about twice that in water. Tables 24 and 25 list reported⁽⁶⁰⁾ hail and ice crystal distributions. Hail can exist at altitudes up to 50,000 to 60,000 ft.

TABLE 24. POSSIBLE HAILSTONE SIZE DISTRIBUTION

Diameter Range (cm)	Maximum Hailstone Diameter (Centimeters)		
	3 cm	6 cm	10 cm
	No. Hailstones/Cubic Meter		
0-1	22.*	9.*	7.*
1-2	0.8	0.35	0.27
2-3	0.17	0.075	0.058
3-4	--	0.027	0.021
4-5	--	0.013	0.010
5-6	--	0.0007	0.005
6-7	--	--	0.003
7-8	--	--	0.002
8-9	--	--	0.0015
9-10	--	--	0.001
Equivalent R (mm/hr)	250	300	500
2 (mm ⁶ /m ³) 10 cm radar	5×10^7	5.5×10^7	5.4×10^7
Equivalent L (g/m ³)	3.8	3.3	4.3

* Probably a considerable underestimate of the smallest stones in this range.

TABLE 25. ICE CRYSTAL CONTENT OF CLOUD

Air Temperature (°C)	Altitude Range (ft)	Ice Crystal Content (Gram/m ³)	Horizontal Extent (Miles)
0 to -20	10,000 - 30,000 (3 - 9 km)	8.0	0.5
		5.0	3.0
		2.0	50.
		1.0	300.
-20 to -40	15,000 - 40,000 (4.5 - 12 km)	5.0	3.
		2.0	10.
		1.0	50.
		0.5	300.

Over temperature range 0 to -10°C, assume that ice crystals may be mixed with water drops (with maximum diameter of 2 mm) to up to content of 1 gm/m³ or half the total content, whichever is less; the total content remaining unchanged. Mean diameter may be taken as 1 mm.

Precipitation has been measured by use of radar reflectivity factor Z which is directly proportional to $\sum N_i D_i^6$ which in turn is related to rainfall rate R . For example, one relation⁽⁵⁾ for all storms is $Z(\text{mm}^6/\text{m}^3) = 372 R(\text{mm/hr})^{1.47}$.

A non-metallic surface can acquire a slightly negative charge from rain impact. Values of charge per drop have been cited⁽⁶¹⁾ as 0.37 (cloudburst) to 0.0064 (moderate rain) esu/drop.

(A copy of the papers presented at the Third International Conference on Rain Erosion and Associated Phenomena (1970) was not available at the time of this writing.)

REFERENCES

- (1) "A Rain Survey of Rain Simulation Techniques", Ser. No. 52.0, The Journal of the JANAF Fuze Committee (May 3, 1967).
- (2) Laws, J., "Measurement of Fall Velocity of Waterdrops and Raindrops", Transaction of American Geophysical Union, Part 3 (1941).
- (3) Booker, J., "Facilities at Royal Aircraft Establishment for Simulation of Flight Through Rain", TR 67245 (October 1967).
- (4) Simpson, M. H., "Rain Test Procedures Research 2nd Report Correlation of Drop Size with Climatic Region and Type of Rain", R-1851, Frankford Arsenal, Philadelphia, Pa. (June 1967).
- (5) Stout, G. E., et al, "Summary of Radar-Rainfall Research, 1952-1968", TR ECOM-02071-3 from Illinois State Water Survey, University of Illinois, Urbana, Illinois to U.S. Army Electronics Command, Fort Monmouth, N.J. Atmospheric Sciences Laboratory (October 1968).
- (6) Marshall, J., Palmer, W., "The Distribution of Raindrops and Size", Journal of Meteorology, Vol. 5 (August 1949).
- (7) Smith, M. R., "Rain-Erosion Tests on Walleye", NWC TP 5281, Naval Weapons Center, China Lake, California (November 1971).
- (8) Lynn, J., "Development of Simulated Rain Test for Impact Fuze", FV-1898, Franklin Institute, Philadelphia, Pa. (January 18, 1956 to October 18, 1956).
- (9) Mueller, E. A., Sims, A. L., "Calibration and Comparison of Simulated Rainfields with Natural Rains", Report R-1993 from Illinois State Water Survey to Frankford Arsenal (February 1971).
- (10) Mueller, E. A., Sims, A. L., "Effects of Rainfall and Drop Size on the M564 Fuze", Report R-1909, Illinois State Water Survey to Frankford Arsenal (October 1968).

- (11) Billions, N. S., "A Study of Raindrop Size Distributions and Probability of Occurrence", Report No. RR-TR-65-1, U.S. Army Missile Command, Redstone Arsenal, Ala. (January 1965).
- (12) Lucey, G. K., "A Rain Impact Analysis for an Artillery PD System", HDL-TM-72-15, Harry Diamond Laboratories, Washington, D.C. (May 1972).
- (13) Ivankoe, E., "Rain Sensitivity Tests on M557 and M557E1 (XM712E2)", PATR 3966, Picatinny Arsenal, Dover, N.J. (August 1969).
- (14) Reynolds, M. C., "Rain Measurement and Simulation for Supersonic Erosion Studies", SCR-474, Sandia Laboratories, Albuquerque, N.M. (February 1962).
- (15) "Study of Liquid and Solid Particle Impacts", Contract Rt 64, TRW 17286-6001-P0-00, from TRW Systems Group, Redondo Beach, California to Ballistic Research Laboratories, Aberdeen, Md. (March 1972).
- (16) Askin, D., Sikra, J. (Frankford Arsenal), "Rainfall as an Environmental Factor", Note In Proceedings of the Ballistic Environmental Measurements Symposium for Tube-Fired Munitions, BRL, Aberdeen, Md. (May 1972).
- (17) Jenkins, D. C., Booker, J. D., "A Photographic Study of the Impact Between Water Drops and a Surface Moving at High Speed", Tech. Note Mech. Eng. 275, Royal Aircraft Establishment, England (November 1958).
- (18) Heymann, F. J., "Synopsis of Final Comparisons Between the Speed of Erosion and Impact Parameters", paper presented at Second International Conference on Rain Erosion and Associated Phenomena, Meersburg (August 1967), N68-19401-427.
- (19) Savic, P., Boulton, G. T., "The Fluid Flow Associated with the Impact of Liquid Drops with Solid Surfaces", Report No. MT-26, National Research Council of Canada, Ottawa (May 1965).
- (20) Engel, O. G., "Waterdrop Collisions with Solid Surfaces", Journal of Research, National Bureau of Standards, 54 (5), 281-298 (May 1955).
- (21) Engel, O. G., "Note on Particle Velocity in Collisions Between Liquid Drops and Solids", Journal of Research, NBS, 64A (6), 497-498 (November-December 1960).
- (22) Engel, O. G., "Resistance of White Sapphire and Hot-Pressed Alumina to Collision with Liquid Drops", Journal of Research, NBS, 64A (6), 499-512 (November-December 1960).
- (23) Hancox, N. L., Brunton, J. H., "The Erosion of Solids by the Repeated Impact of Liquid Drops", Phil. Trans. Roy. Soc., London, A, 260 (1110), 121-139 (1966).
- (24) Kosonocky, S., "Design and Evaluation of a Rain Insensitive Modification to M557E1 Point Detonating Fuze", PATR 3894, Picatinny Arsenal, Dover, N.J. (April 1969).
- (25) Handbook of the Engineering Sciences, Edited by J. H. Potter, D. Van Nostrand, New York (1967), p 1011.
- (26) Inghard, U., Kraushaar, W. L., Introduction to Mechanics, Matter and Waves, Addison-Wesley Publishing Co., Reading, Mass. (1960), p 583.
- (27) Wahl, N. E., "Investigation of the Phenomena of Rain Erosion at Subsonic and Supersonic Speeds", Tech. Report AFML-TR-65-330, from Bell Aerosystems Company for Air Force Materials Laboratory, Wright-Patterson AFB, Ohio (October 1965). (Literature search)

- (28) Roys, G. P., "Operation of an F-106A in Thunderstorms at Supersonic and High Subsonic Airspeeds", ASD-TN-61-97, AD-270037, Aeronautical Systems Division, Wright-Patterson AFB, Ohio (October 1961).
- (29) Brunton, J. H., "Erosion by Liquid Shock", paper presented at Second International Conference on Rain Erosion and Associated Phenomena, Meersburg (August 1967).
- (30) Fyall, A. A., "Single Impact Studies with Liquids and Solids", paper presented at Second International Conference on Rain Erosion and Associated Phenomena, Meersburg (August 1967).
- (31) Hammit, F. G., et al, "Laboratory Scale Devices for Rain Erosion Simulation", paper presented at Second International Conference on Rain Erosion and Associated Phenomena, Meersburg (August 1967).
- (32) Brunton, J. H., Camus, J. J., "The flow of a Liquid Drop During Impact", paper at Third International Conference on Rain Erosion and Associated Phenomena, Hampshire, England (August 1970) summarized by E. Salkovitz, AD 715-100.
- (33) Brunton, J. H., "Cavitation Damage", paper at Third International Conference on Rain Erosion and Associated Phenomena, Hampshire, England (August 1970) summarized by E. Salkovitz.
- (34) Field, J. E., et al, "Erosion Processes", paper at Third International Conference on Rain Erosion and Associated Phenomena, Hampshire, England (August 1970) summarized by E. Salkovitz.
- (35) Wetmore, W. C., "Rain Erosion Damage to Aircraft Structural Parts and Materials at Supersonic Speeds", Aviation Week, 80 (17), 110 (1964).
- (36) Lucey, G. K., Ireland, R., "An Improved Test to Determine Rain-Erosion Resistance in Fuze Nose Cones", HDL-TR-1559, Harry Diamond Laboratories, Washington, D.C. (July 1971).
- (37) Conn, A. F., "Prediction of Rain Erosion Resistance from Measurement of Dynamic Properties", paper at Third International Conference on Rain Erosion and Associated Phenomena, Hampshire, England (August 1970) summarized by E. Salkovitz.
- (38) Weaver, J. M., "Nickel Electroplated Nonconductive Materials for Rain Erosion Protection", Tech. Report AFML-TR-66-398, Air Force Materials Laboratory, Wright-Patterson AFB, Ohio (May 1967).
- (39) Michael, H. J., "Testing and Evaluation of Impact-Abrasion-Erosion Resistant Aircraft Coatings", AFML-TR-68-324, from North American Rockwell Corp. Columbus Division to Air Force Materials Laboratory, Wright-Patterson AFB, Ohio (October 1968).
- (40) "State-of-the-Art Survey of Raindrop Erosion", edited by E. J. Wheelahan, Report No. RS-TR-67-13, U.S. Army Missile Command, Redstone Arsenal, Alabama (November 1967).
- (41) Schmidt, G. F., "Polyurethane Coatings for Rain Erosion Protection", paper presented at Second International Conference on Rain Erosion and Associated Phenomena, Meersburg (August 1967).
- (42) Wahl, N. E., "Design and Operation of Mach 3 Rotating Arm Erosion Test Apparatus", paper at Third International Conference on Rain Erosion and Associated Phenomena, Hampshire, England (August 1970) summarized by E. Salkovitz.
- (43) Gould, G. C., "The Cavitation Erosion of Stellite and Other Metallic Materials", paper at Third International Conference on Rain Erosion and Associated Phenomena, Hampshire, England (August 1970) summarized by E. Salkovitz.

- (44) Sikra, J., Putscher, K., "Rain Erosion Tests of Fuze, MTSQ, M564, in Simulated Rain, Series I-V", Frankford Arsenal, Philadelphia, Pa (December 1968 - July 1971).
- (45) Brunton, J. H., "Erosion by Liquid Shock", paper presented at Second International Conference on Rain Erosion and Associated Phenomena, Meersburg (August 1967).
- (46) Rieger, H., "The Influence of Various Test Parameters on Material Destruction at Drop-Impact", paper at Third International Conference on Rain Erosion and Associated Phenomena, Hampshire, England (August 1970) summarized by E. Salkovitz.
- (47) Mutchler, C. K., Hansen, L. M., "Splash of Waterdrop at Terminal Velocity", *Science*, **169**, 1311-1312 (September 1970).
- (48) Wilson, R. E., "Ceramic-Plastic Composites for Rain Erosion Resistant Randomes", NOLTR 65-63, Naval Ordnance Laboratory, White Oak, Md. (November 1965).
- (49) Walton, J. D., et al, "Rain Erosion of Ceramics at High Mach Numbers", paper presented at Second International Conference on Rain Erosion and Associated Phenomena, Meersburg (August 1967).
- (50) Tatnall, G. J., "Aerodynamic Spike for Drag Reduction and Rain Drop Disintegration at Low Supersonic Velocities", paper presented at Second International Conference on Rain Erosion and Associated Phenomena, Meersburg (August 1967).
- (51) Nicholson, J. E., "Drop Breakup by Airstream Impact", paper presented at Second International Conference on Rain in Erosion and Associated Phenomena, Meersburg (August 1967).
- (52) Liepmann, Rochko, Elements of Gas Dynamics, John Wiley and Sons, New York (1958).
- (53) Handbook of Tables for Applied Engineering Science, Chemical Rubber Co., Cleveland, Ohio (1970), pp 404-414.
- (54) Ranger, A. A., Nichols, J. A., "Water Droplet Breakup in High Speed Airstreams", paper presented at Third International Conference on Rain Erosion and Associated Phenomena, Hampshire, England (August 1970) summarized by E. Salkovitz.
- (55) Waldman, G. D., Reinecke, W. G., Glenn, D. C., "Raindrop Breakup in the Shock Layer of a High-Speed Vehicle", *AIAA Journal*, **10** (9), 1200-1204 (September 1972).
- (56) Reinecke, W. G., McKay, W. L., "Experiments on Water Drop Breakup Behind Mach 3 to 12 Shocks", AVATD-0172-69-RR from AVCO Government Products Group, Lowell, Mass. to Sandia Corporation, Albuquerque, N.M. (June 1969).
- (57) Branson, D. E., et al, "Study of Target Penetration Prediction by High Speed and Ultra High Speed Ballistic Impact", Report No. 634, Hayes International, Birmingham, Alabama (1963).
- (58) Sorenson, N. R., "Systematic Investigation of Crater Formation in Metals", Proceedings of the Seventh Symposium on Hypervelocity Impact, VI (February 1965).
- (59) McNaughtan, I. I., et al, "Hail Impact Studies", paper at Third International Conference on Rain Erosion and Associated Phenomena, Hampshire, England (August 1970) summarized by E. Salkovitz.
- (60) Edwards, L. S., "Airworthiness Requirements for Supersonic Transport Aircraft in a Hydro-meteor Environment", paper presented at Second International Conference on Rain Erosion and Associated Phenomena, Meersburg (August 1967).
- (61) Gunn, R., The Electricity of Rain and Thunderstorms, Terrestrial Magnetism and Atmospheric Electricity (March 1935).

Distribution List

Defense Materiel Specifications & Standards Office

ATTN: Mr. John McAdam
2 Skyline Place
5203 Leesburg Pike-14th Fl
Falls Church, VA 22041

Office of Secretary of Defense
Director of Defense, RES and Engr

ATTN: Mr. R. Thorkelson
Pentagon, Washington, DC 20301

HQTRS, Dept of Army

ATTN: DAMA-CSM Mr. E. Lippi
Washington, DC 20310

Commander

DARCOM

ATTN: DRCDE-DF Mr. E. Boward
5001 Eisenhower Avenue
Alexandria, VA 22333

Commander

US Armament Materiel Readiness Command

ATTN: DRSAR-LEW-F Mr. R. Kotecki DRSAR-QAS Mr. P. Barrette
DRSAR-ASF Mr. V. Bozzer DRSAR-QAL Mr. G. Kenaley
DRSAR-QAM Mr. A. Simpson DRSAR-MA Mr. H. Baren
Rock Island, IL 61299

Commander, Harry Diamond Laboratories

2800 Powder Mill Road, Adelphi, MD 20783

ATTN: DELHD-TD Dr. W. Carter
DELHD-PO Mr. K. Hine
DELHD-DE Mr. I. Flyer
DELHD-IT Mr. J. Cullinane
DELHD-DE-OE Mr. M. Barron
DELHD-IT-E Mr. R. Westlund
DELHD-IT-RT Mr. A. Frydman
DELHD-TA-L Tech. Library

Commander
US Army Armament Research and Development Command,
Dover, NJ 07801
ATTN:

DRDAR-TDS	Mr. V. Lindner	DRDAR-LCN
DRDAR-ASF	Mr. A. Braganca	DRDAR-LCN-C Mr. G.R. Taylor
DRDAR-ASF	Mr. H. MacGrady	DRDAR-LCN-C Mr. G. Demitrack
DRDAR-LCU-SP	Mr. S.J. Ruffini	DRDAR-LCN-M Mr. V. Gentile
DRDAR-TST-S	Mr. R. Joe	DRDAR-LCN-M Mr. L. Horowitz
DRDAR-TST	Mr. W. Bondemore	DRDAR-LCN-T Mr. S. Israels
DRDAR-TSE-EE	Mr. E. Steward	DRDAR-LCN-T Mr. L. Post
DRDAR-LCE	Dr. R.E. Walker	DRDAR-LCN-T Mr. R. Nitzsche
DRDAR-LCE	Mr. L. Avrami	DRDAR-LCN-T Mr. H. Rand
DRDAR-LCE-C	Dr. H. Matsuguma	DRDAR-LCN-T Mr. F. McCann
DRDAR-LCE-D	Mr. F. Correll	DRDAR-LCN-T Mr. A.G. Nash
DRDAR-LCE-D	Mr. R. Wagner	DRDAR-QAD Mr. R. Davis
DRDAR-TSS	Mrs. E. Sommers	DRDAR-QA Mr. H. Lazar
DRCPM-CAWS	Mr. R. DeKline	DRDAR-QAR-E Mr. L. Springer
DRDAR-LCS-E	Ms. G. Weintraub	DRDAR-PMT Mr. G. Zell
DRDAR-SC	Mr. L. Ghazi	DRCPM-TMA-P Mr. F. Steinberg
DRXHE-PTA	Mr. G.R. DeTogni	DRDAR-LCN-C Mr. C. Gelfenstein
DRDAR-TSI-E	Mr. A. Grinoch	

Headquarters, US Army Test and Evaluation Command
ATTN: DRSTE-AD-M Mr. G. Shelton
DRSTE-CM-F Mr. L. Nealley
Aberdeen Proving Ground, MD 21005

Director, Ballistic Research Laboratory
ATTN: DRDAR-BLT-TBD-SCE Mr. D. Silvia
Aberdeen Proving Ground, MD 21005

Commander
Aberdeen Proving Ground, MD 21005
ATTN: STEAP-MT-A Mr. M. Trumbore
STEAP-MT-M Mr. J. Feroli

Commander
Chemical Systems Laboratory ARRADCOM
ATTN: DRDAR-CL
DRDAR-CLN-P Mr. Bach
Aberdeen Proving Ground, MD 21010

Commandant
US Marine Corps
ATTN: AAW-IC Major Peterson
Washington, DC 20380

Commanding General
Firepower Division, Dev. Ctr
ATTN: LTC Maresco
U.S. Marine Corps Development and Education Command
Quantico, VA 22134

Commandant
Headquarters US Marine Corps
Code LMG (Mr. J. Locke)
Washington, DC 20380

Commander
Naval Weapon Support Center
ATTN: Code 30541 Mr. K.L. Holloway
Crane, IN 47522

Office-In-Charge
Naval Ammunition Production Engineering Center (NAVAMPROENG CEN)
ATTN: Code SEA-642524 Mr. L. Wilson
Crane, IN 47522

Commander
US Naval Underwater Systems Center
ATTN: Code 4323
Newport, RI 02840

Commander
Naval Air Systems Command
Department of the Navy
ATTN: Code Air 52021 Eng Div Std Sec
Code Air 541
Washington, DC 20361

Commander
Naval SEA Systems Command, Department of the Navy
ATTN: Code SEA-62Y
Code SEA-642
Code SEA-3112 Mrs. M.I. Pellegrini
Code SEA-04H3 Mr. E.A. Daugherty
Washington, DC 20360

Commander
Naval Ordnance Station
ATTN: Code 5241 Mr. Sigmund S. Stolarz
Code 5211M Engr. Dept Mr. W.A. York
Indian Head, MD 20640

Commander
Naval Weapons Center
ATTN: Code 3351 Mr. R.R. Emerson
Code 6212 Mr. T. Inouye
Code 335 Mr. R. Higuera
China Lake, CA 93555

Commander
Naval Surface Weapons Center
White Oak Laboratory, Silver Spring, MD 20910
ATTN: Code G-44 Mr. F. Gomez, Mr. A. Munach
Code E-21 Mr. J.S. Gott, Mr. C. Fridinger
Code E-35 Mr. D. Smock
Code R-12 Mr. F. Menz
Code G-43 Mr. R. Eby

Commander, Pacific Missile Test Center
ATTN: Code 2252, Mr. M. Ralles, Mr. T. Gurrola
Point Mugu, CA 93042

Commander
Naval Weapons Station
ATTN: Code 3022, Mr. David Heape
Yorktown, VA 23491

Commander
Naval Surface Weapons Center
ATTN: Code N42, Mr. F. Hanzel
Code G32, Mr. R. Morrisette
Dahlgren Laboratory
Dahlgren, VA 22448

HQTRS, USAF Air Systems Command
ATTN: SDWM
SDZA
Andrews Air Force Base
Washington, DC 20331

Commander
Hanscom Air Force Base
ATTN: AFGL-LYD, Mr. P. Pettelman
Hanscom AFB, MA 01731

Commander
Hill Air Force Base
ATTN: OO-ALC/MMWRAE Mr. W. Scott Dolder
Ogden, UT 84406

Armament Development & Test Center
ATTN: AD/SD3M Mr. E.T. Smith
AD/SESS Mr. J. Nichols
AD/TETPA Mr. D.G. Cox
AD/SDEP Mr. C. Thirsk
AD/DLJP Mr. R.C. Erhart, Mr. Don Bednar
Eglin AFB, FL 32542

USA Transportation Engineering Agency (USATEA)

ATTN: MTT-TRG

P.O. Box 6276

Newport News, VA 23606

Commander

US Naval Ammunition Depot

ATTN: Code 805 Mr. R.E. Seely

Earle, NJ 07737

Commander

US Army Missile Command

ATTN: DRSMI-MC Mr. T. DeLong

Redstone Arsenal, AL 35898

USAF Departmental Standardization Office

HA, USAF/LGPMC

Washington, DC 20330

HQ AFLC CASO/LCDSHB

ATTN: Mr. M. Stasio

Federal Center

Battle Creek, MI 49016

Commander

Holloman Air Force Base

ATTN: Test Track Division

Holloman AFB, NM 88330

Commander

Defense Technical Information Center

Cameron Station

Alexandria, VA 22314

Mr. R.W. Strauss

Chairman Fuze Section

American Defense Preparedness Association

c/o Stewart-Warner Corporation

425 13th Street

Washington, DC 20004

RARDE

Ft. Halstead

ATTN: ET3 Branch, Bldg N3, Mr. R. Sculpher

Sevenoaks, Kent, UK